AD-A116 448 MASSACHUSETTS INST OF TECH CAMBRIDGE RESEARCH LAB OF--ETC F/G 17/9
PREDICTION OF BACKSCATTER AND EMISSIVITY OF SNOW AT MILLIMETER --ETC(U)
JAN 80 J A KONG, R T SHIN F08635-78-C-0115
UNCLASSIFIED AFATL-TR-80-33 NL

1 OF 3
AD A
116448

PHOTOGRAPH THIS SHEET

AD-E800481

AD A116448

DTIC ACCESSION NUMBER

III

LEVEL

INVENTORY

Final, Feb. 78 - Sep. '79

Jan. 80

DOCUMENT IDENTIFICATION

Contract F08635-78-C-0115 AFATL-TR-80-33

DISTRIBUTION STATEMENT A

Approved for public release;
Distribution Unlimited

DISTRIBUTION STATEMENT

ACCESSION FOR		
NTIS	GRA&I	☒
DTIC	TAB	☐
UNANNOUNCED		☐
JUSTIFICATION		
BY		
DISTRIBUTION /		
AVAILABILITY CODES		
DIST	AVAIL AND/OR SPECIAL	
A		

DISTRIBUTION STAMP

DTIC
S ELECTE D
JUL 6 1982
D

DATE ACCESSIONED

DTIC
COPY
INSPECTED
2

82 07 06 232

DATE RECEIVED IN DTIC

PHOTOGRAPH THIS SHEET AND RETURN TO DTIC-DDA-2

DTIC FORM OCT 79 70A DOCUMENT PROCESSING SHEET

AD-E 800 481

AFATL-TR-80-33

Jan 80

Prediction of Backscatter and Emissivity of Snow at Millimeter Wavelengths

J. A. Kong
R. T. Shin

MASSACHUSETTS INSTITUTE OF TECHNOLOGY
RESEARCH LABORATORY OF ELECTRONICS
CAMBRIDGE, MASSACHUSETTS 02139

AD A116448

JANUARY 1980

FINAL REPORT FOR PERIOD FEBRUARY 1978-SEPTEMBER 1979

Approved for public release; distribution unlimited

Air Force Armament Laboratory
AIR FORCE SYSTEMS COMMAND ★ UNITED STATES AIR FORCE ★ EGLIN AIR FORCE BASE, FLORIDA

23 06 82

UNCLASSIFIED

SECURITY CLASSIFICATION OF THIS PAGE (When Data Entered)

REPORT DOCUMENTATION PAGE		READ INSTRUCTIONS BEFORE COMPLETING FORM
1. REPORT NUMBER AFATL-TR-80-33	2. GOVT ACCESSION NO. AD-A116 448	3. RECIPIENT'S CATALOG NUMBER
4. TITLE (and Subtitle) PREDICTION OF BACKSCATTER AND EMISSIVITY OF SNOW AT MILLIMETER WAVELENGTHS		5. TYPE OF REPORT & PERIOD COVERED Final Report Feb. 1978 - Sept. 1979
		6. PERFORMING ORG. REPORT NUMBER
7. AUTHOR(s) Jin Au Kong and R. T. Shin		8. CONTRACT OR GRANT NUMBER(s) F08635-78-C-0115
9. PERFORMING ORGANIZATION NAME AND ADDRESS Massachusetts Institute of Technology Research Laboratory of Electronics Cambridge, Massachusetts 02139		10. PROGRAM ELEMENT, PROJECT, TASK AREA & WORK UNIT NUMBERS Program Element: 61102F JON: 2305E110
11. CONTROLLING OFFICE NAME AND ADDRESS Air Force Armament Laboratory Armament Division Eglin AFB, Florida 32542		12. REPORT DATE January 1980
		13. NUMBER OF PAGES 234
14. MONITORING AGENCY NAME & ADDRESS(if different from Controlling Office)		15. SECURITY CLASS. (of this report) Unclassified
		15a. DECLASSIFICATION/DOWNGRADING SCHEDULE

16. DISTRIBUTION STATEMENT (of this Report)

Approved for public release; distribution unlimited.

17. DISTRIBUTION STATEMENT (of the abstract entered in Block 20, if different from Report)

18 SUPPLEMENTARY NOTES

Availability of this report is specified on verso of front cover.

19 KEY WORDS (Continue on reverse side if necessary and identify by block number)

Active Remote Sensing
Born Approximation
Remote Sensing of Snow
Passive Remote Sensing
Modified Radiative Transfer Theory

20 ABSTRACT (Continue on reverse side if necessary and identify by block number)

In both the active and passive microwave remote sensing of snowpacks, volume scattering effects due to medium inhomogeneities play a dominant role in the determination of the radar backscattering cross sections and the brightness temperatures. Two theoretical models have been developed to characterize snowpacks: (1) a random medium with a variance, a horizontal correlation length, and a vertical correlation length and, (2) a homogeneous

DD FORM 1 JAN 73 1473

UNCLASSIFIED

SECURITY CLASSIFICATION OF THIS PAGE (When Data Entered)

20. Abstract (continued)

dielectric containing discrete scatterers. The earth terrain is then modelled as layers of such scattering media bounded by air above and a homogeneous half-space below. The development of the theoretical approach is guided by the motivation that data set obtained in a field and plotted as functions of frequency, angle, and polarization must be matched with same set of parameters characterizing the same field. In matching the theoretical results with experimental data collected from snow-ice fields, we summarize the following findings: (1) For snow-ice fields the horizontal correlation length is no less than the vertical correlation length signifying a more laminar structure. The correspondence between the continuum random medium and the discrete spherical scatterer model can be verified when the vertical correlation length is equal to the horizontal correlation length. (2) The vertically polarized backscattering cross section σ_{vv} is always greater than the horizontally polarized backscattering cross section σ_{hh} for half-space scattering media and may become small for a two-layer model. (3) To account for diurnal change exhibited by snow fields in both the active and passive remote sensing cases, a three-layer model with a thin top layer caused by solar illumination must be used.

PREFACE

This is a final report on U.S. Air Force/Eglin Contract F08635-78-C-0115 on prediction of backscatter and emissivity of snow at millimeter wavelengths for the period covering February 1978 - September 1979. This work has been sponsored by the Air Force Armament Laboratory and performed by Massachusetts Institute of Technology, Research Laboratory of Electronics, Cambridge, Massachusetts 02139.

The Public Affairs Office has reviewed this report, and it is releasable to the National Technical Information Service (NTIS), where it will be available to the general public, including foreign nationals.

This technical report has been reviewed and is approved for publication.

FOR THE COMMANDER

Barnes E Holder Jr.

BARNES E. HOLDER, Jr., Colonel, USAF
Chief, Guided Weapons Division

(The reverse of this page is blank)

TABLE OF CONTENTS

LIST OF FIGURES

SECTION I
INTRODUCTION

In this report the work accomplished during this program is summarized. In Section II and Section III, the completed theoretical work for active and passive remote sensing is summarized. In Section IV the work done on deriving the modified radiative transfer theory which includes the coherent effects is summarized, and the work on the rough surface effects is summarized in Section V. The experimental and ground-truth studies are summarized in Section VI. Section VII lists the computer programs with comment cards, equations used in the programs, list of symbols, and input-output formats. Publications are listed in Section VIII and the Appendices are listed in Section IX.

The comprehensive review of the remote sensing theories and the experiments pertaining to snow is included in Appendix A.

SECTION II
ACTIVE REMOTE SENSING

In the active remote sensing of earth terrain, theoretical models have been developed which can be classified under two categories: (1) wave models and (2) radiative transfer models. In both cases, the earth terrain of interest is treated as a random medium with a correlation function characterizing the size of inhomogeneities and the contrast in fluctuation strength as compared with the background dielectric constant. The model of a continuous random medium has been found to be versatile and useful in the analysis and interpretation of backscattering data collected from snow and vegetation fields (Reference 1). This model can be developed in a straightforward manner and is able to match the essential angular and spectral behavior in the collected backscattering data.

WAVE MODELS

In this approach the scattering of electromagnetic waves by a layer of random media with three-dimensional correlation functions has been solved by applying Born approximations to the wave equation. Carrying to first order in albedo, analytical results for the bistatic scattering coefficients and the backscattering cross sections have been derived (Reference 2) which account for volume scattering effects. It was found that as a result of the effect of the second boundary, the horizontally polarized return σ_{hh} can be greater than the vertically polarized return σ_{vv}, whereas for a half-space random medium σ_{vv} is always greater than σ_{hh}.

As more realistic simulation of earth terrain for active remote sensing, analytical expressions for the backscattering cross sections have been derived (Reference 3) for a stratified random medium by applying the first-order Born approximation. In the

special case of a three-layer random medium, two maxima are found in the spectral dependence of the backscattering due to resonance scattering within each random layer. The theoretical results also are found to compare favorably with data obtained from vegetation and snow-ice fields.

The Born approximation has been carried to second order in the albedo to obtain backscattering cross sections that account for depolarization effects in a two-layer random medium (Reference 4). It was found that the first- and second-order theoretical results, together with a consistent set of parameters, are able to match the essential features of like- and cross-polarized backscattering data gathered from the same target area.

RADIATIVE TRANSFER MODELS

In this approach bistatic scattering cross sections for a half space random medium are derived (Reference 5) by using the radiative transfer theory, which deals directly with radiation intensities by assuming incoherence and far-field interactions. An iterative process is applied to solve the integral equations to both first and second order in albedo. The first-order results yield backscattering cross sections which account for the like-polarized return. The second-order results, as in the case of the wave approach, exhibit depolarization effects in the backscattered power. The angular and spectral dependence of the backscattering cross sections have been illustrated numerically.

SECTION III
PASSIVE REMOTE SENSING

In the microwave remote sensing of snow, volume scattering effects play a dominant role in brightness temperature measurements. The scattering effects can be accounted for by considering the scattering to be due to either discrete scattering centers imbedded in a homogeneous medium (discrete scatterer approach) or by random inhomogeneities in a medium (random medium approach). Both the discrete scatterer approach and the random medium approach with radiative transfer theory have been used to study the effect of volume scattering. Even though the radiative transfer approach deals only with the intensities of the field quantities and neglects their coherent nature, it has an advantage in that it is simple and, more importantly, accounts for multiple scattering effects.

In the discrete scatterer approach, a Mie scattering model with radiative transfer theory was used to solve the problem of microwave thermal emission from a scattering layer on top of a homogeneous medium (Reference 6). The result was applied to the interpretation of experimental data obtained from various snow measurements. The spectral and the angular dependences of the brightness temperatures showed good agreement between theory and experiment. The brightness temperature as a function of snow depths was also interpreted. It was observed that as the snow depth increased, the brightness temperature increased when the subsurface was an aluminum plate due to the fact that the plate was cold and snow absorption induced a brightening effect. The brightness temperature decreased when the subsurface was soil, due to the face that snow scattering induced a darkening effect.

In the process of matching the data obtained from snow fields, the phenomenon of diurnal change where the brightness temperature

decreased as a function of frequency in the morning and increased in the afternoon was encountered. In order to explain this phenomenon, the results were extended by adding a homogeneous layer on top of the scattering layer (Reference 7). The effect of a homogeneous layer was incorporated in a set of effective boundary conditions for the scattering medium. The effect of the surface layer was also illustrated by plotting the brightness temperatures as functions of frequency and viewing angle for different layer thicknesses, dielectric constants, and fractional volume of the scatterers. It was found that (1) the brightness temperature increased when the loss tangent of the surface layer was increased and when the fractional volume occupied by the scatterers was decreased, (2) in the absence of the surface layer the brightness temperature was usually decreasing as a function of frequency, and (3) the presence of the homogeneous layer might cause the brightness temperature to increase with frequency.

The random medium approach with radiative transfer theory was also used to obtain results from an N-scattering layer model with laminar structure (Reference 8). The propagation matrix formulation was used to obtain the analytical solutions. The results were illustrated with a two-scattering layer model in order to study the dependence of the brightness temperature variations on the layer thickness, variance, correlation length, and permittivity. It was found that usually the brightness temperature increased when the loss tangents increased and decreased when the variances and the correlation lengths increased. For the case of a homogeneous layer on top of a scattering layer, the fact that the brightness temperature could be increased as a function of frequency while for the case of only a scattering layer the brightness temperature decreased as a function of frequency was illustrated.

SECTION IV
MODIFIED RADIATIVE TRANSFER THEORY

The most useful theoretical approach in the active remote sensing of earth terrain is the phenomenological radiative transfer (RT) theory. The RT theory deals directly with intensities, and energy conservation is guaranteed as a consequence of the coupled first-order differential equations. However, the limitation of the RT theory is that it assumes incoherent interactions among the specific intensities. When interference effects among specific intensities become important, a modified radiative transfer (MRT) theory where coherence is included must be used. MRT equations have been developed for a two-layer one-dimensional random medium, by applying the nonlinear approximation to Dyson's equation and the ladder approximation to the Bethe-Salpeter equation. These approximations have been shown to be energetically consistent and therefore appropriate in the development of a radiative transport theory. Additional constructive interference terms not accounted for in phenomenological transport theories are found to occur due to the presence of the bottom boundary.

More recently, MRT equations have been derived (Reference 9) for active remote sensing of a half-space random medium with three-dimensional variations. The standard RT theory is shown to follow as a limiting case of the MRT theory.

SECTION V
ROUGH SURFACE EFFECTS

In passive remote sensing of geophysical surfaces, the quantity of particular interest is the emissivity which, by reciprocity and energy conservation, is equal to one minus the reflectivity. The reflectivity is calculated in terms of bistatic reflectivities as defined by Peake. Stogryn's solution for the emissivity of a rough surface with the principle of reciprocity has been in use for many years. The rough surface bistatic coefficients are calculated by using a combination of Huygen's principle and geometrical optic approach. Transmissivity of a rough surface was not considered because it is not needed in the calculation of the emissivity. The bistatic transmission coefficients for a dielectric interface were calculated using the same approaches as in the calculation of the bistatic reflection coefficients (Reference 10). It was then shown that the resultant reflectivity and transmissivity do not add to unity, indicating violation of energy conservation. This nonconservation of energy leads to a nonunique definition of emissivity calculated with this approach.

In the calculation for the emissivity, numerical integration has to be carried out for two angular variables θ_s and ϕ_s in the upper hemisphere. The computation is usually very inefficient because the integrand, for the case of small slope, is sharply peaked in the specular direction. Thus the results must be accurate enough in order to differentiate between a rough surface and a specular surface. The integral representation of the reflectivity and the transmissivity were modified in terms of the bistatic coefficients. It was then shown that the sum of the modified reflectivity and the modified transmissivity is unity. Thus conservation of energy is observed. Furthermore, the modified reflectivity and transmissivity integrals can be evaluated asymptotically and made

to exhibit the net rough surface effects as compared to a specular surface.

SECTION VI
EXPERIMENTAL AND GROUND-TRUTH STUDIES

EXPERIMENTAL STUDIES

Participation in an experiment that took place in the Rocky Mountains near Winter Park, Colorado, during March 1978 (Reference 11) was made. This was a joint effort with a team from NASA Goddard Space Flight Center and National Bureau of Standards to investigate the microwave hydrologic properties of snow. To isolate many of the electromagnetic emission characteristics of snow, a 35 GHz radiometer was used to measure the brightness temperatures of man-made and natural snow on an aluminum plate. In particular, the following topics were investigated: (1) angular dependence of the brightness temperature as snow depth increases, (2) change in the measured brightness temperature as a target made of aluminum foil is placed on top of a snow layer, and (3) diurnal changes. The aluminum plate was used to reduce the uncertainties concerning the subsurface electromagnetic properties of the snow pack.

GROUND-TRUTH STUDIES

The ground-truth measurements for snow fields in the Rome, New York area and the Rogers City, Michigan area were obtained during the months of January and February 1979. These measurements were made in connection with the AIR FORCE SAR IMAGING flights in order to make a meaningful interpretation of the data. The ground-truth measurements for the snow fields include snow profile characteristics, free water content measurements, and depth measurements. Snow profile characteristics were obtained from a pit dug in the field, by identifying the various layers, and recording the temperature, average grain size, density, and thickness of each layer. For the free water content measurements, a freezing calorimetric technique

was used to find the percentage by weight of free water present in the snow. The depth measurements were made approximately 20 meters apart in the snow field.

In the Rome, New York area the measurements were made at four sites referred to as Rome A, Rome E, Ava B and Ava C. Two SAR imaging flights were made on January 16 and January 29, 1979. The ground-truth acquired on these two days were supplemented by the measurements made on six other days. In the Rogers City, Michigan area the measurements were made at two test sites referred to as Site E and Site F on February 7 and 8, 1979 in relation to the flight made on February 5, 1979. The detailed ground-truth measurements are included in Appendices B and C.

SECTION VII

COMPUTER PROGRAMS

PROGRAM LAMINAR

Introduction

This program is based upon the thesis by B. Djermakoye (S.M. and E.E., M.I.T., 1978). The brightness temperature from a three-layer random medium (Figure 1) with laminar structure is calculated from radiative transfer theory. The inhomogeneous temperature profiles are also included. The sky temperature is also taken into account in the program.

Two versions of this program are listed here. One is to find the brightness temperature versus angles (Version I). The other one is to find the brightness temperature versus the frequency (Version II).

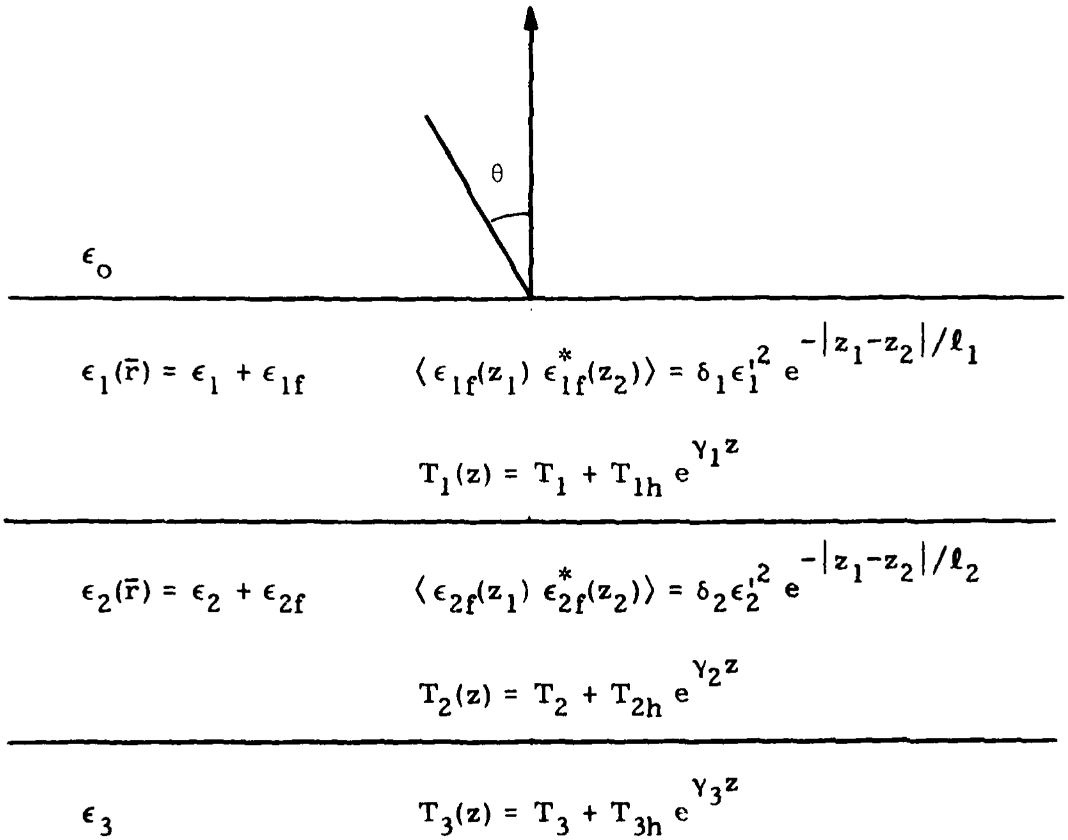

Figure 1. Geometrical Configuration of the Problem for Program LAMINAR

Equations

The radiative transfer equations governing the upward propagating intensity I_{un} and the downward propagating intensity I_{dn} in region n are

$$\frac{d}{dz} I_{un} = -\kappa_{en} I_{un} + \kappa_{an} B_n(z) + \frac{\kappa_{sn}}{2} \left[P_{fn} I_{un} + P_{bn} I_{dn}\right] \tag{1a}$$

$$\frac{d}{dz} I_{dn} = \kappa_{en} I_{dn} - \kappa_{an} B_n(z) - \frac{\kappa_{sn}}{2} \left[P_{fn} I_{dn} + P_{bn} I_{un}\right], \tag{1b}$$

where

$$B_n = \frac{K}{\lambda^2} \frac{\epsilon_n'}{\epsilon_o} T_n(z) \qquad n = 1, 2, 3 \tag{2}$$

$$k_n = \omega\sqrt{\mu\epsilon_n'} \qquad n = 1, 2, 3 \tag{3}$$

$$\kappa_{en} = \kappa_{an} + \kappa_{sn} \qquad n = 1, 2 \tag{4}$$

$$T_1(z) = T_1 + T_{1h}\, e^{\gamma_1 z} \tag{5a}$$

$$T_2(z) = T_2 + T_{2h}\, e^{\gamma_2 z} \tag{5b}$$

$$T_3(z) = T_3 + T_{3h}\, e^{\gamma_3 z}. \tag{5c}$$

K is the Boltzmann constant and λ is the free-space wavelength. The scattering coefficient κ_{sn}, the absorption coefficient κ_{an}, and the scattering phase functions have been determined. We have, for vertical polarization,

$$\kappa_{an} = \frac{\epsilon_n''}{\epsilon_n'} \frac{k_n}{\cos\theta_n} \tag{6}$$

$$\kappa_{sn} = \frac{k_n^2 \Delta_n \ell_n}{2 \cos^2\theta_n} \left[\frac{1 + 4k_n^2 \ell_n^2 \cos^2\theta_n + \cos^2 2\theta_n}{1 + 4k_n^2 \ell_n^2 \cos^2\theta_n} \right] \qquad n = 1,2 \tag{7a}$$

$$\kappa_{sn} = 0 \quad \text{in region 3.} \tag{7b}$$

$$P_{bn} = \frac{2 \cos^2 2\theta_n}{1 + 4k_n^2 \ell_n^2 \cos^2\theta_n + \cos^2 2\theta_n} \qquad n = 1,2 \tag{8}$$

$$P_{fn} = 2 - P_{bn} \qquad n = 1,2 \tag{9}$$

or for horizontal polarization

$$\kappa_{sn} = \frac{k_n^2 \Delta_n \ell_n}{\cos^2\theta_n} \left[\frac{1 + 2k_n^2 \ell_n^2 \cos^2\theta_n}{1 + 4k_n^2 \ell_n^2 \cos^2\theta_n} \right] \qquad n = 1,2 \tag{10a}$$

$$\kappa_{s3} = 0 \tag{10b}$$

$$P_{bn} = \frac{1}{1 + 2k_n^2 \ell_n^2 \cos^2\theta_n} \tag{11}$$

$$P_{fn} = 2 - P_{bn} \qquad n = 1,2. \tag{12}$$

The solutions:

$$I_{1u} = \eta_1 A_1 e^{\alpha_1 z} + B_1 e^{-\alpha_1 z} + C_1 + D_1 e^{\gamma_1 z} \tag{13a}$$

$$I_{1d} = A_1 e^{\alpha_1 z} + \eta_1 B_1 e^{\alpha_1 z} + C_1 + D_1' e^{\gamma_1 z} \tag{13b}$$

$$I_{2u} = \eta_2 A_2 e^{\alpha_2 z} + B_2 e^{-\alpha_2 z} + C_2 + D_2 e^{\gamma_2 z} \tag{14a}$$

$$I_{2d} = A_2 e^{\alpha_2 z} + \eta_2 B_2 e^{-\alpha_2 z} + C_2 + D_2' e^{\gamma_2 z} \tag{14b}$$

$$I_{3u} = E + G' e^{\gamma_3 z} \tag{15a}$$

$$I_{3d} = H e^{\alpha_3 z} + E + G e^{\gamma_3 z} \tag{15b}$$

with

$$D_1' = \xi_1' D_1 \qquad D_2' = \xi_2' D_2 \tag{16}$$

$$\xi_1' = \frac{\alpha_1^2 + \gamma_1 K_{a1}}{\alpha_1^2 - \gamma_1 K_{a1}} \qquad \xi_2' = \frac{\alpha_2^2 + \gamma_2 K_{a2}}{\alpha_2^2 - \gamma_2 K_{a2}} \tag{17}$$

$$\eta_1 = \frac{\alpha_1 - K_{a1}}{\alpha_1 + K_{a1}} \qquad \eta_2 = \frac{\alpha_2 - K_{a2}}{\alpha_2 + K_{a2}}. \tag{18}$$

$$\alpha_1 = K_{e1}\{(1-\tilde{\omega}_1)[1 - (\tilde{\omega}_1/2)P_{f1} + (\tilde{\omega}_1/2)P_{b1}]\}^{1/2} \tag{19a}$$

$$\alpha_2 = K_{e2}\{(1-\tilde{\omega}_2)[1 - (\tilde{\omega}_2/2)P_{f2} + (\tilde{\omega}_2/2)P_{b2}]\}^{1/2}. \tag{19b}$$

If we identify the scattering albedo,

$$\tilde{\omega}_1 = K_{s1}/K_{e1}. \tag{20}$$

The brightness temperature is found by

$$T_B = \frac{\lambda^2 \epsilon_o}{K\epsilon_{1m}'} (1 - r_{01}) I_{1u}\Big|_{z=0} \tag{21}$$

or

$$T_B = \frac{\lambda^2 \epsilon_o (1 - r_{01})}{K\epsilon_{1m}'} [\eta_1 A_1 + B_1 + C_1 + D_1]. \tag{22}$$

With

$$B_1 = \frac{N}{D} \tag{23}$$

where

$$\begin{aligned}
N = \{ & [(r_{12}-1)\, C_1 a_2 a_3 + (r_{12}\xi_1' - 1)\, D_1 a_2 a_3\, e^{-\gamma_1 d_1} \\
& + \tilde{t}_{12}(C_2 + D_2\, e^{-\gamma_2 d_1})\, a_2 a_3 + \tilde{t}_{12}\eta_2 a_2 M]\, e^{\alpha_2(d_2-d_1)} \\
& - [(r_{12}-1)\, C_1 a_1 a_4 + r_{12}\xi_1' - 1)\, D_1 a_1 a_4\, e^{-\gamma_1 d_1} \\
& + \tilde{t}_{12}(C_2 + D_2\, e^{-\gamma_2 d_1})\, a_1 a_4 + \tilde{t}_{12}\, a_1 M]\, e^{-\alpha_2(d_2-d_1)} \}\, e^{-\alpha_1 d_1} \\
& + \tilde{t}_{12} I_1 (a_3 - \eta_2 a_4)\, e^{-\alpha_1 d_1} \\
& + \{ [(r_{12} - \eta_1)\, \epsilon_1 a_2 a_3 + \tilde{t}_{12}\tilde{t}_{21}\epsilon_1 \eta_2 a_2]\, e^{\alpha_2(d_2-d_1)} \\
& - [\tilde{t}_{21}\tilde{t}_{12}\epsilon_1 a_1 + (r_{12}-\eta_1)\, \epsilon_1 a_1 a_4]\, e^{-\alpha_2(d_2-d_1)} \}\, e^{-2\alpha_1 d_1}
\end{aligned} \tag{24}$$

$$\begin{aligned}
D = \{ & [(1 - r_{12}\eta_1)\, a_2 a_3\, e^{\alpha_2(d_2-d_1)} \\
& - (1 - r_{12}\eta_1)\, a_1 a_4\, e^{-\alpha_2(d_2-d_1)}] \\
& + [-\tilde{t}_{21}\tilde{t}_{12}\eta_1\eta_2 a_2\, e^{\alpha_2(d_2-d_1)} \\
& + \tilde{t}_{21}\tilde{t}_{12}\eta_1 a_1\, e^{-\alpha_2(d_2-d_1)}]\}
\end{aligned} \tag{25}$$

$$\begin{aligned}
(\eta_2 - r_{23}) &= a_1 \qquad & (1 - \eta_2 r_{23}) &= a_2 \\
(1 - \eta_2 r_{12}) &= a_3 \qquad & (\eta_2 - r_{12}) &= a_4 .
\end{aligned} \tag{26}$$

$$\tilde{t}_{12} = t_{12}\,\frac{\epsilon'_{1m}}{\epsilon'_{2m}} \qquad\qquad \tilde{t}_{21} = t_{12}\,\frac{\epsilon'_{2m}}{\epsilon'_{1m}} \tag{27}$$

$$\epsilon_1 = \frac{(r_{01}-1)C_1 + (r_{01}-\xi'_1)D_1}{(1-r_{01}\eta_1)} \tag{28}$$

$$\epsilon_2 = -\frac{(\eta_1 - r_{01})}{(1-r_{01}\eta_1)}$$

$$A_1 = \epsilon_1 + \epsilon_2 B_1 \tag{29}$$

$$A_2 = \frac{I_1}{a_1}\,e^{\alpha_3 d_2} - \frac{a_2 B_2}{a_1}\,e^{2\alpha_2 d_2}.$$

$$I_1 = r_{23}-1)C_2 + (\xi'_2 r_{23}-1)D_2\,e^{-\gamma_2 d_2} + \tilde{t}_{23}(E+G'\,e^{-\gamma_3 d_2}) \tag{30}$$

$$M = (r_{12}-1)C_2 + D_2(r_{12}-\xi'_2)\,e^{-\gamma_2 d_1} + (C_1 + \xi'_1 D_1\,e^{-\gamma_1 d_1})\,\tilde{t}_{21} \tag{31}$$

$$C_1 = A'_1 T_1 \qquad\qquad C_2 = A'_2 T_2 \qquad\qquad E = A'_3 T_3 \tag{32}$$

(where the A'_1 should not be confused with the coefficient in I_{1u}).

$$(K/\lambda^2) = \frac{\epsilon'_{1m}}{\epsilon_o} = A'_1.$$

$$(K/\lambda^2)\,\frac{\epsilon'_{2m}}{\epsilon_o} = A'_2 \tag{33}$$

$$(K/\lambda^2)\,\frac{\epsilon'_{3m}}{\epsilon_o} = A'_3.$$

Symbols

Fortran Symbols	Notation	Explanations
TETA	θ	Incident angle (in radians)
EX1, EX2, EX3	k_1, k_2, k_3	Propagation constants
E1M, E2M, E3M	$\epsilon_1', \epsilon_2', \epsilon_3'$	Real part of $\epsilon_1, \epsilon_2, \epsilon_3$
QS1, QS2, QS3	$\cos\theta_1, \cos\theta_2, \cos\theta_3$	
KA1P, KA1	$2k_1''/\cos\theta_1$	Absorption coefficients (as defined in the paper).
KA2P, KA2	$2k_2''/\cos\theta_2$	
KA3P, KA3	$2k_3''/\cos\theta_3$	
PFE1, PF1	P_{f1} (TE)	Equations (12), (11)
PFE2, PF2	P_{f2} (TE)	Equations (12), (11)
PBE1, PB1	P_{b1} (TE)	Equation (11)
PBE2, PB2	P_{b2} (TE)	Equation (11)
PBM1, PB1	P_{b1} (TM)	Equation (8)
PBM2, PB2	P_{b2} (TM)	Equation (8)
PFM1, PF1	P_{f1} (TM)	Equations (8), (9)
PFM2, PF2	P_{f2} (TM)	Equations (8), (9)
KSE1	κ_{s1} (TE)	Equation (10)
KSE2	κ_{s2} (TE)	Equation (10)
KSM1	κ_{s1} (TM)	Equation (7)
KSM2	κ_{s2} (TM)	Equation (7)
KE1	κ_{e1}	Equation (4)
KE2	κ_{e2}	Equation (4)
RF01	r_{01}	Reflectivities
RF12	r_{12}	"

Fortran Symbols	Notation	Explanations
R01TE	R_{01}	TE reflection coefficients
R12TE	R_{12}	" " "
R01TM	S_{01}	TM reflection coefficients
R12TM	S_{12}	" " "
N1	η_1	Equation (18)
N2	η_2	Equation (18)
XI1	ξ_1'	Equation (17)
XI2	ξ_2'	Equation (17)
AA1	A_1'	Equation (33)
AA2	A_2'	Equation (33)
AA3	A_3'	Equation (33)
T01	t_{01}	Transmissivities
T12	t_{12}	"
TS10	$\tilde{t}_{10}$	Equation (27)
TS12	$\tilde{t}_{12}$	Equation (27)
TS23	$\tilde{t}_{23}$	Equation (27)
TS21	$\tilde{t}_{21}$	Equation (27)
I1	I_1	Equation (30)
M	M	Equation (31)
EP1	ϵ_1	Equation (28)
EP2	ϵ_2	Equation (28)
A	A_1	Equation (29)
IU	I_{1u} $(z = 0)$	Equation (13a)
TB	T_B	Equation (22)

Features

1. Version I. T_B versus incident angles.

   Version II. T_B versus frequency.

2. No subroutines.

Input-Output Format

1. Version I, T_B versus incident angles.

   Data cards format for input:

(1) FORMAT (2F7.4, 2F7.4, 2F5.1); ϵ_1', ϵ_1'', ϵ_2', ϵ_2'', ϵ_3', ϵ_3''

(2) FORMAT (2F6.3, 2F8.5); Δ_1, Δ_2, ℓ_1, ℓ_2

(3) FORMAT (2F6.3, I2, F5.1, I2, F6.1); d_1, d_2, IH, Freq., NEM, T_{sky}.

IH = 0; case of two layers

IH = 1; case of three layers

NEM = 0; TM case

NEM = 1; TE case

(4) FORMAT (3F6.1, 3F4.1, 3F4.1); T_1, T_2, T_3, TH1, TH2, TH3, γ_1, γ_2, γ_3

2. Version II, T_B versus frequency.

   Data cards format for input:

(1) FORMAT (2F7.4, 2F7.4, 2F5.1); ϵ_1', ϵ_1'', ϵ_2', ϵ_2'', ϵ_3', ϵ_3''

(2) FORMAT (2F6.3, 2F8.5); Δ_1, Δ_2, ℓ_1, ℓ_2

(3) FORMAT (2F6.3, I2, I3, I2, F6.1); d_1, d_2, IH, ITETA(θ), NEM, T_{sky}.

ITETA is the incident angle in degrees (integer m).

(4) FORMAT (3F6.1, 3F4.1, 3F4.1); T_1, T_2, T_3, T_{h1}, T_{h2}, T_{h3}, γ_1, γ_2, γ_3

```
C
C                 PROGRAM LAMINAR NO.1
C
C B. DJERMAKOYE (1978)
C S.L.CHUANG(7,1979)
C  LAMINAR,THREE LAYER MODEL
C  RADIATIVE TRANSFER THEORY
C  BRITENESS TEMPERATURE VERSUS INCIDENT ANGLES.
C  THIS PROGRAM FOLLOWS THE PAPER 'RADIATIVE TRANSFER THEORY
C  FOR THE REMOTE SENSING OF LAYERED RANDOM MEDIA' BY
C  B. DJERMAKOYE AND J. A. KONG.
C  AND THE S.M. &E.E. THESIS OF B. DJERMAKOYE,MIT,1978.
      REAL  KA1P,KA2P,KA3P,KSE1,KSE2,KSE1P,KSE2P,KE1P,KE2P
      COMPLEX  R01TE,R12TE,R23TE,R01TM,R12TM,R23TM
      COMPLEX RR1,RR2,RR3
      REAL  G,KSM1,KSM2,KSM1P,KSM2P,KE1PP,KE2PP
      REAL KA1,KA2,KA3,KM1,KM2,KS1,KS2
      REAL KE1,KE2,N1,N2,I1,M,NUM1,NUM2,NUM3
      REAL NUM4,NUM5,NUM,IU,AA(500,6)
      COMPLEX  R23,G1,G2,G3
      COMPLEX R01,E1,E2,E3,R12,EX1,EX2,EX3
      COMPLEX  IX,JX
      NVARS=2
      NPT=16
      NORDER=0
      NPLOT=0
      IDIM=500
      JDIM=6
      IX=(1.0,0.0)
      JX=(0.0,1.0)
  77  FORMAT(2F7.4,2F7.4,2F5.1)
 10   CONTINUE
C  E1,E2,AND E3 ARE THE COMPLEX DIELECTRIC CONSTANTS
C  IN EACH REGION.
      READ(5,77,END=1) E1,E2,E3
  79  FORMAT(2F6.3,2F8.5)
C   DEL1 AND DEL2 ARE THE VARIANCES,CL1 AND CL2 ARE THE
C  CORRELATION LENGTHS IN VERTICAL DIRECTION.
      READ(5,79,END=1) DEL1,DEL2,CL1,CL2
C  D1 AND D2 ARE THE DEPTHS OF THE FIRST AND SECOND LAYER,
C  MEASURED FROM THE TOP SURFACE. NOTE D2 IS NOT THE
C  THICKNESS OF THE SECOND LAYER UNLESS D1=0.
C  IH=0 CASE OF TWO LAYERS.
C  IH=1(NOT 0) CASE OF THREE LAYERS.
C  FREQ IS THE FREQUENCY.
C  NEM=0 VERTICAL POLARIZATION(TM) CASE.
C  NEM=1(NOT 0),HORIZONTAL POLARIZATION(TE) CASE.
C  TSKY IS THE SKY TEMPERATURE WHICH IS LESS THAN 7 DEGREES
C  GENERALLY.
      READ(5,78,END=1) D1,D2,IH,FREQ,NEM,TSKY
  78  FORMAT(2F6.3,I2,F5.1,I2,F6.1)
C  FOR INHOMOGENEOUS TEMPERATURE PROFILES:
C  T1(Z)=T1+TH1*EXP(GAM1*Z),SIMINARLY FOR T2(Z) AND T3(Z),
C  WE ASSIGN APPROPRIATE VALUES FOR T1,TH1,GAM1 ETC.
C  FOR HOMOGENEOUS TEMPERATURE PROFILES:
```

```
C  TH1=TH2=TH3=0.   GAM1=GAM2=GAM3=0.
      READ(5,331) T1,T2,T3,TH1,TH2,TH3,GAM1,GAM2,GAM3
  331 FORMAT(3F6.1,3F4.1,3F4.1)
      IF(IH.EQ.0)  WRITE(6,333)  IH
 333  FORMAT(1H 'IH=',I2,' CASE OF TWO LAYER')
      IF(IH.NE.0)  WRITE(6,334)  IH
 334  FORMAT(1H 'IH=',I2,' CASE OF THREE LAYER')
      IF(NEM.EQ.0)  WRITE(6,666) FREQ
 666  FORMAT(1H 'FREQUENCY(GHZ)=',F5.1,' TM CASE')
      IF(NEM.NE.0)  WRITE(6,667)FREQ
 667  FORMAT(1H 'FREQUENCY(GHZ)=',F5.1,' TE CASE')
      WRITE(6,335) DEL1,DEL2,CL1,CL2,D1,D2
 335  FORMAT(1H 'DEL1=',F6.4,' DEL2=',F6.4,' CL1=',F7.5,' CL2=',
     1F7.5,' D1=',F6.3,' D2=',F6.3)
      WRITE(6,336) E1,E2,E3
 336  FORMAT(1H 'E1=',2F7.4,' E2=',2F7.4,' E3=',2F8.4)
      WRITE(6,337) T1,T2,T3,TH1,TH2,TH3,GAM1,GAM2,GAM3
 337  FORMAT(1H 'T1=',F5.1,' T2=',F5.1,' T3=',F5.1,'TH1=',F5.1
     1,' TH2=',F5.1,' TH3=',F5.1,' GAM1=',F4.1,' GAM2=',F4.1,
     1' GAM3=',F4.1)
      DO 115 I=1,NPT
C  CORRESPONDING TO EACH I THE ANGLE 5*I DEGREES IS
C  THE ANGLE OF INCIDENCE.
      TETA=FLOAT(I)*5.0
      EX1=20.9*FREQ*CSQRT(E1)
      EX2=20.9*FREQ*CSQRT(E2)
      EX3=20.9*FREQ*CSQRT(E3)
C  EX1,EX2,EX3 ARE THE PROPAGATION CONSTANTS IN EACH
C  REGION. E1M,E2M,E3M ARE THE REAL PARTS.
      E1M=REAL(E1)
      E2M=REAL(E2)
      E3M=REAL(E3)
      ARG=(3.14*TETA)/180.0
C  IN THE FOLLOWING WE CALCULATE COS(TETA) IN EACH
C  REGION,QS1,QS2,QS3,BY SNELL'S LAW.
      S1=(1.-(SIN(ARG)**2)/E1M)
      S2=(1.-(SIN(ARG)**2)/E2M)
      S3=(1.-(SIN(ARG)**2)/E3M)
      QS1=SQRT(S1)
      QS2=SQRT(S2)
      QS3=SQRT(S3)
      CS1=(2.*S1)-1.
      CS2=(2.*S2)-1.
C  THE ABSORPTION COEFFICIENTS IN THIS PAPER ARE DEFINED
C  AS     KA1=2*(IMAGINARY PART OF K1)/COS(TETA1)
C            =E1''*K1'/(E1'*COS(TETA1))
C          HERE E1' IS THE REAL PART AND E1'' THE IMAGINARY
C          PART OF E1.  COS(TETA1) IS QS1.
      KA1P=2.*AIMAG(EX1)/QS1
      KA2P=2.*AIMAG(EX2)/QS2
      KA3P=2.*AIMAG(EX3)/QS3
C THE KA'S GIVE THE VALUE OF THE ABSORPTION COEFFICIENT IN EACH LAYER.
      KA1=KA1P
      KA2=KA2P
      KA3=KA3P
```

```
      KM1=REAL(EX1)
      KM2=REAL(EX2)
C  DEFINE RR0,RR1,RR2,RR3, TO FIND REFLECTIVITIES BETWEEN
C  TWO MEDIA: RF01,RF12,RF23.
      G0=(1.-SIN(ARG)**2)
      RR0=SQRT(G0)
      G1=(E1-SIN(ARG)**2)
      RR1=CSQRT(G1)
      G2=(E2-SIN(ARG)**2)
      RR2=CSQRT(G2)
      G3=(E3-SIN(ARG)**2)
      RR3=CSQRT(G3)
      IF (NEM.EQ.0) GO TO 111
C THIS SECTION CONSIDERS TE WAVES AND DEFINES THE SCATTERING PARAMETERS
C FOR THIS CASE.KSE IS THE SCATTERING EXTINCTION COEFFICIENT,PFE
C AND PBE DEFINE THE FORWARD AND BACKWARD SCATTERING PHASE FUNCTIONS.
C RF DEFINES THE REFLECTIVITIES AT THE DIFFERENT BOUNDARIES.
      PFE1=(1.+4.*((KM1*CL1)**2)*S1)/(1.+2.*((KM1*CL1)**2)*S1)
      PBE1=1./(1.+2.*((KM1*CL1)**2)*S1)
      KSE1=((KM1**2)*DEL1*CL1/QS1)/PFE1
      PFE2=(1.+4.*((KM2*CL2)**2)*S2)/(1.+2.*((KM2*CL2)**2)*S2)
      PBE2=1./(1.+2.*((KM2*CL2)**2)*S2)
      KSE2=((KM2**2)*DEL2*CL2/QS2)/PFE2
      KSE1P=KSE1/QS1
      KSE2P=KSE2/QS2
      R01TE=(RR0-RR1)/(RR0+RR1)
      R12TE=(RR1-RR2)/(RR1+RR2)
      R23TE=(RR2-RR3)/(RR2+RR3)
      RF01=CABS(R01TE)**2
      RF12=CABS(R12TE)**2
      RF23=CABS(R23TE)**2
      PF1=PFE1
      PB1=PBE1
      PF2=PFE2
      PB2=PBE2
      KE1P=KA1P+KSE1P
      KE2P=KA2P+KSE2P
      KE1=KE1P
      KE2=KE2P
      KS1=KSE1P
      KS2=KSE2P
      GO TO 222
C THIS SECTION CONSIDERS TM WAVES AND DEFINES THE SCATTERING PARAMETERS
C THE NOTATION UTILIZED IS SIMILAR TO THE TE CASE.
  111 PFM1=2.*(1.+4.*((KM1*CL1)**2)*S1)/(1.+4.*((KM1*CL1)**2)*S1+
     1(CS1**2))
      PBM1=2.*(CS1**2)/(1.+4.*((KM1*CL1)**2)*S1+(CS1**2))
      KSM1=(KM1**2)*DEL1*CL1/(QS1*PFM1)
      PFM2=2.*(1.+4.*((KM2*CL2)**2)*S2)/(1.+4.*((KM2*CL2)**2)*S2+
     1(CS2**2))
      PBM2=2.*(CS2**2)/(1.+4.*((KM2*CL2)**2)*S2+(CS2**2))
      KSM2=(KM2**2)*DEL2*CL2/(QS2*PFM2)
      KSM1P=KSM1/QS1
      KSM2P=KSM2/QS2
      R01TM=((E1*RR0)-RR1)/((E1*RR0)+RR1)
```

```
      R12TM=((E2*RR1)-(E1*RR2))/((E2*RR1)+(E1*RR2))
      R23TM=((E3*RR2)-(E2*RR3))/((E3*RR2)+(E2*RR3))
      RF01=CABS(R01TM)**2
      RF12=CABS(R12TM)**2
      RF23=CABS(R23TM)**2
      PF1=PFM1
      PF2=PFM2
      PB1=PBM1
      PB2=PBM2
      KE1PP=KA1P+KSM1P
      KE2PP=KA2P+KSM2P
      KE1=KE1PP
      KE2=KE2PP
      KS1=KSM1P
      KS2=KSM2P
C THE W'S REFER TO THE SCATTERING ALBEDO.
 222  W1=KS1/KE1
      W2=KS2/KE2
C THE FOLLOWING SECTION COMPUTES THE BRIGHTNESS TEMPERATURE ACCORDING
C TO EQUATION 12(PAGE 36) IN THE THESIS.
C  IN THE FOLLOWING ALL THE PAGE NO.S REFER TO THE THESIS.
  88  T11=SQRT(1.-PF1*(W1/2.)+PB1*(W1/2.))
      T22=SQRT(1.0-PF2*(W2/2.0)+PB2*(W2/2.0))
      A1=KE1*T11*SQRT(1.0-W1)
      A2=KE2*T22*SQRT(1.0-W2)
      GF1=0.5*KS1*PF1
      GB1=0.5*KS1*PB1
      N1=(A1-KA1)/(A1+KA1)
C     THE PARAMETERS A1,A2 ARE DERIVED IN THE APPENDIX A
C     OF THE THESIS IN TERMS OF ALPHA'S.
C      N1 APPEARS IN PAGE 33 OF THE THESIS.
      IF (GB.LT.(.1*GF1).OR.W1.LE.0.3) N1=GB1/(A1+KE1-GF1)
      GF2=0.5*KS2*PF2
      GB2=0.5*KS2*PB2
      N2=(A2-KA2)/(A2+KA2)
C      N2 IS DEFINED IN PAGE 33.
C     MOST OF THE TERMS FOLLOWING ARE DEFINED IN P.28-36.
      IF (GB2.LT.(.1*GF2).OR.W2.LE.0.3)  N2=GB2/(A2+KE2-GF2)
  99  AA1=E1M
      AA2=E2M
      AA3=E3M
C     XI1,XI2 ARE DEFINED IN P.33.
      XI1=((A1**2)+GAM1*KA1)/((A1**2)-GAM1*KA1)
      XI2=((A2**2)+GAM2*KA2)/((A2**2)-GAM2*KA2)
C     HERE C1,C2,E ARE DEFINED IN P.36.
C     IN THE FOLLOWING WE FIND C1,D11(D1 IN THESIS),B,A,
C     FOR IU IN EQ.11.
  66  C1=AA1*T1
      C2=AA2*T2
      E=AA3*T3
      DD11=((A1**2)-GAM1*KA1)*AA1*TH1
      DD12=(A1**2)-(GAM1**2)
      D11=DD11/DD12
      D22=0.0
      IF(IH.EQ.0) GO TO 55
```

```
      DD21=((A2**2)-GAM2*KA2)*AA2*TH2
      DD22=(A2**2)-(GAM2**2)
      D22=DD21/DD22
C  THE TRANSMITIVITIES BETWEEN TWO MEDIA ARE T12,T23,T01.
   55 T12=1.-RF12
      T01=1.-RF01
      TS10=T01*E1M
      EP1=((RF01-1.0)*C1+(RF01-XI1)*D11+(TS10*TSKY))/(1.0-RF01*N1)
      EP2=((-1.0)*(N1-RF01))/(1.0-RF01*N1)
      G=(KA3*TH3*AA3)/(GAM3+KA3)
   44 T23=1.-RF23
      TS12=(T12*E1M)/(E2M)
      TS23=(T23*E2M)/(E3M)
      TS21=(T12*E2M)/(E1M)
      A11=N2-RF23
      A22=1.0-N2*RF23
      A33=1.0-N2*RF12
      A44=N2-RF12
      AR1=GAM2*D2
      Y1=0.0
      IF (AR1.LT.40.0) Y1=EXP(-AR1)
      AR2=GAM3*D2
      Y2=0.0
      IF (AR2.LT.40.0) Y2=EXP(-AR2)
      I1=(RF23-1.0)*C2+((XI2*RF23)-1.0)*D22*Y1+TS23*(E+G*Y2)
C     I1 APPEARS IN P.36.
      HX3=RF12-N1
      HX1=RF12-1.0
      HX2=RF12*XI1-1.0
      AR3=GAM2*D1
      AR4=GAM1*D1
      Y3=0.0
      Y4=0.0
      IF (AR3.LT.40.0) Y3=EXP(-AR3)
      IF (AR4.LT.40.0)  Y4=EXP(-AR4)
      M=HX1*C2+(RF12-XI2)*D22*Y3+(C1+XI1*D11*Y4)*TS21
C     M APPEARS IN P.36.
      HH1=(HX1*C1)+(HX2*D11*Y4)+TS12*(C2+D22*Y3)
      HH2=HX3*A33+(T12**2)*N2
      HH3=HX3*A44+(T12**2)
      NUM1=((HH1*A22*A33)+(TS12*N2*A22*M))
      AR5=2.*A2*(D2-D1)
      AR6=A1*D1
      Y5=0.0
      Y6=0.0
      IF (AR5.LT.40.0) Y5=EXP(-AR5)
      IF (AR6.LT.40.0) Y6=EXP(-AR6)
      AR8=A2*(D2-D1)
      Y8=0.0
      IF (AR8.LT.40.0) Y8=EXP(-AR8)
      NUM2=(HH1*A11*A44+TS12*A11*M)*Y5
      NUM3=TS12*I1*(A33-N2*A44)*Y6*Y8
      NUM4=(HH2*EP1*A22)
      NUM5=(HH3*EP1*A11)*Y5
      AR7=2.0*A1*D1
```

```
      Y7=0.0
      IF (AR7.LT.40.0) Y7=EXP(-AR7)
      NUM=(NUM1-NUM2)*Y6+NUM3+(NUM4-NUM5)*Y7
      DN1=((A33*A22)-(A11*A44*Y5))
      DN2=(((-1.0)*N2*A22)+(A11*Y5))
      DEN=(1.0-RF12*N1)*DN1+N1*(T12**2)*DN2
      DENO=DEN+((N1-RF12)*EP2*DN1+(T12**2)*EP2*DN2)*Y7
      B=NUM/DENO
      A=EP1+EP2*B
      IU=(N1*A)+B+C1+D11
C     IU IS THE UPWARD INTENSITY AT Z=0. (SEE P.35 EQ.11).
      TB=(((1.0-RF01)*IU)/E1M)+(RF01*TSKY)
      AA(I,2)=TB
C  AA(I,2) IS THE BRITENESS TEMPERATURE CORRESPONDING TO
C   THE INCIDENT ANGLE 5*I DEGREES.
C  AA(I,1) IS THE INCIDENT ANGLE 5*I DEGREES.
      AA(I,1)=TETA
  115 CONTINUE
      NLINES=80
  100 CONTINUE
      DO 103 JI=1,NVARS
      WRITE(6,*)  W2
      WRITE(6,*)  (AA(IL,JI),IL=1,NPT)
  103 CONTINUE
      GO TO 10
    1 CONTINUE
      CALL EXIT
      STOP
      END
```

```
C
C          PROGRAM LAMINAR NO.2
C
C   B.DJERMAKOYE(1978)
C   S.L.CHUANG(7,1979)
C   LAMINAR,THREE-LAYER MODEL
C   RADIATIVE TRANSFER THEORY
C   BRITENESS TEMPERATURE VERSUS FREQUENCY.
C   THIS PROGRAM FOLLOWS THE PAPER 'RADIATIVE TRANSFER THEORY
C   FOR THE REMOTE SENSING OF LAYERED MEDIA' BY
C   B. DJERMAKOYE AND J. A. KONG.
C   AND THE THESIS OF B. DJERMAKOYE 92(SM EEE DEGREES),MIT,1978.
      REAL  KA1P,KA2P,KA3P,KSE1,KSE2,KSE1P,KSE2P,KE1P,KE2P
      COMPLEX  R01TE,R12TE,R23TE,R01TM,R12TM,R23TM
      COMPLEX RR1,RR2,RR3
      REAL  G,KSM1,KSM2,KSM1P,KSM2P,KE1PP,KE2PP
      REAL KA1,KA2,KA3,KM1,KM2,KS1,KS2
      REAL KE1,KE2,N1,N2,I1,M,NUM1,NUM2,NUM3
      REAL NUM4,NUM5,NUM,IU,AA(500,6)
      COMPLEX  R23,G1,G2,G3
      COMPLEX R01,E1,E2,E3,R12,EX1,EX2,EX3
      COMPLEX  IX,JX
      NVARS=2
      NPT=30
      NORDER=0
      NPLOT=0
      IDIM=500
      JDIM=6
      IX=(1.0,0.0)
      JX=(0.0,1.0)
  77  FORMAT(2F7.4,2F7.4,2F5.1)
 10   CONTINUE
C   E1,E2,AND E3 ARE THE COMPLEX DIELECTRIC CONSTANTS
C   IN EACH REGION.
      READ(5,77,END=1) E1,E2,E3
  79  FORMAT(2F6.3,2F8.5)
C   DEL1 AND DEL2 ARE THE VARIANCES,CL1 AND CL2 ARE THE
C   CORRELATION LENGTHS IN VERTICAL DIRECTION.
      READ(5,*,END=1) DEL1,DEL2,CL1,CL2
C   D1 AND D2 ARE THE DEPTHS OF THE FIRST AND SECOND LAYER,
C   MEASURED FROM THE TOP SURFACE. NOTE D2 IS NOT THE
C   THICKNESS OF THE SECOND LAYER UNLESS D1=0.
C   IH=0 CASE OF TWO LAYERS.
C   IH=1(NOT 0) CASE OF THREE LAYERS.
C   FREQ IS THE FREQUENCY.
C   NEM=0 VERTICAL POLARIZATION(TM) CASE.
C   NEM=1(NOT 0) HORIZONTAL POLARIZATION(TE) CASE.
C   TSKY IS THE SKY TEMPERATURE WHICH IS LESS THAN 7 DEGREES
C   GENERALLY.
      READ(5,*,END=1) D1,D2,IH,ITETA,NEM,TSKY
  78  FORMAT(2F6.3,I2,I3,I2,F6.1)
C   FOR INHOMOGENEOUS TEMPERATURE PROFILES:
C   T1(Z)=T1+TH1*EXP(GAM1*Z),SIMILARLY FOR T2(Z) AND T3(Z),
C   WE ASSIGN APPROPRIATE VALUES FOR T1,TH1,GAM1,ETC.
C   FOR HOMOGENEOUS CASE:
```

```
C   TH1=TH2=TH3=0.   GAM1=GAM2=GAM3=0.
      READ(5,*) T1,T2,T3,TH1,TH2,TH3,GAM1,GAM2,GAM3
  331 FORMAT(3F6.1,3F4.1,3F4.1)
      IF(IH.EQ.0)  WRITE(6,333)  IH
  333 FORMAT(1H 'IH=',I2,' CASE OF TWO LAYER')
      IF(IH.NE.0)  WRITE(6,334)  IH
  334 FORMAT(1H 'IH=',I2,' CASE OF THREE LAYER')
      IF(ITETA.EQ.0) WRITE(6,89) ITETA
   89 FORMAT(1H 'ITETA=',I2,' NADIR OBSERVATION')
      IF(NEM.EQ.0)  WRITE(6,666) ITETA
  666 FORMAT(1H 'ITETA=',I2,' TM CASE')
      IF(NEM.NE.0)  WRITE(6,667) ITETA
  667 FORMAT(1H 'ITETA=',I2,' TE CASE')
      WRITE(6,335) DEL1,DEL2,CL1,CL2,D1,D2
  335 FORMAT(1H 'DEL1=',F6.4,' DEL2=',F6.4,' CL1=',F7.5,' CL2=',
     1F7.5,' D1=',F6.3,' D2=',F6.3)
      WRITE(6,336) E1,E2,E3
  336 FORMAT(1H 'E1=',2F7.4,' E2=',2F7.4,' E3=',2F8.4)
      WRITE(6,337) T1,T2,T3,TH1,TH2,TH3,GAM1,GAM2,GAM3
  337 FORMAT(1H 'T1=',F5.1,' T2=',F5.1,' T3=',F5.1,'TH1=',F5.1
     1,' TH2=',F5.1,' TH3=',F5.1,' GAM1=',F4.1,' GAM2=',F4.1,
     1' GAM3=',F4.1)
      DO 115 I=1,NPT
      FREQ=FLOAT(I)*2.0
C   CORRESPONDING TO EACH I WE CALCULATE BRITENESS TEMPERATURE
C   FOR FREQUENCY 2*I GHZ.
      EX1=20.9*FREQ*CSQRT(E1)
      EX2=20.9*FREQ*CSQRT(E2)
      EX3=20.9*FREQ*CSQRT(E3)
C   EX1,EX2,EX3 ARE THE PROPAGATION CONSTANTS IN EACH REGION.
C   E1M,E2M,E3M ARE THEIR REAL PARTS.
      E1M=REAL(E1)
      E2M=REAL(E2)
      E3M=REAL(E3)
      ARG=(3.14*ITETA)/180.0
C   IN THE FOLLOWING WE CALCULATE COS(TETA) IN EACH REGION,
C   I. E. QS1,QS2,QS3,ACCORDING TO SNELL'S LAW.
      S1=(1.-(SIN(ARG)**2)/E1M)
      S2=(1.-(SIN(ARG)**2)/E2M)
      S3=(1.-(SIN(ARG)**2)/E3M)
      QS1=SQRT(S1)
      QS2=SQRT(S2)
      QS3=SQRT(S3)
      CS1=(2.*S1)-1.
      CS2=(2.*S2)-1.
C   THE ABSORPTION COEFFICIENTS IN THIS PAPER ARE DEFINED
C   AS    KA1=2*(IMAGINARY PART OF K1)/COS(TETA1)
C              =E1''*K1'/(E1'*COS(TETA1)
C         HERE E1' IS THE REAL PART AND E1'' THE IMAGINARY
C         PART OF E1.  COS(TETA1) IS QS1.
      KA1P=2.*AIMAG(EX1)/QS1
      KA2P=2.*AIMAG(EX2)/QS2
      KA3P=2.*AIMAG(EX3)/QS3
C THE KA'S GIVE THE VALUE OF THE ABSORPTION COEFFICIENT IN EACH LAYER.
      KA1=KA1P
```

```
      KA2=KA2P
      KA3=KA3P
      KM1=REAL(EX1)
      KM2=REAL(EX2)
C  DEFINE RR0,RR1,RR2,RR3 TO FIND THE REFLECTIVITIES BETWEEN
C  TWO MEDIA: RF01,RF12,RF23.
      G0=(1.-SIN(ARG)**2)
      RR0=SQRT(G0)
      G1=(E1-SIN(ARG)**2)
      RR1=CSQRT(G1)
      G2=(E2-SIN(ARG)**2)
      RR2=CSQRT(G2)
      G3=(E3-SIN(ARG)**2)
      RR3=CSQRT(G3)
      IF (NEM.EQ.0) GO TO 111
C THIS SECTION CONSIDERS TE WAVES AND DEFINES THE SCATTERING PARAMETERS
C FOR THIS CASE.KSE IS THE SCATTERING EXTINCTION COEFFICIENT,PFE
C AND PBE DEFINE THE FORWARD AND BACKWARD SCATTERING PHASE FUNCTIONS.
C RF DEFINES THE REFLECTIVITIES AT THE DIFFERENT BOUNDARIES.
      PFE1=(1.+4.*((KM1*CL1)**2)*S1)/(1.+2.*((KM1*CL1)**2)*S1)
      PBE1=1./(1.+2.*((KM1*CL1)**2)*S1)
      KSE1=((KM1**2)*DEL1*CL1/QS1)/PFE1
      PFE2=(1.+4.*((KM2*CL2)**2)*S2)/(1.+2.*((KM2*CL2)**2)*S2)
      PBE2=1./(1.+2.*((KM2*CL2)**2)*S2)
      KSE2=((KM2**2)*DEL2*CL2/QS2)/PFE2
      KSE1P=KSE1/QS1
      KSE2P=KSE2/QS2
      R01TE=(RR0-RR1)/(RR0+RR1)
      R12TE=(RR1-RR2)/(RR1+RR2)
      R23TE=(RR2-RR3)/(RR2+RR3)
      RF01=CABS(R01TE)**2
      RF12=CABS(R12TE)**2
      RF23=CABS(R23TE)**2
      PF1=PFE1
      PB1=PBE1
      PF2=PFE2
      PB2=PBE2
      KE1P=KA1P+KSE1P
      KE2P=KA2P+KSE2P
      KE1=KE1P
      KE2=KE2P
      KS1=KSE1P
      KS2=KSE2P
      GO TO 222
C THIS SECTION CONSIDERS TM WAVES AND DEFINES THE SCATTERING PARAMETERS
C THE NOTATION UTILIZED IS SIMILAR TO THE TE CASE.
  111 PFM1=2.*(1.+4.*((KM1*CL1)**2)*S1)/(1.+4.*((KM1*CL1)**2)*S1+
     1(CS1**2))
      PBM1=2.*(CS1**2)/(1.+4.*((KM1*CL1)**2)*S1+(CS1**2))
      KSM1=(KM1**2)*DEL1*CL1/(QS1*PFM1)
      PFM2=2.*(1.+4.*((KM2*CL2)**2)*S2)/(1.+4.*((KM2*CL2)**2)*S2+
     1(CS2**2))
      PBM2=2.*(CS2**2)/(1.+4.*((KM2*CL2)**2)*S2+(CS2**2))
      KSM2=(KM2**2)*DEL2*CL2/(QS2*PFM2)
      KSM1P=KSM1/QS1
```

```
      KSM2P=KSM2/QS2
      R01TM=((E1*RR0)-RR1)/((E1*RR0)+RR1)
      R12TM=((E2*RR1)-(E1*RR2))/((E2*RR1)+(E1*RR2))
      R23TM=((E3*RR2)-(E2*RR3))/((E3*RR2)+(E2*RR3))
      RF01=CABS(R01TM)**2
      RF12=CABS(R12TM)**2
      RF23=CABS(R23TM)**2
      PF1=PFM1
      PF2=PFM2
      PB1=PBM1
      PB2=PBM2
      KE1PP=KA1P+KSM1P
      KE2PP=KA2P+KSM2P
      KE1=KE1PP
      KE2=KE2PP
      KS1=KSM1P
      KS2=KSM2P
C THE W'S REFER TO THE SCATTERING ALBEDO.
 222  W1=KS1/KE1
      W2=KS2/KE2
C THE FOLLOWING SECTION COMPUTES THE BRIGHTNESS TEMPERATURE ACCORDING
C TO EQUATION 12(PAGE 36) IN THE THESIS.
C  IN THE FOLLOWING THE PAGE NO. REFER TO THE THESIS.
  88  T11=SQRT(1.-PF1*(W1/2.)+PB1*(W1/2.))
      T22=SQRT(1.0-PF2*(W2/2.0)+PB2*(W2/2.0))
      A1=KE1*T11*SQRT(1.0-W1)
      A2=KE2*T22*SQRT(1.0-W2)
      GF1=0.5*KS1*PF1
      GB1=0.5*KS1*PB1
      N1=(A1-KA1)/(A1+KA1)
C  THE PARAMETERS A1,A2 ARE DERIVED IN THE APPENDIX A
C  OF THE THESIS IN TERMS OF ALPHA'S.
C  N1 IS IN PAGE 33.
      IF (GB.LT.(.1*GF1).OR.W1.LE.0.3) N1=GB1/(A1+KE1-GF1)
      GF2=0.5*KS2*PF2
      GB2=0.5*KS2*PB2
      N2=(A2-KA2)/(A2+KA2)
C  N2 IS DEFINED IN PAGE 33 AS ETA(GREEK).
C  MOST OF THE TERMS FOLLOWING ARE DEFINED IN PP.28-36.
      IF (GB2.LT.(.1*GF2).OR.W2.LE.0.3)  N2=GB2/(A2+KE2-GF2)
  99  AA1=E1M
      AA2=E2M
      AA3=E3M
C  XI1,XI2 ARE IN PAGE 33.
      XI1=((A1**2)+GAM1*KA1)/((A1**2)-GAM1*KA1)
      XI2=((A2**2)+GAM2*KA2)/((A2**2)-GAM2*KA2)
C  HERE C1,C2,E ARE DEFINED IN P.36.
C  IN THE FOLLOWING WE FIND C1,D11(D1 IN THESIS),B,A,
C  TO CALCULATE IU IN EQUATION 11.
  66  C1=AA1*T1
      C2=AA2*T2
      E=AA3*T3
      DD11=((A1**2)-GAM1*KA1)*AA1*TH1
      DD12=(A1**2)-(GAM1**2)
      D11=DD11/DD12
```

```
      D22=0.0
      IF(IH.EQ.0) GO TO 55
      DD21=((A2**2)-GAM2*KA2)*AA2*TH2
      DD22=(A2**2)-(GAM2**2)
      D22=DD21/DD22
C  THE TRANSMITIVITIES BETWEEN ARE T12,T23,T01.
 55   T12=1.-RF12
      T01=1.-RF01
      TS10=T01*E1M
      EP1=((RF01-1.0)*C1+(RF01-XI1)*D11+(TS10*TSKY))/(1.0-RF01*N1)
      EP2=((-1.0)*(N1-RF01))/(1.0-RF01*N1)
      G=(KA3*TH3*AA3)/(GAM3+KA3)
 44   T23=1.-RF23
      TS12=(T12*E1M)/(E2M)
      TS23=(T23*E2M)/(E3M)
      TS21=(T12*E2M)/(E1M)
      A11=N2-RF23
      A22=1.0-N2*RF23
      A33=1.0-N2*RF12
      A44=N2-RF12
      AR1=GAM2*D2
      Y1=0.0
      IF (AR1.LT.40.0) Y1=EXP(-AR1)
      AR2=GAM3*D2
      Y2=0.0
      IF (AR2.LT.40.0) Y2=EXP(-AR2)
      I1=(RF23-1.0)*C2+((XI2*RF23)-1.0)*D22*Y1+TS23*(B+G*Y2)
C  I1 IS DEFINED IN P.36.
      HX3=RF12-N1
      HX1=RF12-1.0
      HX2=RF12*XI1-1.0
      AR3=GAM2*D1
      AR4=GAM1*D1
      Y3=0.0
      Y4=0.0
      IF (AR3.LT.40.0) Y3=EXP(-AR3)
      IF (AR4.LT.40.0)  Y4=EXP(-AR4)
      M=HX1*C2+(RF12-XI2)*D22*Y3+(C1+XI1*D11*Y4)*TS21
C  M APPEARS IN P.36.
      HH1=(HX1*C1)+(HX2*D11*Y4)+TS12*(C2+D22*Y3)
      HH2=HX3*A33+(T12**2)*N2
      HH3=HX3*A44+(T12**2)
      NUM1=((HH1*A22*A33)+(TS12*N2*A22*M))
      AR5=2.*A2*(D2-D1)
      AR6=A1*D1
      Y5=0.0
      Y6=0.0
      IF (AR5.LT.40.0) Y5=EXP(-AR5)
      IF (AR6.LT.40.0) Y6=EXP(-AR6)
      AR8=A2*(D2-D1)
      Y8=0.0
      IF (AR8.LT.40.0) Y8=EXP(-AR8)
      NUM2=(HH1*A11*A44+TS12*A11*M)*Y5
      NUM3=TS12*I1*(A33-N2*A44)*Y6*Y8
      NUM4=(HH2*EP1*A22)
```

```
      NUM5=(HH3*EP1*A11)*Y5
      AR7=2.0*A1*D1
      Y7=0.0
      IF (AR7.LT.40.0) Y7=EXP(-AR7)
      NUM=(NUM1-NUM2)*Y6+NUM3+(NUM4-NUM5)*Y7
      DN1=((A33*A22)-(A11*A44*Y5))
      DN2=(((-1.0)*N2*A22)+(A11*Y5))
      DEN=(1.0-RF12*N1)*DN1+N1*(T12**2)*DN2
      DENO=DEN+((N1-RF12)*EP2*DN1+(T12**2)*EP2*DN2)*Y7
      B=NUM/DENO
      A=EP1+EP2*B
      IU=(N1*A)+B+C1+D11
C  IU IS THE UPWARD INTENSITY AT Z=0.(SEE P.35,EQ.11).
      TB=(((1.0-RF01)*IU)/E1M)+(RF01*TSKY)
      AA(I,2)=TB
C  AA(I,2) IS THE BRITENESS TEMPERATURE CORRESPONDING TO
C  THE INCIDENT ANGLE 5*I DEGREES.
C  AA(I,1) IS JUST THIS ANGLE 5*I DEGREES.
      AA(I,1)=FREQ
  115 CONTINUE
      NLINES=80
  100 CONTINUE
      DO 103 JI=1,NVARS
      WRITE(6,*)   W2
      WRITE(6,*)   (AA(IL,JI),IL=1,NPT)
  103 CONTINUE
      GO TO 10
    1 CONTINUE
      CALL EXIT
      STOP
      END
```

PROGRAM INVARIANT IMBEDDING

Introduction

In this program we solve the thermal microwave emission from a slab random medium with nonuniform scattering, absorption, and temperature profiles using radiative transfer theory (Figure 2). With the method of invariant imbedding, the boundary value problem of RT equations is converted to an initial value problem starting at zero thickness. The invariant imbedding technique incorporates the boundary conditions of radiative transfer equations in the new equations. They are in the form of first-order ordinary differential equations and are solved by the Runge-Kutta method in this program. The case of a laminar structure with TE polarization is considered.

Reference: "Thermal microwave emission from a random inhomogeneous layer over a homogeneous medium using the method of invariant imbedding," by L. Tsang and J.A. Kong, Radio Science, Vol. 12, No. 2, pp. 185-194, March-April 1977.

Notes: The frequency and incident angle can be changed in the program. The program we show here is for fixed angle and fixed frequency. To find T_B for different frequencies (or different angles) we just modify the DO loop (896 and 100) by changing FREQ (or DEG).

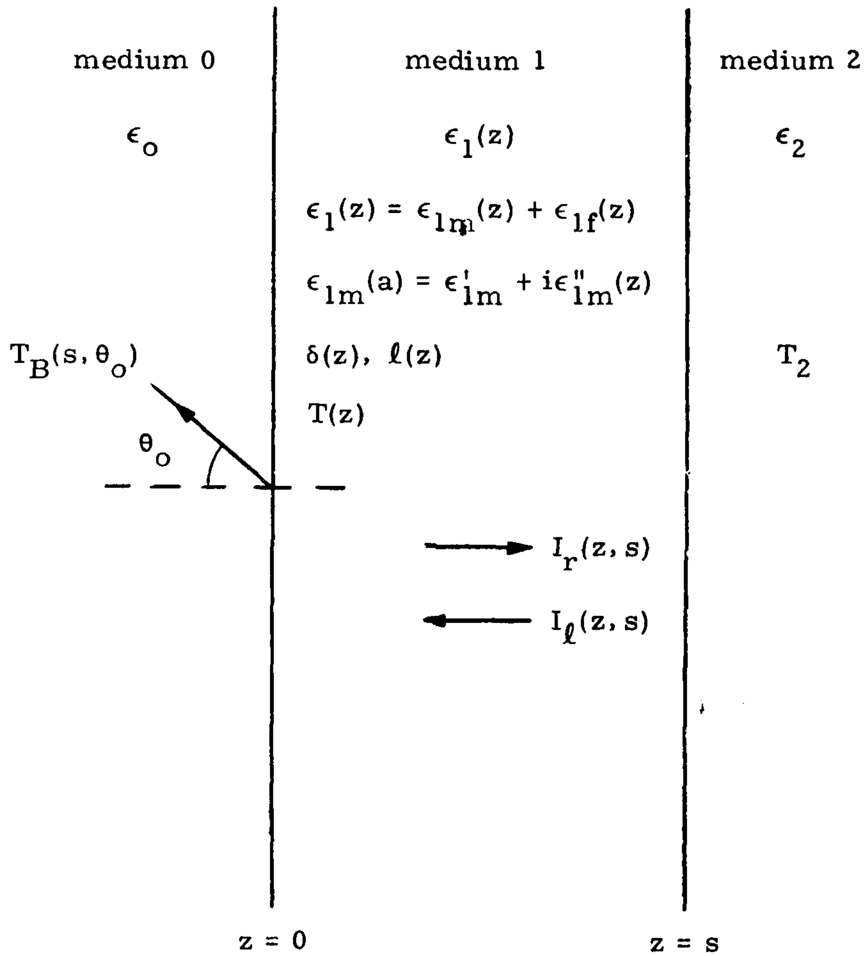

Figure 2. Geometrical Configuration of the Problem for Program INVARIANT IMBEDDING

Equations

Consider Fig. 2 with the correlation function for $\epsilon_{1f}(z)$ of the form

$$\langle \epsilon_{1f}(z_1)\, \epsilon_{1f}(z_2) \rangle = \delta(z)\, \epsilon_{2m}'\, \exp\left[- \frac{|z_1 - z_2|}{\ell(z)}\right], \tag{1}$$

where $z = (z_1 + z_2)/2$. The inhomogeneous scattering, absorption and temperature profiles are characterized by $\delta(z)$ and $\ell(z)$, $\kappa_{ao}(z) = (\epsilon_1''(z)/\epsilon_1')\, k_1'$, and $T(z)$.

In the program, we consider these cases:

$$\delta(z) = \delta_o + \delta_d\, e^{-\delta_r z} \tag{2}$$

$$\ell(z) = \ell_o + \ell_d\, e^{-\ell_r z} \tag{3}$$

$$\ell_t(z) \cong (\epsilon_1''(z)/\epsilon_1') = \ell_{to} + \ell_{td}\, e^{-\ell_{tr} z} \tag{4}$$

$$T(z) = T_o + T_d\, e^{-T_r z}, \tag{5}$$

where δ_o, δ_d, δ_r, ℓ_o, ℓ_d, ℓ_r, ℓ_{to}, ℓ_{td}, ℓ_{tr}, T_o, T_d, and T_r are all constants. The four invariant imbedding equations obtained in the paper are

$$\frac{dR(s)}{ds} = b(s) + 2p(s)\, R(s) + q(s)\, R^2(s) \tag{6}$$

$$\frac{dt(s)}{ds} = \{p(s) + q(s)\, R(s)\}\, t(s) \tag{7}$$

$$\frac{dT_R(s)}{ds} = [p(s) + R(s)q]\, T_R(s) + [pR(s) + b(s)]\, t_{12} T_2$$
$$+ \kappa_a T(s)[1 + R(s)(1 + r_{12})] \tag{8}$$

$$\frac{dT_B(s)}{ds} = t_{01}t(s)[T_R(s)\ q(s) + p(s)\ t_{12}T_2 + \kappa_a(s)\ T(s)(1+r_{12})] \tag{9}$$

with the initial conditions

$$R(s=0) = \frac{r_{01}}{1 - r_{01}r_{12}} \tag{10}$$

$$t(s=0) = \frac{1}{1 - r_{01}t_{12}} \tag{11}$$

$$T_R(s=0) = \frac{r_{01}r_{12}}{1 - r_{01}r_{12}}\ T_2 \tag{12}$$

$$T_B(s=0) = \frac{t_{01}t_{12}}{1 - r_{01}r_{12}}\ T_2, \tag{13}$$

where

$$p(s) = -\kappa_e(s) + f(s) + b(s)\ r_{12} \tag{14}$$

$$q(s) = (1+r_{12}^2)\ b(s) - 2r_{12}[\kappa_e(s) - f(s)]. \tag{15}$$

The total extinction coefficient profile $\kappa_e(z)$ is

$$\kappa_e(z) = \kappa_a(z) + \kappa_s(z) \tag{16}$$

where

$$\kappa_a(z) = \kappa_{ao}(z)/\cos\theta \tag{17}$$

$$\kappa_s(z) = \kappa_{so}(z)/\cos\theta \tag{18}$$

and $f(z), b(z)$ are defined as

$$f(z) = \kappa_s(z)\frac{P_f(z)}{2} \tag{19}$$

$$b(z) = \kappa_s(z)\, \frac{P_b(z)}{2} \, . \tag{20}$$

For TE polarization considered in the program, we have

$$r_{01} = \left| \frac{\sqrt{k_o^2 - k_m'^2 \sin^2\theta} - k_m' \cos\theta}{\sqrt{k_o^2 - k_m'^2 \sin^2\theta} + k_m' \cos\theta} \right|^2 \tag{21}$$

$$r_{12} = \left| \frac{k_m' \cos\theta - \sqrt{k_2^2 - k_m'^2 \sin^2\theta}}{k_m' \cos\theta + \sqrt{k_2^2 - k_m'^2 \sin^2\theta}} \right|^2 \tag{22}$$

$$\kappa_{so}(z) = \frac{k_m'^2 \delta(z)\, \ell(z)}{\cos\theta} \left(\frac{1 + 2k_m'^2 \ell^2(z) \cos^2\theta}{1 + 4k_m'^2 \ell^2(z) \cos^2\theta} \right) \tag{23}$$

$$P_f(z) = \frac{1 + 4k_m'^2 \ell^2(z) \cos^2\theta}{1 + 2k_m'^2 \ell^2(z) \cos^2\theta} \tag{24}$$

$$P_b(z) = \frac{1}{1 + 2k_m'^2 \ell^2(z) \cos^2\theta} \, , \tag{25}$$

where θ should be the angle in medium 1. The viewing angle θ_o for the brightness temperature $T_B(s)$ as observed by a radiometer in region 0 is related to θ by Snell's law:

$$\sin\theta_o = \frac{\epsilon_1'}{\epsilon_o} \sin\theta. \tag{26}$$

We have the set of the initial value problem, Eqs. (6)-(9), (10)-(13), which is easier to solve (than the original boundary value problem) with the numerical method.

We use the IMSL ROUTINE – DVERK to solve the differential equations (6)-(9) by the Runge-Kutta method.

Symbols

Fortran Symbols	Notation	Explanations
DL	ϵ_1'	Real part of permittivity in medium 1
DL2	ϵ_2'	Real part of permittivity in medium 2
LT2	ϵ_2''/ϵ_2'	Loss tangent, medium 2
TEMPO	T_o	
TEMPD	T_d	$T(z) = T_o + T_d e^{-T_r z}$
TEMPR	T_r	
TEMP	$T(z)$	
DELO	δ_o	
DELD	δ_d	$\delta(z) = \delta_o + \delta_d e^{-\delta_r z}$
DELR	δ_r	
DEL	$\delta(z)$	
CLO	ℓ_o	
CLD	ℓ_d	$\ell(z) = \ell_o + \ell_d e^{-\ell_r z}$
CLR	ℓ_r	
CL	$\ell(z)$	
LTO	ℓ_{to}	
LTD	ℓ_{td}	$\ell_t(z) = \ell_{to} + \ell_{td} e^{-\ell_{tr} z}$
LTR	ℓ_{tr}	
LT	$\ell_t(z)$	
DEG	θ_o	Medium 0 (in degrees)
TAI	θ_o	Medium 0 (in radians)
CTI	$\cos \theta_o$	

Fortran Symbols	Notation	Explanations
TAT	θ	Medium 1 (in radians)
FREQ	frequency	Frequency
WAVE	ω	
KO	k	Wave number in medium 0
KIMR	k_1'	Real part of k_1
NT	k_1'/k	
K2	k_2	Complex
T01	t_{01}	Transmissivities
T12	t_{12}	"
R01	r_{01}	Reflectivities
R12	r_{12}	"
T12P	$1 + r_{12}$	
T12P2	$1 + r_{12}^2$	
RD	$1 - r_{01}r_{12}$	
R, Y(1)	R(s)	Reflectivity function
T, Y(2)	t(s)	Transmissivity function
TRN, Y(3)	$T_R(s)/T_2$	"Reflected" temperature, normalized
TBN, Y(4)	$T_B(s)/T_2$	"Brightness" temperature, normalized
KA	$\kappa_{ao}(s)$	
KS	$\kappa_{so}(s)$	
KAP	$\kappa_s(s) = \kappa_{ao}(s)/\cos\theta$	Eq. (17)
KSP	$\kappa_s(s) = \kappa_{so}(s)/\cos\theta$	Eq. (18)

Fortran Symbols	Notation	Explanations
F1	$P(s)$	As defined in Eq. (14)
F12	$2P(s)$	Eq. (14)
F2	$q(s)$	Eq. (15)
G(1)	$dR(s)/ds$	Derivative of $R(s)$
G(2)	$dt(s)/ds$	Derivative of $t(s)$
G(3)	$\frac{1}{T_2}\frac{dT_R(s)}{ds}$	Derivative of $T_R(s)/T_2$
G(4)	$\frac{1}{T_2}\frac{dT_B(s)}{ds}$	Derivative of $T_B(s)/T_2$

Features

(a) SUBROUTINE RHS(N, Z, Y, G)

This subroutine is to calculate the right-hand sides of Eqs. (6)-(9) (with Eqs. (8) and (9) normalized by T_2, i.e., $(dT_R(z)/dz)/T_2$, $(dT_B(z)/ds)/T_2$), and evaluate at each z, the vectors $\overline{Y}(z)$ and $\overline{G}(z)$.

$$\overline{Y}(z) = \begin{pmatrix} R(z) \\ t(z) \\ T_R(a)/T_2 \\ T_B(z)/T_2 \end{pmatrix}, \qquad G(z) = \frac{d\overline{Y}(z)}{dz} .$$

N is the number of equations. N = 4 in this program.

(b) Call DVERK(N, RHS, Z, Y, XEND, TOL, IND, C, N, W, IER)

DVERK is the IMSL ROUTINE to solve the differential equation with the RUNGE-KUTTA-VERNER fifth- and sixth-order method.

N – number of equations (=4)

Z – independent variable

(1) On input, Z supplies the initial value.

(2) On output, Z is replaced with XEND.

Y –

(1) On input, Y(1) . . . Y(N) supply initial values.

(2) On output, Y(1) . . . Y(N) are replaced with an approximate solution at XEND (unless error condition arises).

XEND – value of Z at which solution is desired.

TOL – tolerance for error control (input).

IND – indicator (see the manual of IMSL Library, IMSL LIB-0007).

C – communications vector of length 24.

N – row dimension of the matrix W exactly as specified in the dimension statement in the calling program.

W – workspace matrix. The first dimension of W must be (the above) N, the second must be greater or equal to 9.

IER – ERROR parameter.

(c) To run the program, use:

```
GLOBAL TXTLIB FORTMDD2 IMSL SP CMSLIB

LOAD IMBED

FILEDEF 5 DISK IMBED DATA

START
```

Input and Output Format

(1) Input: $\boxed{\text{free format}}$

The lengths are in centimeters.

```
READ(5,*) DL,DL2,LT2
READ(5,*,END=2) TEMPO, TEMPD, TEMPR, T2
READ(5,*)  DELO,DELD,DELR
READ(5,*)  CLO,CLD,CLR
READ(5,*)  LTO,LTD,LTR.
```

This program is for fixed incident angle and fixed frequency. To vary the incident angles, just change the lines (IMB 00670, IMB 00710, IMB 00720) to:

```
DOO 896  JAK = 1, 17
DEG = FLOAT (JAK-1) * 5.0
```

(Delete "DEG = 0.0").

To vary the frequencies, change the lines (IMB 00750, IMB 00810) to:

```
NPT = 10
DO 100  I = 1, NPT
FREQ = FLOAT (I) * 5.0
```

(Delete the line "FREQ = 10.0").

(2) Output:

(1) DL, DL2, LT2
(2) TEMPO, TEMPD, TEMPR (in order)
(3) DELO, DELD, DELR (in order)

(4) DLO, CLD, CLR (in order)

(5) LTO, LTD, LTR (in order)

(6) T2

(7) DEG = (incident angle in degrees), TAI, TAT (in radians), CST ($\cos\theta_o$)

(8) FREQ (in GHZ), K1MR (k_1' cm^{-1})

(9) Y1234 (Y(1), Y(2), Y(3), Y(4) in this order), i.e., R(z), t(z), $T_R(z)/T_2$, $T_B(z)/T_2$

(10) Z, H, and TB.
Z is the thickness (cm). H is the interval for each change of Z.
TB is the brightness at thickness Z.

```
C
C
C                 PROGRAM  INVARIANT IMBEDDING
C
C
C  L.TSANG(1976).
C  S.L.CHUANG(8,1979),CMS VERSION.
C  THIS PROGRAM SOLVES THE RADIATIVE TRANSFER EQUATIONS WITH THE
C  INVARIANT IMBEDDING APPROACH.  THE PROBLEM CONSIDERED IS A TWO LAYER
C RANDOM MEDIUM WITH A LAMINAR STRUCTURE AND WITH INHOMOGENEOUS
C TEMPERATURE,SCATTERING STRENGTHS,CORRELATION LENGTHS,AND LOSS
C TANGENTS PROFILES.
C THE RESULTANT ORDINARY DIFFERENTIAL EQUATIONS ARE OF THE INITIAL VALUE
C PROBLEM AND ARE SOLVED BY USING THE RUNGE-KUTTA SUBROUTINES.
C THE TE CASE IS CONSIDERED IN THIS PROGRAM
C
C
C
      REAL  Y(4),G(4),RAT(4)
      REAL  C(24),W(4,9)
      REAL  AA(100,3)
      REAL  LT0,LTD,LTR
      REAL  K0,K1MR,K1MI,KA,KSD,KSN,KS,KE,KEMP,LT,LT2,NT
       COMPLEX  K2,DIELE2,IX,JX,K2Z
      COMMON/PARA/R01,T01,R12,T12,T12P,T12P2,K1MR,CST
       COMMON/PARA1/TEMP0,TEMPD,TEMPR,T2
      COMMON/PARA2/DEL0,DELD,DELR
      COMMON/PARA3/CL0,CLD,CLR
      COMMON/PARA4/LT0,LTD,LTR
      EXTERNAL  RHS
      NPT=1
      IX=(1.,0.)
      JX=(0.,1.)
C N IS THE NUMBER OF ORDINARY DIFFERTIAL EQUATIONS . THERE ARE FOUR.
      N=4
      TOL=0.0001
      PI=3.1415926
C  DL IS DIELECTRIC CONSTANT OF RANDOM MEDIUM AND DL2 IS DIELECTRIC
C CONSTANT OF THE BOTTOM HOMOGENEOUS MEDIUM.  LT2 IS LOSS TANGENT OF
C BOTTOM MEDIUM.
      READ(5,*) DL,DL2,LT2
    3 CONTINUE
C  FOR THE SAKE OF ILLUSTRATION, WE ASSUME THE FUNCTIONAL FORM OF THE
C INHOMOGENEOUS PROFILES TO BE EXPONENTIAL.
C TEMP0,TEMPD,TEMPR CHARACTERISE THE TEMPERATURE PROFILE.
C DEL0,DELD,DELR CHARACTERIZE THE SCATTERING STRENGTH PROFILE
C CL0,CLD,CLR CHARACTERIZE THE CORRELATION LENGTH PROFILE.
C LT0,LTD,LTR CHARACTERIZE THE LOSS TANGENT PROFILE.
C T2 IS TEMPERATURE OF BOTTOM MEDIUM.
      READ(5,*,END=2)  TEMP0,TEMPD,TEMPR,T2
      READ(5,*)  DEL0,DELD,DELR
      READ(5,*)  CL0,CLD,CLR
      READ(5,*)  LT0,LTD,LTR
      WRITE(6,788)  DL,DL2,LT2
  788 FORMAT(1H0'DL=',E18.8,' DL2=',E18.8,' LT2=',E18.8)
```

```
      WRITE(6,701)  TEMPO,TEMPD,TEMPR
  701 FORMAT(1H0'TEMPO,TEMPD,TEMPR=',3E18.8)
      WRITE(6,702)  DELO,DELD,DELR
  702 FORMAT(1H0'DELO,DELD,DELR=',3E18.8)
      WRITE(6,703)  CLO,CLD,CLR
  703 FORMAT(1H0'CLO,CLD,CLR=',3E18.8)
      WRITE(6,704)  LTO,LTD,LTR
  704 FORMAT(1H0'LTO,LTD,LTR=',3E18.8)
      WRITE(6,705)  T2
  705 FORMAT(1H0'T2=',E18.8)
      DIELE2=DL2*(IX+JX*LT2)
      DO 896 JAK=1,1
C DEG AND TAI ARE THE OBSERVATION ANGLE IN MEDIUM 0 IN DEGREES  AND
C RADIANS RESPECTIVELY. TAT IS THE CORRESPONDING ANGLE IN RANDOM MEDIUM.
C TAI AND TAT ARE RELATED BY SNELL'S LAW.
C     DEG=FLOAT(JAK-1)*5.0
      DEG=0.0
      TAI=DEG*PI/180.
      CTI=COS(TAI)
      NPT=1
      DO 100 I=1,NPT
C FREQ IS FREQUENCY IN GHZ
C WAVE IS WAVELENGTH IN CENTIMETERS.
C KO IS FREE SPACE WAVENUMBER, K1MR IS WAVE NUMBER IN RANDOM MEDIUM, K2
C IS WAVENUMBER OF BOTTOM MEDIUM.
      FREQ=10.0
      WAVE=30./FREQ
      KO=2.*PI/WAVE
      K1MR=SQRT(DL)*KO
      NT=K1MR/KO
      TAT=ARSIN(SIN(TAI)/NT)
      CST=COS(TAT)
      WRITE(6,2369)  DEG,TAI,TAT,CST
 2369 FORMAT(1H0'DEG=',F12.6,' TAI,TAT=',2F12.6,' CST=',F12.6)
      K2=CSQRT(DIELE2)*KO
      WRITE(6,711)  FREQ,K1MR
  711 FORMAT(1H0'FREQ=',E18.8,' K1MR=',E18.8)
C RO1 AND R12 ARE FRESNEL REFLECTIVITY AT TOP AND BOTTOM BOUNDARIES
C  RESPECTIVELY. TO1 AND T12 ARE THE CORRESPONDING TRANSMISSIVITIES.
      K2Z=CSQRT(K2*K2-(K1MR*SIN(TAT))**2)
      RO1=((KO*CTI-K1MR*CST)/(KO*CTI+K1MR*CST))**2
      R12=CABS((K1MR*CST-K2Z)/(K1MR*CST+K2Z))**2
      TO1=1.-RO1
      T12=1.-R12
      T12P=1.+R12
      T12P2=1.+R12*R12
      RD=1.-RO1*R12
C  THE UNKNOWNS IN THE ORDINARY DIFFERENTIAL EQUATIONS ARE R,T,TRN,TBN
C ACCORDING TO EQS.(6),(7),(8),AND (9).OR EQS.(64A),(64B),(69)AND(70)
C IN CHAPTER 6 OF THE BOOK.
C TRN AND TBN ARE NORMALIZED TO T2.  FIRST WE INITIALIZE R,T,TRN,AND
C TBN ACCORDING TO EQS.(10)-(13),OR EQS.(6.64C),(6.64D),(6.71)AND(6.72)
C IN THE BOOK.
      R=RO1/RD
      T=1./RD
```

```
      TRN=R01*T12/RD                                                    IMB01110
      TBN=T01*T12/RD                                                    IMB01120
C Z CHARACTERIZES THE THICKNESS OF SLAB. VECTOR Y ARE THE UNKNOWNS, AND IMB01130
C VECTOR G ARE THE DERIVATIVES OF THE UNKNOWN AND ARE GIVEN BY THE RIGHTIMB01140
C HAND SIDES OF EQUATIONS (6.64A),(6.64B),(6.69),AND (6.70). VECTOR G ISIMB01150
C CALCULATED IN SUBROUTINE RHS.                                         IMB01160
      Z=0.                                                              IMB01170
      Y(1)=R                                                            IMB01180
      Y(2)=T                                                            IMB01190
      Y(3)=TRN                                                          IMB01200
      Y(4)=TBN                                                          IMB01210
      CALL RHS(N,Z,Y,G)                                                 IMB01220
      TB=Y(4)*T2                                                        IMB01230
      WRITE(6,123)  (Y(II),II=1,N)                                      IMB01240
      H=ABS(Y(1)/G(1))*0.1                                              IMB01250
      WRITE(6,124)  Z,H,TB                                              IMB01260
  123 FORMAT(1H0'Y1234=',4E18.8)                                        IMB01270
  124 FORMAT(1H0'Z=',E18.8,' H=',E18.8,'---TB=',E18.8)                  IMB01280
C NIN IS THE NUMBER OF TIMES WE ITERATE THE ORDINARY DIFFERTIAL         IMB01290
C EQUATIONS.                                                            IMB01300
      NIN=100                                                           IMB01310
      DO 899 IO=1,NIN                                                   IMB01320
      DO 564 LO=1,4                                                     IMB01330
C H IS THE INCREMENTAL INTERVAL IN THICKNESS AND IS CALCULATED ACCORDINGIMB01340
C TO THE VALUES OF Y AND G.                                             IMB01350
      RAT(LO)=1000.0                                                    IMB01360
      IF  (G(LO).NE.0.0.AND.Y(LO).NE.0.0)  RAT(LO)=ABS(Y(LO)/G(LO))     IMB01370
  564 CONTINUE                                                          IMB01380
      H=0.2*AMIN1(RAT(1),RAT(2),RAT(3),RAT(4))                          IMB01390
C WE WANT THICKNESS Z TO FALL ON 50 CM. AND 1000 CM.                    IMB01400
      IF (Z.LT.49.99.AND.(Z+H).GT.50.0)  H=50.0-Z                       IMB01410
      IF  (Z.LT.999.99.AND.(Z+H).GT.1000.0)  H=1000.0-Z                 IMB01420
C DVERK IS THE SUBROUTINE SUPPLIED BY IBM IMSLMATH SOLVING ORDINARY     IMB01430
C DIFFERENTIAL EQUATIONS WITH RUNGE KUTTA METHOD                        IMB01440
     IND=1                                                              IMB01450
     XEND=Z+H                                                           IMB01460
     CALL DVERK(N,RHS,Z,Y,XEND,TOL,IND,C,N,W,IER)                       IMB01470
       TB=Y(4)*T2                                                       IMB01480
     AA(IO,1)=Z                                                         IMB01490
      AA(IO,2)=H                                                        IMB01500
      AA(IO,3)=TB                                                       IMB01510
      IF  (Z.GT.140.0)  GO TO 900                                       IMB01520
  899 CONTINUE                                                          IMB01530
  900 CONTINUE                                                          IMB01540
      DO 654 IP=1,IO                                                    IMB01550
      WRITE(6,653)  (AA(IP,LEUNG),LEUNG=1,3)                            IMB01560
  653 FORMAT(3X,E18.8,3X,E18.8,6X,E18.8)                                IMB01570
  654 CONTINUE                                                          IMB01580
  100 CONTINUE                                                          IMB01590
  896 CONTINUE                                                          IMB01600
      GO TO 3                                                           IMB01610
    2 CONTINUE                                                          IMB01620
      CALL EXIT                                                         IMB01630
      END                                                               IMB01640
       SUBROUTINE  RHS(N,Z,Y,G)                                         IMB01650
```

```
C IN THIS SUBROUTINE RHS, WE CALCULATE THE DERIVATIVES OF THE UNKNOWNS
C R,T,TRN,AND TBN.  THEY ARE CONTAINED IN THE RIGHT HAND SIDES OF
C EQS.(6.64A),(6.64B),(6.69) AND (6.70). THE UNKNOWNS ARE STORED IN
C VECTOR Y AND THE DERIVATIVES ARE STORED IN VECTOR G
      REAL  G(N),Y(N)
      REAL  K0,K1MR,K1MI,KA,KSD,KSN,KS,KE,KEMF,LT,LT2
      REAL  LT0,LTD,LTR
      REAL  KSP,KAP,KEP
      COMMON/PARA/R01,T01,R12,T12,T12P,T12P2,K1MR,CST
       COMMON/PARA1/TEMP0,TEMPD,TEMPR,T2
      COMMON/PARA2/DEL0,DELD,DELR
      COMMON/PARA3/CL0,CLD,CLR
      COMMON/PARA4/LT0,LTD,LTR
C TEMP0,TEMPD,TEMPR CHARACTERISE THE TEMPERATURE PROFILE.
C DEL0,DELD,DELR CHARACTERIZE THE SCATTERING STRENGTH PROFILE
C CL0,CLD,CLR CHARACTERIZE THE CORRELATION LENGTH PROFILE.
C LT0,LTD,LTR CHARACTERIZE THE LOSS TANGENT PROFILE.
C TEMP IS THE TEMPERATURE, CL IS THE CORRELATION LENGTH, DEL IS THE
C SCATTERING STRENGTH AND LT IS THE LOSS TANGENT , ALL AT POSITION Z.
      LT=LT0+LTD*EXP(-LTR*Z)
      DEL=DEL0+DELD*EXP(-Z*DELR)
      CL=CL0+CLD*EXP(-Z*CLR)
      TEMP=TEMP0+TEMPD*EXP(-Z*TEMPR)
      TEMPN=TEMP/T2
      R=Y(1)
      T=Y(2)
      TRN=Y(3)
      TBN=Y(4)
C KS IS SCATTERING COEFFICIENT, KA ABSORPTION COEFFICIENT, KE EXTINCTION
C COEFFICIENT, OM THE ALBEDO.  PF FORWARD PHASE FUNCTION AND PB BACKWARD
C PHASE FUNCTION.
      KSD=1.+(2.*K1MR*CL*CST)**2
      KSN=1.+2.*(K1MR*CL*CST)**2
      KS=DEL*K1MR*K1MR*CL*KSN/(KSD*CST)
      PF=KSD/KSN
      PB=1./KSN
      K1MI=K1MR*LT*0.5
      KA=2.*K1MI
      KE=KS+KA
      OM=KS/KE
      KSP=KS/CST
      KAP=KA/CST
      KEP=KAP+KSP
      F=0.5*KSP*PF
      B=KSP*0.5*PB
       KEMF=KEP-F
      F1=-KEMF+B*R12
      F12=2.*F1
      F2=-2.*KEMF*R12+B*T12P2
       G(1)=B+R*F12+R*R*F2
      G(2)=T*(F1+F2*R)
     G(3)=TRN*F1+B*T12+KAP*TEMPN+R*(TRN*F2+T12*F1+KAP*TEMPN*T12P)
      G(4)=T01*T*(TRN*F2+F1*T12+KAP*T12P*TEMPN)
      RETURN
      END
```

PROGRAM BORN1

Introduction

This program computes the backscattering cross sections per unit area in the first-order Born approximation for a two-layer random medium (Figure 3) for both types of polarizations TE and TM. The program computes the backscattering cross sections as a function of angle (for a given frequency) or as a function of frequency (for a given incident angle). Two correlation functions are considered; the first is laterally Gaussian and vertically exponential, the second is spherical. This program also superimposes very rough surface effects incoherently using the model in the Radar Cross-Section Handbook, Chapter 9. The units used in this program are in the MKS system. The frequency is in Hz.

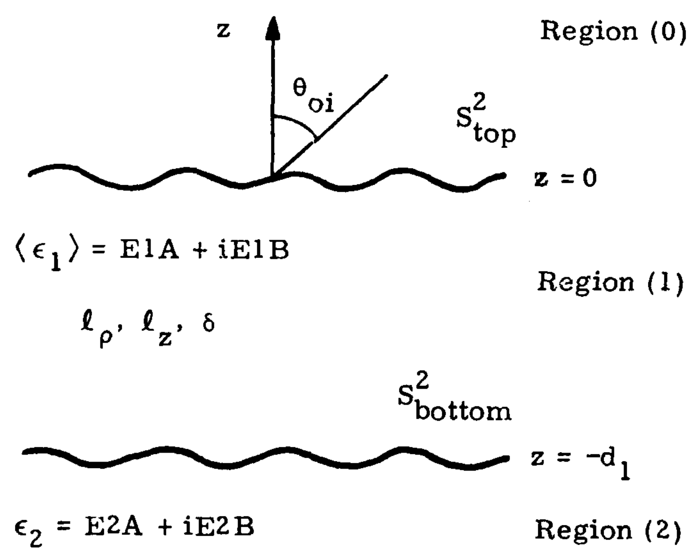

Figure 3. Geometrical Configuration of the Problem for Program BORN1

Equations

The backscattering cross sections per unit area are calculated according to the following equation:

$$\sigma_{hh} = \delta k_1'^4 \pi^2 \frac{|X_{01i}|^4}{|D_{2i}|^4} \left[8d_1 \phi_1(2k_{\perp i}, 0) |R_{12i}|^2 e^{-4k''_{1zi} d_1} \right.$$

$$\left. + (1 + |R_{12i}|^4 e^{-4k''_{1zi} d_1})(1 - e^{-4k''_{1zi} d_1}) \frac{\phi_1(2k_{\perp i}, 2k_{1zi})}{2k''_{1zi}} \right]$$

$$\sigma_{vv} = \delta k_1'^4 \pi^2 \frac{|Y_{01i}|^4}{|F_{2i}|^4} \frac{k_o^4}{|k_1|^4} \left[8d_1 \phi_1(2k_{\perp i}, 0) |S_{12i}|^2 e^{-4k''_{1zi} d_1} \right.$$

$$\left. \frac{|k_{\rho i}^2 - k_{1zi}^2|^2}{|k_1|^4} + (1 + |S_{12i}|^4 e^{-4k''_{1zi} d_1})(1 - e^{-4k''_{1zi} d_1}) \frac{\phi_1(2k_{\perp i}, 2k_{1zi})}{2k''_{1zi}} \right].$$

Two correlation functions are considered in this program: The first is laterally Gaussian and vertically exponential. The corresponding spectral density is

$$\phi_1(\beta_\perp, \beta_z) = \frac{\ell_z \ell_\rho^2 \, e^{-\beta_\perp^2 \ell_\rho^2 / 4}}{4\pi^2 (1 + \beta_z^2 \ell_z^2)}.$$

The second is spherical. The corresponding density is

$$\phi_1(\beta) = \frac{r_o^3 / \pi^2}{[1 + \beta^2 r_o^2]^2}.$$

The rough surface effects are superimposed incoherently using the model in the Radar Cross Section Handbook, Chapter 9.

The rough surface can be either on the top or bottom surface or both.

If the rough surface is on the top layer, then

$$\sigma_{R_{hh}} = \frac{\sec^4\theta_{oi}}{S^2}\left|\frac{k_o - k_1}{k_o + k_1}\right|^2 \exp\left(-\frac{1}{S^2}\tan^2\theta_{oi}\right)$$

$$\sigma_{R_{vv}} = \frac{\sec^4\theta_{oi}}{S^2}\left|\frac{\epsilon_o k_1 - \epsilon_1 k_o}{\epsilon_o k_1 + \epsilon_1 k_o}\right|^2 \exp\left(-\frac{1}{S^2}\tan^2\theta_{oi}\right)$$

If the rough surface is on the bottom layer, then

$$\sigma_{R_{hh}} = \frac{\sec^4\theta_t}{S^2}\left|\frac{k_1 - k_2}{k_1 + k_2}\right|^2 \exp\left(-\frac{1}{S^2}\tan^2\theta_t\right)\exp(-4k''_{1z}d_1)$$

$$\sigma_{R_{vv}} = \frac{\sec^4\theta_t}{S^2}\left|\frac{\epsilon_2 k_1 - \epsilon_1 k_2}{\epsilon_2 k_1 + \epsilon_1 k_2}\right|^2 \exp\left(-\frac{1}{S^2}\tan^2\theta_t\right)\exp(-4k''_{1z}d_1),$$

where

$$\sin\theta_t = \frac{k_o}{k'_1}\sin\theta_{oi}.$$

Thus the total backscattering cross sections are given by

$\sigma_{R_{hh}} + \sigma_{hh}$ for the TE polarization

$\sigma_{R_{vv}} + \sigma_{vv}$ for the TM polarization,

where σ_R (either $\sigma_{R_{hh}}$ or $\sigma_{R_{vv}}$) is that due to the top rough surface or the bottom rough surface or both.

For $\ell, m = 0, 1, 2$,

$$k_\ell = \omega \sqrt{\mu \langle \epsilon_\ell \rangle}$$

$$k_{\ell z} = \sqrt{k_\ell^2 - k_\perp^2}$$

$$R_{\ell m} = \frac{k_{\ell z} - k_{mz}}{k_{\ell z} + k_{mz}}$$

$$S_{\ell m} = \frac{\langle \epsilon_m \rangle k_{\ell z} - \langle \epsilon_\ell \rangle k_{mz}}{\langle \epsilon_m \rangle k_{\ell z} + \langle \epsilon_\ell \rangle k_{mz}}$$

$$X_{\ell m} = 1 + R_{\ell m}$$

$$Y_{\ell m} = 1 + S_{\ell m}$$

$$D_2 = 1 + R_{01} R_{12}\, e^{i2k_{1z}d_1}$$

$$F_2 = 1 + S_{01} S_{12}\, e^{i2k_{1z}d_1}.$$

A subscript "i" indicates that a quantity is to be calculated at the incident wavevector angles in the appropriate region, e.g.,

$$R_{\ell mi} = \frac{k_{\ell zi} - k_{mzi}}{k_{\ell zi} + k_{mzi}} \qquad k_{\ell zi} = \sqrt{k_\ell^2 - k_{\perp i}^2} \qquad k_{\perp i} = k_o \sin \theta_{oi}.$$

The real and imaginary parts of a quantity are denoted by a prime and double primes, respectively, e.g.,

$$k'_{1z} = \mathrm{Re}\,(k_{1z}) \qquad k''_{1z} = \mathrm{Im}\,(k_{1z}).$$

Symbols

Fortran Symbol	Notation	Explanations
D1	d_1	Thickness of the random layer
EPS1	$\langle \epsilon_1 \rangle$	Mean permittivity of the random layer
EPS0, EPS2	ϵ_o, ϵ_3	Permittivities of the free space region and the homogeneous ground, respectively
K0, K1, K2	k_o, k_1, k_2	Wave numbers in the air region (0-region), the first and second regions, respectively
K1Z, K2Z	k_{1z}, k_{2z}	Components of the wave numbers in the z-direction in regions (1) and (2), respectively
R01, R12	R_{01i}, R_{12i}	Reflection coefficients for the TE wave in regions (0) and (1) at the boundaries separating regions (0)-(1) and (1)-(2), respectively, evaluated at θ_{oi}
S01, S12	S_{01i}, S_{12i}	Reflection coefficients for the TM wave in regions (0) and (1) at the boundaries separating regions (0)-(1) and (1)-(2), respectively, evaluated at θ_{oi}
ZRHO	ℓ_ρ	Lateral correlation length of fluctuations in permittivities in the random medium
DEL	δ	Variance of fluctuations in permittivities in the random medium
RO	r_o	Spherical correlation length of fluctuations in permittivities in the random medium
E1A	$\langle \epsilon_1 \rangle' / \epsilon_o$	Real part of the mean dielectric constant in the random medium
E2A	ϵ_2' / ϵ_o	Real part of the dielectric constant in the homogeneous medium (2)
E1B	$\langle \epsilon_1 \rangle'' / \epsilon_o$	Imaginary part of the mean dielectric constant in the random medium

Fortran Symbol	Notation	Explanations
E2B	ϵ_2''/ϵ_o	Imaginary part of the dielectric constant in the homogeneous medium (2)
S2T, S2B	s^2	Mean square slope of the top and bottom rough surfaces, respectively
XINC, X	θ_{oi}	Fixed incidence angle and variable incidence angle, respectively
FREQC, FREQ	f	Constant and variable frequencies, respectively
RSIGH, RSIGV	$\sigma_{R_{hh}}$, $\sigma_{R_{vv}}$	Backscattering cross sections for the TE and TM polarizations, respectively, due to rough surface effects
SIG1, SIG2	σ_{hh}, σ_{vv}	Backscattering cross sections for the TE and TM polarizations, respectively, due to volume scattering

Input and Output Format

(1) The input parameters are:

(i)	ICHECK, ICHOIC	(v)	APT, APB, S2T, S2B
(ii)	FREQ, X	(vi)	ZRHO, ZL, DEL
(iii)	DX, DF, XM, FM	(vii)	E1A, E1B, E2A, E2B
(iv)	FREQC, XINC	(viii)	D1

Sets (i), (ii), (iii), and (iv) are read from a data file named BORN1 DATA (with logical unit number 8). Sets (v), (vi), (vii), and (viii) are input at the users terminal under a free format specification. The user is prompted with a message to enter the parameters of sets (v), (vii), and (viii) in a specified order.

All input parameters are in MKS units, frequency in Hz, and angles in degrees.

Fortran Symbol	Notation	Explanations
ICHOIC		If ICHOIC = 1 we plot SIGMA vs frequency. If ICHOIC = 2 we plot SIGMA vs incident angle.
ICHECK		ICHECK = 1 corresponds to spherical correlation function. In this case ZRHO is set equal to ZL, and the value read for ZHRO (which is equal to that for ZL) is set equal to RO inside the program. ICHECK = 0 corresponds to Gaussian laterally, exponential vertically.
FREQ, FM		Initial and final values of the variable frequency

Fortran Symbol	Notation	Explanations
DF		Increment step of the variable frequency
X, XM		Initial and final values of the variable incident angle
DX		Increment step of the variable incident angle
APT		If APT = 1 top rough surface effects are included. If APT = 0 top rough surface effects are not included.
APB		If APB = 1 bottom rough surface effects are included. If APB = 0 bottom rough surface effects are not included.
S2T, S2B	s^2	Mean square slope of top and bottom rough surfaces, respectively
XINC	θ_{oi}	Fixed incident angle in degrees, if we plot σ vs frequency
FREQC	f	Fixed frequency in HZ, if we plot σ vs angle

(2) The output parameters are: SIGMA VV, SIGMA HH, INC ANGLE (DEG) or FREQUENCY (GHZ).

SIGMA VV, SIGMA HH are the backscattering cross sections per unit area for the TM and TE polarizations, respectively, in dB.

The format in which these appear is E13.7.

INC ANGLE (DEG) is the incidence angle in degrees, if ICHOIC = 2.

FREQUENCY (GHZ) is the frequency in GHZ, if ICHOIC = 1.

The format in which these appear is F6. 3.

```
C                        PROGRAM BORN1
C                         M. ZUNIGA
C
C
C
C     PROGRAM TO COMPUTE BACK SCATTERING CROSS SECTIONS/AREA
C     IN THE FIRST ORDER BORN APPROXIMATION FOR A TWO LAYER RANDOM MED.
C     THIS PROGRAM ALSO SUPERIMPOSES VERY ROUGH SURFACE EFFECTS
C     INCOHERENTLY USING THE MODEL IN BARRECKS PAPER
C
C
C
      COMPLEX EPS1,EPS2,K1,K2,K1Z,K2Z,R10,R12,S10,S12,X01,Y01
      COMPLEX A12I,A10I,D2,E2,ARG,PH
      REAL K0,K1R,K2R,K1ZR,K2ZR,KAZ,KZ
      DATA EPS0,PI,U/8.85E-12,3.14159,1.2566E-6/
C
C     CORRELATION FUNCTION (A) IS SPHERICAL
C     CORRELATION FUNCTION (C) IS GAUSSIAN LATERALLY AND EXPONENTIAL
C     VERTICALLY
C     ICHECK=1 CORRESPONDS TO CORRELATION FUNCTION (A)
C     ICHECK=0 CORRESPONDS TO CORRELATION FUNCTION (C)
C
C     IF ICHOIC=1 WE PLOT SIGMA VS. FREQUENCY
C     IF ICHOIC=2 WE PLOT SIGMA VS. INC. ANGLE
C
      READ(8,*) ICHECK,ICHOIC
C
C     FREQ IS THE INITIAL VALUE OF THE VARIABLE FREQ. , IN HZ.
C     X IS THE INITIAL VALUE OF THE VARIABLE INC. ANGLE ,IN DEG.
C
      READ (8,*)FREQ,X
      X=X*PI/180.
C
C     DX IS THE INCREMENT STEP OF THE VARIABLE INC. ANGLE,IN DEG.
C     DF IS THE INCREMENT STEP OF THE VARIABLE FREQ. ,IN HZ.
C     XM IS THE FINAL VALUE OF THE VARIABLE INC. ANGLE ,IN DEG.
C     FM IS THE FINAL VALUE OF THE VARIABLE FREQ.,IN HZ
C
      READ(8,*) DX,DF,XM,FM
C
C     FREQC IS THE FIXED FREQ.,IN HZ.,IF WE PLOT SIGMA VS. ANGLE
C     XINC IS THE FIXED INC. ANGLE IN DEG.,IF WE PLOT SIGMA VS. FREQUENCY
C
      READ(8,*)FREQC,XINC
      WRITE(6,111)
  111 FORMAT(3X,'ENTER APT,APB,S2T AND S2B IN THAT ORDER')
C
C     IF APT=1 TOP ROUGH SURFACE EFFECTS ARE INCLUDED
C     IF APT=0 TOP ROUGH SURFACE EFFECTS ARE NOT INCLUDED
C     IF APB=1 BOTTOM ROUGH SURFACE EFFECTS ARE INCLUDED
C     IF APB=0 BOTTOM ROUGH SURFACE EFFECTS ARE NOT INCLUDED
C
C     S2T DENOTES THE MEAN SQUARE SLOPE AT THE TOP SURFACE
C     S2B DENOTES THE MEAN SQUARE SLOPE AT THE BOTTOM SURFACE
```

```
C
      READ(5,*)APT,APB,S2T,S2B
      WRITE(6,2)
    2 FORMAT(1X,'ENTER LRHO AND LZ IN M. , ALSO ENTER DEL IN THAT ORDER'
     *)
C
C     ZRHO DENOTES THE LATERAL CORRELATION LENGH OF FLUCTUATION IN
C     PERMITTIVITY OF THE RANDOM MEDIUM,IN M.
C     ZL DENOTES THE VERTICAL CORRELATION LENGH ,IN M.
C     DEL DENOTES THE VARIANCE OF FLUCTUATION IN PERMITTIVITY IN THE
C     RANDOM MEDIUM
C
C     IF ICHECK=1(SPHERICAL CASE) ZRHO IS SET EQUAL TO ZL
C     THE VALUE READ FOR ZRHO(WHICH IS THE SAME AS THAT FOR ZL) IS SET
C     EQUAL TO RO INSIDE THE PROGRAM
C     RO IS THE SPHERICAL CORRELATION LENGTH OF FLUCTUATION IN
C     PERMITTIVITY OF THE RANDOM MEDIUM
C
      READ(5,*) ZRHO,ZL,DEL
      WRITE(6,3)
    3 FORMAT(1X,'ENTER E1A,E1B,E2A AND E2B IN THAT ORDER')
C
C     E1A IS THE REAL PART OF THE MEAN DIELECTRIC CONSTANT IN THE RANDOM
C     MEDIUM
C     E2A IS THE REAL PART OF THE DIELECTRIC CONSTANT IN THE HOMOGENEOUS
C     MEDIUM
C     E1B IS THE IMAGINARY PART OF THE MEAN DIELECTRIC CONSTANT IN THE
C     RANDOM MEDIUM
C     E2B IS THE IMAGINARY PART OF THE DIELECTRIC CONSTANT IN THE
C     HOMOGENEOUS MEDIUM
C
      READ(5,*)E1A,E1B,E2A,E2B
      WRITE(6,197)
  197 FORMAT(3X,'ENTER D1 IN METERS')
C
C     D1 IS THE DEPTH OF THE RANDOM MEDIUM
C
      READ(5,*)D1
      DX=DX*PI/180.
      XM=XM*PI/180.
      RO=ZRHO
C
C     EPS1 IS THE COMPLEX MEAN PERMITTIVITY IN THE RANDOM MEDIUM (1)
C     EPS2 IS THE COMPLEX PERMITTIVITY IN THE HOMOGENEOUS MEDIUM (2)
C
      EPS1=EPS0*CMPLX(E1A,E1B)
      EPS2=EPS0*CMPLX(E2A,E2B)
C
C      IF ICHOIC=2 FIX FREQUENCY
C
      IF(ICHOIC.EQ.2) FREQ=FREQC
      ACOR=1.
      MSQ=2
C
C      IPOL=0 CORRESPONDS TO TE --IPOL=1 CORRESPONDS TO TM
```

```
C      IPOL  MUST ALWAYS HAVE INITIAL VALUE=0
C
       IPOL=0
       IF(ICHECK.EQ.0) ACOR=0.
       IF(ICHECK.EQ.0) RO=ZL
       IF(ICHECK.EQ.0) MSQ=1
       IF(ICHECK.EQ.1) WRITE(6,8)
       IF(ICHECK.EQ.0) WRITE(6,9)
     8 FORMAT(3X,'CORRELATION FUNCTION A(SPHERICAL)')
     9 FORMAT(3X,'CORRELATION FUNCTION C(GAUSSIAN LATERALLY EXPONENTIAL '
     *,'VERTICALLY)')
       IF(APT.EQ.0..AND.APB.EQ.1.)WRITE(6,113)
       IF(APB.EQ.0..AND.APT.EQ.1.) WRITE(6,114)
       IF(APT.EQ.1..AND.APB.EQ.1.) WRITE(6,115)
       IF(APT.EQ.0..AND.APB.EQ.0.) WRITE(6,116)
   113 FORMAT(3X,'ONLY BOTTOM ROUGH SURFACE EFFECTS ARE INCLUDED')
   114 FORMAT(3X,'ONLY TOP ROUGH SURFACE EFFECTS ARE INCLUDED')
   115 FORMAT(3X,'BOTH TOP AND BOTTOM ROUGH SURFACE EFFECTS ARE INCLUDED'
     *)
   116 FORMAT(3X,'NO ROUGH SURFACE EFFECTS ARE INCLUDED')
       FRET=FREQC/1.0E+9
       IF(ICHOIC.EQ.2) WRITE(6,24) FRET
    24 FORMAT(3X,'FREQUENCY(GHZ)=',F7.3)
C
C      IF ICHOIC=1 FIX INC ANGLE
C
       IF(ICHOIC.EQ.1) X=XINC*(PI/180.)
       IF(ICHOIC.EQ.1) WRITE(6,25) XINC
    25 FORMAT(3X,'INC ANGLE(DEG)=',F7.3)
       IF(ICHOIC.EQ.1) WRITE(6,26)
    26 FORMAT(3X,'SIGMA VV                  SIGMA HH                  FREQUENCY(GHZ
     1)')
       IF(ICHOIC.EQ.2) WRITE(6,27)
    27 FORMAT(3X,'SIGMA VV                  SIGMA HH                  INC ANGLE(DE
     1G)')
       ICOUNT=0
    18 CONTINUE
       W=2.*PI*FREQ
C
C     K0,K1,K2 ARE THE WAVE NUMBERS IN THE AIR [(0)-REGION],THE FIRST ,
C     AND THE SECOND REGIONS RESPECTIVELY
C
       K0=W*SQRT(U*EPS0)
       K2=W*CSQRT(U*EPS2)
       K1=W*CSQRT(U*EPS1)
       K1R=REAL(K1)
     5 CONTINUE
       Y=COS(X)
       YS=SIN(X)
       KZ=K0*Y
C
C     K1Z,K2Z ARE THE COMPONENTS OF THE WAVE NUMBER IN THE Z-DIRECTION
C     IN REGIONS (1) AND (2) RESPECTIVELY
C
       K1Z=CSQRT(K1*K1-K0*K0*YS*YS)
```

```
      K2Z=CSQRT(K2*K2-K0*K0*YS*YS)
      K1ZR=REAL(K1Z)
      K2ZR=REAL(K2Z)
      KAZ=2.*AIMAG(K1Z)
C
C     R01,R12 ARE THE REFLECTION COEFFICIENTS FOR TE WAVES IN REGIONS
C     (0) & (1) AT THE BOUNDERIES SEPERATING REGIONS (0)-(1) & (1)-(2)
C     RESPECTIVELY
C     R10=-R01
C
      R10=(K1Z-KZ)/(K1Z+KZ)
      R12=(K1Z-K2Z)/(K1Z+K2Z)
C
C     S01,S12 ARE THE REFLECTION COEFFICIENTS FOR TM WAVES IN REGIONS
C     (0) & (1) AT THE BOUNDERIES SEPERATING REGIONS (0)-(1)
C     & (1)-(2) RESPECTIVELY
C     S10=-S01
C
      S10=(EPS0*K1Z-EPS1*KZ)/(EPS0*K1Z+EPS1*KZ)
      S12=(EPS2*K1Z-EPS1*K2Z)/(EPS2*K1Z+EPS1*K2Z)
      Y01=1.-S10
      X01=1.-R10
      PHAS=2.*D1*KAZ
      ARG=COS(K1ZR*2.*D1)+CMPLX(0.,1.)*SIN(K1ZR*2.*D1)
C
C     THE FOLLOWING STEP IS TO AVOID THE UNDERFLOW RESULTING FROM THE
C     LARGE NEGATIVE POWER OF THE EXPONENTIAL FUNCTION
C
      IF(PHAS.GT.20.) PHAS=20.
      PH=ARG*EXP(-PHAS/2.)
C
C     THE FOLLOWING SECTION COMPUTES THE BACKSCATTERING CROSS SECTIONS
C     PER UNIT AREA DUE TO VOLUME SCATTERING
C
      D2=1.-R10*R12*PH
      E2=1.-S10*S12*PH
      A10I=R10
      A12I=R12
      COEF1=DEL*(R0**3)*(K1R**4)*(CABS(X01)**4)
      COEF1=COEF1/(CABS(D2)**4)
      COEF2=DEL*(R0**3)*(K1R**4)*(CABS(Y01)**4)
      COEF2=COEF2/(CABS(E2)**4)
      COEF2=COEF2*((CABS(K0/K1)**8))
      CCOR=ZL*ZRHO*ZRHO*EXP(-K0*K0*ZRHO*ZRHO*YS*YS)
      IF(ICHECK.EQ.1) CCOR=4.*(R0**3)
      COEF1=COEF1*CCOR/(4.*(R0**3))
      COEF2=COEF2*CCOR/(4.*(R0**3))
      AN=CABS((K1Z/K0)**2+YS*YS)
      AN=AN**2
      BN=CABS((K1Z/K0)**2-YS*YS)
      BN=BN**2
      IF(IPOL.EQ.0) GO TO 10
      A10I=S10
      A12I=S12
   10 IF(IPOL.EQ.0) AN=1.
```

```
      IF(IPOL.EQ.0) BN=1.
      T1=(1.-EXP(-PHAS))/(KAZ*(1.+RO*RO*4.*K1ZR*K1ZR+4.*RO*RO*ACOR*KO*KO
     1*YS*YS)**NSQ)
      T1=T1*(1.+(CABS(A12I)**4)*EXP(-PHAS))
      T2=(8.*D1*EXP(-PHAS)*(CABS(A12I)**2))
      T2=T2/((1.+4.*RO*RO*ACOR*KO*KO*YS*YS)**2)
      C=COEF2
      IF(IPOL.EQ.0) C=COEF1
      SIG=C*(T1*AN+T2*BN)
      IF(IPOL.EQ.0) SIG1=SIG
      IF(IPOL.EQ.1) SIG2=SIG
      IF(IPOL.EQ.1) GO TO 30
      IF(IPOL.EQ.0) IPOL=1
      IF(ICHOIC.EQ.1.AND.IPOL.EQ.1) GO TO 18
      IF(ICHOIC.EQ.2.AND.IPOL.EQ.1) GO TO 5
   30 CONTINUE
      ZZ=X*(180./PI)
      IF(ICHOIC.EQ.1) ZZ=FREQ/1.0E+9
C
C    END OF BACKSCATTERING CROSS SECTIONS / AREA DUE TO VOLUME
C    SCATTERING
C
C     ROUGH SURFACE AT TOP CALCULATION FOLLOWS
C
      S2=S2T
      AP=APT
      XI=X
      RR=CABS((KO-K1)/(KO+K1))
      SS=CABS((EPS0*K1-EPS1*KO)/(EPS0*K1+EPS1*KO))
      TN2=(SIN(XI)/COS(XI))**2
      CHECK2=TN2/S2
      IF(CHECK2.GT.70.) RSIGV=0.
      IF(CHECK2.GT.70.) GO TO 98
      SC4=1./(COS(XI)*COS(XI)*COS(XI)*COS(XI))
      RSIGV=(AP/S2)*SC4*SS*SS*EXP(-TN2/S2)
   98 CONTINUE
      RSIGH=RSIGV*RR*RR/(SS*SS)
C
C     END TOP ROUGH SURFACE CALCULATION
C
C     ROUGH SURFACE AT BOTTOM CALCULATION BEGINS
C
      XI2=ARSIN((KO/K1R)*SIN(X))
      RR=CABS((K1-K2)/(K1+K2))
      SS=CABS((EPS1*K2-EPS2*K1)/(EPS1*K2+EPS2*K1))
      TN2=(SIN(XI2)/COS(XI2))**2
      CHECK2=TN2/S2B
      IF(CHECK2.GT.70.)RSIGVB=0.
      IF(CHECK2.GT.70.)GO TO 107
      SC4=1./(COS(XI2)**4)
      RSIGVB=(APB/S2B)*SC4*SS*SS*EXP(-CHECK2)
  107 CONTINUE
      RSIGHB=RSIGVB*RR*RR/(SS*SS)
      RSIGVB=RSIGVB*EXP(-PHAS)
      RSIGHB=RSIGHB*EXP(-PHAS)
```

```
C
C     END BOTTOM ROUGH SURFACE CALCULATION
C
      RSIGV=RSIGV+RSIGVB
      RSIGH=RSIGH+RSIGHB
      SIG1=SIG1+RSIGH
      SIG2=SIG2+RSIGV
      SIG1=10.*ALOG10(SIG1)
      SIG2=10.*ALOG10(SIG2)
      WRITE(6,19) SIG2,SIG1,ZZ
   19 FORMAT(3X,E13.7,6X,E13.7,9X,F7.3)
      ICOUNT=ICOUNT+1
      IPOL=0
      IF(ICHOIC.EQ.2) X=X+DX
      IF(ICHOIC.EQ.1) FREQ=FREQ+DF
      IF(ICHOIC.EQ.2.AND.X.LT.XM) GO TO 5
      IF(ICHOIC.EQ.1.AND.FREQ.LT.FM) GO TO 18
      WRITE(6,96) ICOUNT
   96 FORMAT(3X,'ICOUNT=',I7)
      STOP
      END
```

PROGRAM BORNM

Introduction

This program computes the backscattering cross sections per unit area in the first-order Born approximation for a three-layer random medium (Figure 4) for both types of polarizations TE and TM. The program computes the backscattering cross sections as a function of angle (for a given frequency) or as a function of frequency (for a given incident angle). The correlation function considered is laterally Gaussian and vertically exponential. This program also superimposes very rough surface effects incoherently using the model in Barrick's paper. The units used in this program are in the MKS system. The frequency is in Hz.

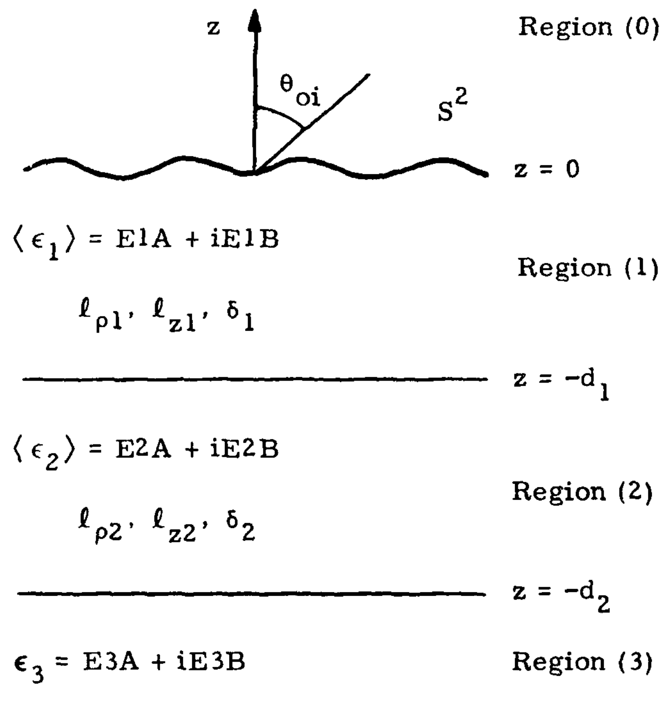

Figure 4. Geometrical Configuration of the Problem for Program BORNM

<u>Equations</u>

The backscattering cross sections per unit are calculated according to the following equations:

$$\sigma_{hh} = \delta_1 k_1'^4 \pi^2 \frac{|X_{01i}|^4}{|D_{2i}|^4} \Bigg[8d_1 \phi_1(2k_{\perp i}, 0) \left| R_{12i} + R_{23i}\, e^{i2k_{2zi}(d_2-d_1)} \right|^2$$

$$\left| 1 + R_{12i}R_{23i}\, e^{i2k_{2zi}(d_2-d_1)} \right|^2 e^{-4k''_{1zi}d_1} + \left(\left| R_{12i} + R_{23i}\, e^{i2k_{2zi}(d_2-d_1)} \right|^4 \right.$$

$$\left. e^{-4k''_{1zi}d_1} + \left| 1 + R_{12i}R_{23i}\, e^{i2k_{2zi}(d_2-d_1)} \right|^4 \right) (1 - e^{-4k''_{1zi}d_1})$$

$$\frac{\phi_1(2k_{\perp i}, 2k_{1zi})}{2k''_{1zi}} \Bigg]$$

$$+ \delta_2 k_2'^4 \pi^2 \frac{|X_{01i}|^4 \, |X_{2i}|^4}{|D_{2i}|^4} \Bigg[8(d_2-d_1)\, \phi_2(2k_{\perp i}, 0) |R_{23i}|^2$$

$$e^{-4k''_{2zi}(d_2-d_1)}\, e^{-4k''_{1zi}d_1}$$

$$+ \left(|R_{23i}|^4 e^{-4k''_{2zi}(d_2-d_1)} + 1 \right) (1 - e^{-4k''_{2zi}(d_2-d_1)})\, e^{-4k''_{1zi}d_1} \frac{\phi_2(2k_{\perp i}, 2k_{2zi})}{2k''_{2zi}} \Bigg]$$

$$\sigma_{vv} = \delta_1 k_1'^4 \pi^2 \frac{|Y_{01i}|^4}{|E_{2i}|^4} \frac{k_o^4}{|k_1|^4} \left[8d_1 \phi_1(2k_{\perp i}, 0) \left| S_{12i} + S_{23i}\, e^{i2k_{2zi}(d_2-d_1)} \right|^2 \right.$$

$$\left| 1 + S_{12i} S_{23i}\, e^{i2k_{2zi}(d_2-d_1)} \right|^2 e^{-4k''_{1zi} d_1} \frac{|k_{\rho i}^2 - k_{1zi}^2|^2}{|k_1|^4}$$

$$+ \left(\left| S_{12i} + S_{23i}\, e^{i2k_{2zi}(d_2-d_1)} \right|^4 e^{-4k''_{1zi} d_1} \right.$$

$$\left. + \left| 1 + S_{12i} S_{23i}\, e^{i2k_{2zi}(d_2-d_1)} \right|^4 \right)(1 - e^{-4k''_{1zi} d_1}) \left. \frac{\phi_1(2k_{\perp i}, 2k_{1zi})}{2k''_{1zi}} \right]$$

$$+ \delta_2 k_2'^4 \pi^2 \frac{|Y_{01i}|^4 \, |Y_{12i}|^4}{|E_{2i}|^4} \frac{k_o^4}{|k_2|^4} \left[8(d_2 - d_1)\, \phi_2(2k_{\perp i}, 0) \right.$$

$$|S_{23i}|^2 e^{-4k''_{2zi}(d_2-d_1)} \frac{|k_{\rho i}^2 - k_{1zi}^2|^2}{|k_2|^4} e^{-4k''_{1zi} d_1}$$

$$\left. + (|S_{23i}|^4 e^{-4k''_{1zi}(d_2-d_1)} + 1)(1 - e^{-4k''_{2zi}(d_2-d_1)})\, e^{-4k''_{1zi} d_1} \frac{\phi_2(2k_{\perp i}, 2k_{2zi})}{2k''_{2zi}} \right].$$

The correlation function considered in this program is laterally Gaussian and vertically exponential. The corresponding spectral density is

$$\phi_m(\beta_\perp, \beta_z) = \frac{\ell_{zm} \ell_{\rho m}^2 \, e^{-\beta_\perp^2 \ell_{\rho m}^2 / 4}}{4\ ^2(1 + \beta_z^2 \ell_{zm}^2)}.$$

The rough surface effects which are superimposed incoherently using the model in Barrick's paper are given by the following equations (the rough surface is on the top layer):

$$\sigma_{R_{hh}} = \frac{\sec^4\theta_{oi}}{S^2} \left|\frac{k_o - k_1}{k_o + k_1}\right|^2 \exp\left(-\frac{1}{S^2}\tan^2\theta_{oi}\right)$$

$$\sigma_{R_{vv}} = \frac{\sec^4\theta_{oi}}{S^2} \left|\frac{\epsilon_o k_1 - \epsilon_1 k_o}{\epsilon_o k_1 + \epsilon_1 k_o}\right|^2 \exp\left(-\frac{1}{S^2}\tan^2\theta_{oi}\right).$$

And the total backscattering cross sections are given by

$\sigma_{R_{hh}} + \sigma_{hh}$ for the TE polarization

$\sigma_{R_{vv}} + \sigma_{vv}$ for the TM polarization

where, for $\ell, m = 0, 1, 2, 3$,

$$k_\ell = \omega\sqrt{\mu\langle\epsilon_\ell\rangle}$$

$$k_{\ell z} = \sqrt{k_\ell^2 - k_\perp^2}$$

$$R_{\ell m} = \frac{k_{\ell z} - k_{mz}}{k_{\ell z} + k_{mz}}$$

$$S_{\ell m} = \frac{\langle\epsilon_m\rangle k_{\ell z} - \langle\epsilon_\ell\rangle k_{mz}}{\langle\epsilon_m\rangle k_{\ell z} + \langle\epsilon_\ell\rangle k_{mz}}$$

$$X_{\ell m} = 1 + R_{\ell m}$$

$$Y_{\ell m} = 1 + S_{\ell m}$$

$$E_2 = 1 + S_{12}S_{23}\, e^{i2k_{2z}(d_2-d_1)} + S_{01}[S_{12} + S_{23}\, e^{i2k_{2z}(d_2-d_1)}]e^{i2k_{1z}d_1}$$

$$D_2 = 1 + R_{12}R_{23}\, e^{i2k_{2z}(d_2-d_1)} + R_{01}[R_{12} + R_{23}\, e^{i2k_{2z}(d_2-d_1)}]e^{i2k_{1z}d_1}.$$

A subscript "i" indicates that a quantity is to be evaluated at the incident wavevector angles in the appropriate region, e.g.,

$$R_{\ell mi} = \frac{k_{\ell zi} - k_{mzi}}{k_{\ell zi} + k_{mzi}} \qquad k_{\ell zi} = \sqrt{k_\ell^2 - k_{1i}^2} \qquad k_{1i} = k_o \sin\theta_{oi}.$$

The real and imaginary parts of a quantity are denoted by a prime and double primes, respectively, e.g.,

$$k'_{1z} = \mathrm{Re}\,(k_{1z}) \qquad k''_{1z} = \mathrm{Im}\,(k_{1z}).$$

Symbols

Fortran Symbol	Notation	Explanations
D1	d_1	Thickness of first random layer
D2	d_2	Thickness of first and second random layers
EPS1, EPS2	$\langle\epsilon_1\rangle, \langle\epsilon_2\rangle$	Mean permittivities of the first and second random layers, respectively
EPS0, EPS3	ϵ_o, ϵ_3	Permittivities of free space region and the homogeneous ground, respectively
K0, K1, K2, K3	k_o, k_1, k_2, k_3	Wave numbers in the air region (0-region), the first, second, and third regions, respectively
K1Z, K2Z, K3Z	k_{1z}, k_{2z}, k_{3z}	Components of the wave number in the z-direction in regions (1), (2), and (3), respectively
R01, R12, R23	$R_{01i}, R_{12i}, R_{23i}$	Reflection coefficients for the TE waves in regions (0), (1), and (2) at the boundaries separating regions (0)-(1), (1)-(2), and (2)-(3), respectively, evaluated at θ_{oi}
S01, S12, S23	$S_{01i}, S_{12i}, S_{23i}$	Reflection coefficients for the TM waves in regions (0), (1), and (2) at the boundaries separating regions (0)-(1), (1)-(2), and (2)-(3), respectively, evaluated at θ_{oi}

Fortran Symbol	Notation	Explanations
ZRHO1, ZRHO2	$\ell_{\rho 1}, \ell_{\rho 2}$	Lateral correlation lengths of fluctuation in permittivities in first and second regions, respectively
ZL1, ZL2	ℓ_{z1}, ℓ_{z2}	Vertical correlation lengths of fluctuation in permittivities in first and second regions, respectively
DEL1, DEL2	δ_1, δ_2	Variances of fluctuations in permittivities in first and second regions, respectively
E1A, E2A	$\langle \epsilon_1 \rangle' / \epsilon_o, \langle \epsilon_2 \rangle' / \epsilon_o$	Real parts of the mean dielectric constant in random media (1) and (2), respectively
E3A	ϵ_3' / ϵ_o	Real part of the dielectric constant in the homogeneous medium (3)
E1B, E2B	$\langle \epsilon_1 \rangle'' / \epsilon_o, \langle \epsilon_2 \rangle'' / \epsilon_o$	Imaginary parts of the mean dielectric constant in random media (1) and (2), respectively
E3B	$\epsilon_3'' / \epsilon_o$	Imaginary part of the dielectric constant in the homogeneous medium (3)
S2	s^2	Mean square slope of the rough surface
XINC, X	θ_{oi}	Fixed incidence angle and variable incidence angle, respectively
RSIGH, RSIGV	$\sigma_{R_{hh}}, \sigma_{R_{vv}}$	Backscattering cross sections for the TE and TM polarizations, respectively, due to rough surface effects
SIG1, SIG2	σ_{hh}, σ_{vv}	Backscattering cross sections for the TE and TM polarizations, respectively, due to volume scattering
FREQC, FREQ	f	Constant and variable frequencies, respectively

Features

A subroutine function called COR(KO, X, RL, RZ, K2R) is built into the program to compute the spectral density corresponding to a correlation function which is laterally Gaussian and vertically exponential.

It computes this spectral density according to the following equation:

$$\phi_m(\beta_\perp, \beta_z) = \frac{\ell_{zm}\ell_{\rho m}^2 \, e^{-\beta_\perp^2 \ell_{\rho m}^2/4}}{4\pi^2(1+\beta_z^2\ell_{zm}^2)}.$$

$\ell_{zm}, \ell_{\rho m}$ are the vertical and lateral correlation lengths in the m^{th} random layer, and the corresponding Fortran symbols are RZ, RL. The corresponding Fortran symbol for β_z is K2R.

Input and Output Format

(1) The input parameters are:

(i) ICHOIC

(ii) F, XO

(iii) DX, DF, XM, FM

(iv) AP, S2

(v) ZRHO1, ZRHO2, ZL1, ZL2, DEL1, DEL2

(vi) E1A, E1B, E2A, E2B, E3A, E3B

(vii) D1, D2

(viii) XINC or FREQC

Sets (i), (ii), and (iii) are read from a data file (with logical unit number 8) with the name BORNM DATA. Sets (iv), (v), (vi), (vii), and (viii) are input at the users terminal under a free format specification. The user is prompted with a message to enter the parameters of sets (iv), (v), (vi), (vii), and (viii) in a specified order.

All input parameters are in MKS units, frequency in Hz, and angles in degrees.

Fortran Symbol	Notation	Explanations
ICHOIC		If ICHOIC = 1 we plot SIGMA vs frequency. If ICHOIC = 2 we plot SIGMA vs incident angle
F, FM		Initial and final values of the variable frequency
DF		Increment step of the variable frequency
XO, XM		Initial and final values of the variable incident angle
DX		Increment step of the variable incident angle

Fortran Symbol	Notation	Explanations
AP		If AP = 1 rough surface effects are included. If AP = 0 rough surface effects are not included.
S2	s^2	Mean square slope of the rough surface
XINC	θ_{oi}	Fixed incident angle in degrees. If ICHOIC = 2, do not enter XINC. Instead, enter FREQC (each value of FREQC should be entered on a separate line).
FREQC	f	Fixed frequency in HZ, if we plot σ vs angle. If ICHOIC = 1, do not enter FREQC. Instead, enter XINC (each value of XINC should be entered on a separate line).

(2) The output parameters are: SIGMA VV, SIGMA HH, INC ANGLE (DEG) or FREQUENCY (GHZ).

SIGMA VV, SIGMA HH are the backscattering cross sections per unit area for the TM and TE polarizations, respectively, in dB. The format in which these appear is E13.7.

INC ANGLE (DEG) is the incident angle in degrees, if ICHOIC = 2. FREQUENCY (GHZ) is the frequency in GHZ, if ICHOIC = 1. The format in which these appear is F6.3.

```
C                         *PROGRAM BORNM*
C                    M. ZUNIGA - T. HABASHY
C
C
C
C     PROGRAM TO COMPUTE BACK SCATTERING CROSS SECTIONS/AREA IN THE
C     FIRST ORDER BORN APPROXIMATION FOR A THREE LAYER RANDOM MED.
C     THIS PROGRAM ALSO SUPERIMPOSES VERY ROUGH SURFACE EFFECTS
C     INCOHERENTLY USING THE MODEL IN BARRECKS PAPER
C
C
C
      COMPLEX EPS1,EPS2,EPS3,K1,K2,K3,K1Z,K2Z,K3Z
      COMPLEX X01,X12,Y01,Y12,D21,E2,AN1,BN1,A12I,A23I,ARG1,ARG2,PH1,PH2
      COMPLEX R10,R12,R23,S10,S12,S23
      REAL K0,K1R,K2R,K1ZR,K2ZR,KAZ1,KAZ2
      DATA EPS0,PI,U/8.85E-12,3.14159,1.2566E-6/
C
C     IF ICHOIC=1 WE PLOT SIGMA VS FREQ.
C     IF ICHOIC=2 WE PLOT SIGMA VS INC. ANGLE
C
      READ(8,*)ICHOIC
C
C     F IS THE INITIAL VALUE OF THE VARIABLE FREQ.,IN HZ.
C     XO IS THE INITIAL VALUE OF THE VARIABLE INC. ANGLE,IN DEG.
C
      READ(8,*) F,XO
C
C     DX IS THE INCREMENT STEP OF THE VARIABLE INC. ANGLE,IN DEG.
C     DF IS THE INCREMENT STEP OF THE VARIABLE FREQ.,IN HZ.
C     XM IS THE FINAL VALUE OF THE VARIABLE INC. ANGLE,IN DEG.
C     FM IS THE FINAL VALUE OF THE VARIABLE FREQ.,IN HZ.
C
      READ(8,*) DX,DF,XM,FM
      WRITE(6,1)
    1 FORMAT(3X,'IF APT=1 TOP ROUGH SURFACE EFFECTS ARE INCLUDED'/,3X,
     *'IF APT=0 TOP ROUGH SURFACE EFFECTS ARE NOT INCLUDED'/,3X,
     *'IF APB=1 BOTTOM ROUGH SURFACE EFFECTS ARE INCLUDED'/,3X,
     *'IF APB=0 BOTTOM ROUGH SURFACE EFFECTS ARE NOT INCLUDED'/,1X,
     *'ENTER APT,APB,S2T AND S2B IN THAT ORDER')
C
C     IF APT=1 TOP ROUGH SURFACE EFFECTS ARE INCLUDED
C     IF APT=0 TOP ROUGH SURFACE EFFECTS ARE NOT INCLUDED
C     IF APB=1 BOTTOM ROUGH SURFACE EFFECTS ARE INCLUDED
C     IF APB=0 BOTTOM ROUGH SURFACE EFFECTS ARE NOT INCLUDED
C     BY TOP ROUGH SURFACE WE MEAN ROUGH SURFACE AT THE INTERFACE
C      SEPERATING REGIONS (0) AND (1)
C     BY BOTTOM ROUGH SURFACE WE MEAN ROUGH SURFACE AT THE INTERFACE
C      SEPERATING REGIONS (2) AND (3)
C
C     S2T DENOTES THE MEAN SQUARE SLOPE AT THE TOP SURFACE
C     S2B DENOTES THE MEAN SQUARE SLOPE AT THE BOTTOM SURFACE
C
      READ(5,*)APT,APB,S2T,S2B
      WRITE(6,2)
```

```
    2 FORMAT(3X,'ENTER LRHO1,LRHO2,LZ1 AND LZ2 IN M.,ALSO ENTER DEL1',
     *' AND DEL2 IN THAT',/,1X,'ORDER')
C
C     ZRHO1,ZRHO2 DENOTE THE LATERAL CORRELATION LENGTHS OF FLUCTUATION
C     IN PERMITTIVITIES IN FIRST AND SECOND REGIONS RESPECTIVELY,IN M.
C     ZL1,ZL2 DENOTE THE VERTICAL CORRELATION LENGTHS,ALSO IN M.
C     DEL1,DEL2 DENOTE THE VARIANCES OF FLUCTUTIONS IN PERMITTIVITIES
C     IN FIRST AND SECOND REGIONS RESPECTIVELY
C
      READ(5,*)ZRHO1,ZRHO2,ZL1,ZL2,DEL1,DEL2
      WRITE(6,3)
    3 FORMAT(3X,'ENTER E1A,E1B,E2A,E2B,E3A AND E3B IN THAT ORDER')
C
C     E1A AND E2A ARE THE REAL PARTS OF THE MEAN DIELECTRIC CONSTANT IN
C     RANDOM MEDIA (1) AND (2) RESPECTIVELY
C     E3A IS THE REAL PART OF THE DIELECTRIC CONSTANT IN THE HOMOGENEOUS
C     MEDIUM (3)
C     E1B AND E2B ARE THE IMAGINARY PARTS OF THE MEAN DIELECTRIC CONSTANT
C     IN RANDOM MEDIA (1) AND (2) RESPECTIVELY
C     E3B IS THE IMAGINARY PART OF THE DIELECTRIC CONSTANT IN THE
C     HOMOGENEOUS MEDIUM (3)
C
      READ(5,*)E1A,E1B,E2A,E2B,E3A,E3B
      WRITE(6,4)
    4 FORMAT(3X,'ENTER D1 AND D2 IN METERS IN THAT ORDER')
C
C     D1 IS THE DEPTH OF THE FIRST REGION
C     D2 IS THE DEPTH OF THE FIRST AND SECOND REGIONS
C
      READ(5,*)D1,D2
      DX=DX*PI/180.
      XM=XM*PI/180.
C
C     EPS1 AND EPS2 ARE THE COMPLEX MEAN PERMITTIVITIES IN REGIONS
C     (1) AND (2) RESPECTIVELY
C     EPS3 IS THE COMPLEX PERMITTIVITY IN THE HOMOGENEOUS MEDIUM
C     (3)
C
      EPS1=EPSO*CMPLX(E1A,E1B)
      EPS2=EPSO*CMPLX(E2A,E2B)
      EPS3=EPSO*CMPLX(E3A,E3B)
      IF(APT.EQ.0..AND.APB.EQ.1.)WRITE(6,911)
      IF(APB.EQ.0..AND.APT.EQ.1.)WRITE(6,912)
      IF(APT.EQ.1..AND.APB.EQ.1.)WRITE(6,913)
      IF(APT.EQ.0..AND.APB.EQ.0.)WRITE(6,914)
  911 FORMAT(3X,'ONLY BOTTOM ROUGH SURFACE EFFECTS ARE INCLUDED')
  912 FORMAT(3X,'ONLY TOP ROUGH SURFACE EFFECTS ARE INCLUDED')
  913 FORMAT(3X,'BOTH TOP AND BOTTOM ROUGH SURFACE EFFECTS ARE INCLUDED'
     *)
  914 FORMAT(3X,'NO ROUGH SURFACE EFFECTS ARE INCLUDED')
  107 CONTINUE
      IF(ICHOIC.EQ.2)GO TO 111
C
C    XINC IS THE FIXED INC. ANGLE,IN DEG. _ IF ICHOIC = 2 DO NOT ENTER
C    XINC ,  INSTEAD ENTER FREQC [EACH VALUE OF FREQC SHOULD BE ENTERED
```

```
C     ON A SEPERATE LINE]
C
      READ(8,*,END=106)XINC
      FREQ=F
      GO TO 112
C
C     FREQC IS THE FIXED FREQ.,IN HZ. - IF ICHOIC = 1 DO NOT ENTER FREQC
C     INSTEAD ENTER XINC [EACH VALUE OF XINC SHOULD BE ENTERED ON A
C     SEPERATE LINE]
C
  111 READ(8,*,END=106)FREQC
      X=XC
      FRET=FREQC/1.0E+9
  112 IF(ICHOIC.EQ.2)GO TO 61
      X=XINC*(PI/180.)
      WRITE(6,25)XINC
   25 FORMAT(3X,'INC ANGLE(DEG)=',F7.3)
      WRITE(6,26)
   26 FORMAT(5X,'SIGMA VV',11X,'SIGMA HH',9X,'FREQUENCY(GHZ)')
      GO TO 18
   61 FREQ=FREQC
      WRITE(6,24)FRET
   24 FORMAT(3X,'FREQUENCY(GHZ)=',F7.3)
      WRITE(6,27)
   27 FORMAT(5X,'SIGMA VV',11X,'SIGMA HH',9X,'INC ANGLE(DEG)')
   18 W=2.*PI*FREQ
C
C     K0,K1,K2,K3 ARE THE WAVE NUMBERS IN THE AIR REGION [(0)-REGION],
C     THE FIRST , SECOND AND THIRD REGIONS RESPECTIVELY
C
      K0=W*SQRT(U*EPS0)
      K1=W*CSQRT(U*EPS1)
      K2=W*CSQRT(U*EPS2)
      K3=W*CSQRT(U*EPS3)
      K1R=REAL(K1)
      K2R=REAL(K2)
C
C     IPOL=0 CORRESPONDS TO TE POLARIZATION
C     IPOL=1 CORRESPONDS TO TM POLARIZATION
C
    5 IPOL=0
      AN=1.
      BN=1.
      Y=COS(X)
      YS=SIN(X)
C
C     K1Z,K2Z,K3Z ARE THE COMPONENTS OF THE WAVE NUMBER IN THE
C     Z-DIRECTION IN REGIONS (1),(2)&(3) RESPECTIVELY
C
      K1Z=CSQRT(K1*K1-K0*K0*YS*YS)
      K2Z=CSQRT(K2*K2-K0*K0*YS*YS)
      K3Z=CSQRT(K3*K3-K0*K0*YS*YS)
      K1ZR=REAL(K1Z)
      K2ZR=REAL(K2Z)
      KAZ1=2.*AIMAG(K1Z)
```

```
      KAZ2=2.*AIMAG(K2Z)
C
C     R01,R12,R23 ARE THE REFLECTION COEFFICIENTS FOR TE WAVES IN REGIONS
C     (0),(1)&(2) AT THE BOUNDERIES SEPERATING REGIONS (0)-(1),(1)-(2)
C     &(2)-(3) RESPECTIVELY
C     R10=-R01
C
      R10=(K1Z-K0*Y)/(K1Z+K0*Y)
      R12=(K1Z-K2Z)/(K1Z+K2Z)
      R23=(K2Z-K3Z)/(K2Z+K3Z)
      A12I=R12
      A23I=R23
C
C     S01,S12,S23 ARE THE REFLECTION COEFFICIENTS FOR TM WAVES IN REGIONS
C     (0),(1)&(2) AT THE BOUNDERIES SEPERATING REGIONS (0)-(1),(1)-(2)
C     &(2)-(3) RESPECTIVELY
C     S10=-S01
C
      S10=(EPS0*K1Z-EPS1*K0*Y)/(EPS0*K1Z+EPS1*K0*Y)
      S12=(EPS2*K1Z-EPS1*K2Z)/(EPS2*K1Z+EPS1*K2Z)
      S23=(EPS3*K2Z-EPS2*K3Z)/(EPS3*K2Z+EPS2*K3Z)
      X01=1.-R10
      X12=1.+R12
      Y01=1.-S10
      Y12=1.+S12
      PHAS1=D1*KAZ1
      PHAS2=(D2-D1)*KAZ2
      PHAS3=D2*KAZ2
C
C     THE FOLLOWING THREE STEPS ARE TO AVOID THE UNDERFLOW RESULTING FROM
C     THE HIGH NEGATIVE POWER OF THE EXPONENTIAL FUNCTION
C
      IF(PHAS1.GT.18.)PHAS1=18.
      IF(PHAS2.GT.18.)PHAS2=18.
      IF(PHAS3.GT.18.)PHAS3=18.
      ARG1=COS(2.*D1*K1ZR)+CMPLX(0.,1.)*SIN(2.*D1*K1ZR)
      ARG2=COS(2.*(D2-D1)*K2ZR)+CMPLX(0.,1.)*SIN(2.*(D2-D1)*K2ZR)
      PH1=ARG1*EXP(-PHAS1)
      PH2=ARG2*EXP(-PHAS2)
C
C     THE FOLLOWING SECTION COMPUTES THE BACKSCATTERING CROSS SECTIONS
C     /AREA DUE TO VOLUME SCATTERING
C
      D21=1.+R12*R23*PH2-R10*(R12+R23*PH2)*PH1
      E2=1.+S12*S23*PH2-S10*(S12+S23*PH2)*PH1
      C1=PI*PI*((CABS(X01/D21))**4)
      C2=C1*DEL2*(K2R**4)*((CABS(X12))**4)
      C1=C1*DEL1*(K1R**4)
      GO TO 10
   20 AN1=((K0*YS)**2-K1Z*K1Z)
      AN=((CABS(AN1))**2)/((CABS(K1))**4)
      BN1=((K0*YS)**2-K2Z*K2Z)
      BN=((CABS(BN1))**2)/((CABS(K2))**4)
      A12I=S12
      A23I=S23
```

```
      C1=PI*PI*((CABS(Y01/E2))**4)*(K0**4)                              BOR02210
      C2=C1*DEL2*(K2R**4)*((CABS(Y12))**4)/((CABS(K2))**4)              BOR02220
      C1=C1*DEL1*(K1R**4)/((CABS(K1))**4)                               BOR02230
   10 T1=(CABS(A12I+A23I*PH2))**2                                       BOR02240
      T2=(CABS(1.+A12I*A23I*PH2))**2                                    BOR02250
      T3=8.*D1*T1*T2*EXP(-2.*PHAS1)*COR(K0,X,ZRHO1,ZL1,0.0)*AN          BOR02260
      T3=T3+(T1*T1*EXP(-2.*PHAS1)+T2*T2)*(1.-EXP(-2.*PHAS1))*           BOR02270
     *COR(K0,X,ZRHO1,ZL1,K1ZB)/KAZ1                                     BOR02280
      T4=8.*(D2-D1)*((CABS(A23I))**2)*EXP(-PHAS2)*COR(K0,X,ZRHO2,ZL2,0.)BOR02290
     **EXP(-PHAS1)*EXP(-PHAS3)*BN                                       BOR02300
      T4=T4+(((CABS(A23I))**4)*EXP(-2.*PHAS2)+1.)*(1.-EXP(-2.*PHAS2))   BOR02310
     **EXP(-2.*PHAS1)*COR(K0,X,ZRHO2,ZL2,K2ZR)/KAZ2                     BOR02320
      SIG=C1*T3+C2*T4                                                   BOR02330
      IF(IPOL.EQ.1)GO TO 30                                             BOR02340
      SIG1=SIG                                                          BOR02350
      IPOL=1                                                            BOR02360
      GO TO 20                                                          BOR02370
   30 SIG2=SIG                                                          BOR02380
C                                                                       BOR02390
C    END OF BACKSCATTERING CROSS SECTIONS/AREA DUE TO VOLUME SCATTERING BOR02400
C                                                                       BOR02410
C    ROUGH SURFACE CALCULATION FOLLOWS,USING THE MODEL IN BARRECKS PAPERBOR02420
C                                                                       BOR02430
C    ROUGH SURFACE AT TOP,CALCULATION FOLLOWS                           BOR02440
C                                                                       BOR02450
      S2=S2T                                                            BOR02460
      AP=APT                                                            BOR02470
C                                                                       BOR02480
C    RR IS THE TE.,SS IS THE TM.,REFLECTION COEFFICIENT AT 0 INCIDENT   BOR02490
C    ANGLE AS REQUIRED FOR THE ROUGH SURFACE CALCULATION.               BOR02500
C                                                                       BOR02510
      RR=CABS((K0-K1)/(K0+K1))                                          BOR02520
      SS=CABS((EPS0*K1-EPS1*K0)/(EPS0*K1+EPS1*K0))                      BOR02530
      TN2=(SIN(X)/COS(X))**2                                            BOR02540
      CHECK2=TN2/S2                                                     BOR02550
      IF(CHECK2.GT.70.)RSIGVB=0.                                        BOR02560
      IF(CHECK2.GT.70.)GO TO 98                                         BOR02570
      SC4=1./(COS(X)**4)                                                BOR02580
      RSIGV=(AP/S2)*SC4*SS*SS*EXP(-TN2/S2)                              BOR02590
   98 RSIGH=RSIGV*RR*RR/(SS*SS)                                         BOR02600
C                                                                       BOR02610
C    END OF TOP ROUGH SURFACE CALCULATION                               BOR02620
C                                                                       BOR02630
C    ROUGH SURFACE AT BOTTOM,CALCULATION FOLLOWS                        BOR02640
C                                                                       BOR02650
      XI2=ARSIN((K0/K2R)*SIN(X))                                        BOR02660
      RR=CABS((K2-K3)/(K2+K3))                                          BOR02670
      SS=CABS((EPS2*K3-EPS3*K2)/(EPS2*K3+EPS3*K2))                      BOR02680
      TN2=(SIN(XI2)/COS(XI2))**2                                        BOR02690
      CHECK2=TN2/S2B                                                    BOR02700
      IF(CHECK2.GT.70.)RSIGV=0.                                         BOR02710
      IF(CHECK2.GT.70.)GO TO 102                                        BOR02720
      SC4=1./(COS(XI2)**4)                                              BOR02730
      RSIGVB=(APB/S2B)*SC4*SS*SS*EXP(-CHECK2)                           BOR02740
  102 CONTINUE                                                          BOR02750
```

```
      RSIGHB=RSIGVB*RR*RR/(SS*SS)
      PHAS=2.*(PHAS1+PHAS2)
      IF(PHAS.GT.18.)PHAS=18.
      RSIGVB=RSIGVB*EXP(-PHAS)
      RSIGHB=RSIGHB*EXP(-PHAS)
C
C     END OF BOTTOM ROUGH SURFACE CALCULATION
C
      RSIGV=RSIGV+RSIGVB
      RSIGH=RSIGH+RSIGHB
      SIG1=SIG1+RSIGH
      SIG2=SIG2+RSIGV
      SIG1=10.*ALOG10(SIG1)
      SIG2=10.*ALOG10(SIG2)
      ZZ=X*(180./PI)
      IF(ICHOIC.EQ.1)ZZ=FREQ/1.0E+9
      WRITE(6,19)SIG2,SIG1,ZZ
   19 FORMAT(3X,E13.7,6X,E13.7,9X,F7.3)
      IF(ICHOIC.EQ.2)X=X+DX
      IF(ICHOIC.EQ.1)FREQ=FREQ+DF
      IF(ICHOIC.EQ.2.AND.X.LT.XM)GO TO 5
      IF(ICHOIC.EQ.1.AND.FREQ.LT.FM)GO TO 18
      GO TO 107
  106 STOP
      END
C
C     THE FOLLOWING IS A FUNCTION SUBROUTINE TO CALCULATE THE SPECTRAL
C     DENSITY CORRESPONDING TO A CORRELATION FUNCTION WHICH IS GAUSSIAN
C     LATERALLY AND EXPONENTIAL VERTICALLY
C
      FUNCTION COR(K0,X,RL,RZ,K2R)
      REAL K0,K2R
      Y=SIN(X)
      PI=3.14159
      TRS=K0*K0*RL*RL*Y*Y
      IF(TRS.GT.18.)TRS=18.
      COR=RZ*RL*RL*EXP(-TRS)/(4.*PI*PI*(1.+4.*K2R*K2R*RZ*RZ))
      RETURN
      END
```

SECTION VIII
PUBLICATIONS

The work performed during the period of February 1, 1978 - September 30, 1979 has been published in the categories of:

A. referred journal articles
B. conference papers
C. technical reports

A. Referred Journal Articles

A.1 L. Tsang and J. A. Kong, "Radiative transfer theory for active remote sensing of half space random media," Radio Science 13, no. 5, 763-774, Sept.-Oct. 1978.

A.2 L. Tsang and J. A. Kong, "Radiative transfer theory for scattering by layered media," Journal of Applied Physics 50, 2465-2469, April 1979.

A.3 L. Tsang and J. A. Kong, "Wave theory for microwave remote sensing of a half-space random medium with three-dimensional variations," Radio Science 14, no. 3, 359-369, May-June 1979.

A.4 J. A. Kong, R. Shin, J. C. Shiue, and L. Tsang, "Theory and experiment for passive microwave remote sensing of snowpacks," Journal of Geophysical Research 84, no. B10, 5669-5673, Sept. 1979.

A.5 M. A. Zuniga, T. M. Habashy, and J. A. Kong, "Active remote sensing of layered random media," IEEE Transactions on Geoscience Electronics GE-17, no. 4, 296-302, Oct ber 1979.

A.6 B. Djermakoye and J. A. Kong, "Radiative-transfer theory for the remote sensing of layered random media," Journal of Applied Physics 50, no. 11, 6600-6604, November 1979.

A.7 M. Zuniga and J. A. Kong, "Active remote sensing of random media," Journal of Applied Physics 51, 74-79, January 1980.

A.8 L. Tsang and J. A. Kong, "Energy conservation for reflectivity and transmissivity at a very rough surface," Journal of Applied Physics 51, 673-680, January 1980.

A.9 M. Zuniga, J. A. Kong, and L. Tsang, "Depolarization effects in the active remote sensing of random media," Journal of Applied Physics 51, 2315-2325, May 1980.

B. Conference Papers

B.1 J. C. Shiue, J. A. Kong, H. A. Boyne, A. T. Chang, D. A. Ellerbruch, and L. Tsang, "Microwave remote sensing of snow pack characteristics," URSI/USNC Symposium, May 18, 1978.

B.2 J. A. Kong, L. Tsang, and B. Djermakoye, "Remote sensing of a buried scattering layer," URSI/USNC Symposium, May 18, 1978.

B.3 J. A. Kong, M. Caulfield, J. C. Shiue, R. Shin, and L. Tsang, "Single frequency microwave remote sensing of snow on an aluminum plate," International Symposium on Antennas and Propagation, Japan, August 1978.

B.4 J. A. Kong, L. Tsang, B. Djermakoye, R. Shin, and J. C. Shiue, "Passive microwave remote sensing of snowpacks," URSI Meeting, Boulder, Colorado, November 6-9, 1978.

B.5 J. A. Kong, L. Tsang, M. Zuniga, and R. Shin, "Theoretical models and approaches for active and passive microwave remote sensing," URSI Meeting, Seattle, Washington, June 1979.

B.6 J. A. Kong, M. Zuniga, L. Tsang, and R. Shin, "Experimental data matching for active and passive microwave remote sensing," URSI Meeting, Seattle, Washington, June 1979.

B.7 J. A. Kong, L. Tsang, M. Zuniga, R. Shin, J. C. Shiue, and A. T. C. Chang, "Theoretical modelling and experimental data matching for active and passive microwave remote sensing of earth terrain," Symposium on Terrain Profiles and Contours in EM Wave Propagation, AGARD/NATO Meeting, Norway, September 1979.

B.8 J. A. Kong, M. Zuniga, T. Habashy, L. Tsang, R. Shin, and B. Djermakoye, "Random medium model applied to active and passive microwave remote sensing of earth terrain," URSI Meeting, Boulder, Colorado, November 5-8, 1979.

C. Reports

C.1 R. T. Shing and M. A. Zuniga, "Ground-truth of snow fields in the Rome, New York area during January 1979," Technical Report, MIT, 1979.

C.2 R. T. Shin and M. A. Zuniga, "Ground-truth of snow fields in the Rogers City, Michigan area during February 1979," Technical Report, MIT, 1979.

SECTION IX
LIST OF APPENDICES

Appendix A

"Review of remote sensing theories and experiments pertaining to snow," Report to AIR FORCE/EGLIN, Contract F08635-78-C-0115, MIT, 1978.

Appendix B

"Ground-truth of snow fields in the Rome, New York area during January 1979," R. T. Shin and M. A. Zuniga, Technical Report, MIT, 1979.

Appendix C

"Ground-truth of snow fields in the Rogers City, Michigan area during February 1979," R. T. Shin and M. A. Zuniga, Technical Report, MIT, 1979.

REFERENCES

1. J. A. Kong, L. Tsang, M. Zuniga, R. Shin, J. C. Shiue, and A. T. C. Chang, "Theoretical modelling and experimental data matching for active and passive microwave remote sensing of earth terrain," Symposium on Terrain Profiles and Contours in EM Wave Propagation, AGARD/NATO Meeting, Norway, September 1979.

2. M. Zuniga and J. A. Kong, "Active remote sensing of random media," J. Appl. Phys., 51, 74-79, January 1980.

3. M. A. Zuniga, T. M. Habashy, and J. A. Kong, "Active remote sensing of layered random media," IEEE Transactions on Geoscience Electronics, GE-17, no. 4, 296-302, October 1979.

4. M. Zuniga, J. A. Kong, and L. Tsang, "Depolarization effects in the active remote sensing of random media," J. Appl. Phys., 51, 2315-2325, May 1980.

5. L. Tsang and J. A. Kong, "Radiative transfer theory for active remote sensing of half space random media," Radio Science, 13, no. 5, 763-775, Sept.-Oct. 1978.

6. J. A. Kong, R. Shin, J. C. Shiue, and L. Tsang, "Theory and experiment for passive microwave remote sensing of snowpacks," J. Geophys. Res., 84, no. B10, 5669-5673, Sept. 1979.

7. L. Tsang and J. A. Kong, "Radiative transfer theory for scattering by layered media," J. Appl. Phys., 50, 2465-2469, April 1979.

8. B. Djermakoye and J. A. Kong, "Radiative transfer theory for the remote sensing of layered random media," J. Appl. Phys., 50, 6600-6604, November 1979.

9. L. Tsang and J. A. Kong, "Wave theory for microwave remote sensing of a half-space random medium with three-dimensional variations," Radio Science, 14, no. 3, 359-369, May-June 1979.

10. L. Tsang and J. A. Kong, "Energy conservation for reflectivity and transmissivity at a very rough surface," J. Appl. Phys., 51, 673-680, January 1980.

11. J. A. Kong, M. Caulfield, J. C. Shiue, R. Shin, and L. Tsang, "Single frequency microwave remote sensing of snow on an aluminum plate," International Symposium on Antennas and Propagation, Japan, August 1978.

APPENDIX A

REVIEW OF REMOTE SENSING THEORIES AND EXPERIMENTS PERTAINING TO SNOW

APPENDIX A CONTENTS

SECTION I
REMOTE SENSING THEORIES

In the remote sensing of snow it is well known that volume scattering due to medium inhomogeneity plays a dominant role. This requires that all theoretical models be accountable for the scattering properties of snow. The effects of volume scattering have been accounted for by characterizing a medium either as a random medium or as a homogeneous background medium containing discrete scatterers. Theoretical models of a vertically structured nonrandom medium (References 1-4) cannot be applied to the remote sensing of snow since the volume scattering properties of snow are not accounted for.

The active and the passive remote sensing theories of snow are reviewed separately in this report. In active sensing we are interested in the reflection coefficients, and the backscattering cross sections. In passive remote sensing we are interested in the brightness temperature and the emissivity. While the primary interest in radar studies lies in the backscattering cross sections, both the reflection coefficients and the bistatic scattering coefficients are of significance to passive remote sensing theories. However, papers on active remote sensing which may have applications in passive remote sensing are not reviewed again in the passive section unless such applications are specifically developed in those papers.

A. Active

(1) Random Medium Model.

Stogryn (Reference 5) considered the electromagnetic scattering by a bounded medium whose dielectric constant contains a small random part and a nonrandom part which can vary as a func-

tion of depth. First order perturbation theory by Karal and Keller (Reference 166) is used to derive equations satisfied by the mean fields and random components of the fields. The reflection coefficient is derived by solving the equations satisfied by the mean fields. Then the bistatic scattering coefficients are derived by first solving for the random component of the field and then taking the expected value of the product of random component of the field and its complex conjugate. The cross-polarized scattering coefficients are shown to vanish in the backscattering direction. This is expected since only the first-order terms are considered and contribution to the cross-polarized scattering coefficients in the backscattering direction comes from the higher-order terms. Also, the assumption that the correlation lengths are small compared to the wavelength is made which makes his results applicable in the low-frequency limit when such assumption is satisfied.

Tsang and Kong (Reference 6) investigated the problem of scattering by a slab random medium with a laminar structure and bounded by a different dielectric on each side for a normally incident monochromatic plane wave. The renormalization method gives rise to the Dyson equation for the mean field and the Bethe-Salpeter equation for the covariance of the field in the random medium. A two-variable expansion technique is used to solve for the zeroth-order mean Green's function from the Dyson equation under the nonlinear approximation. The mean Green's function is then used to derive modified radiative transfer (MRT) equations from the Bethe-Salpeter equation under the ladder approximation. The MRT equations are solved for a two-layer random medium and the reflectivity at normal incidence is determined.

Tsang and Kong (Reference 7) also studied scattering of electromagnetic waves by a half-space random medium with three-dimensional correlation functions. For a plane wave incident upon a random half-space, the scattered fields in nonrandom medium are obtained by employing the dyadic Green's function for a half-space medium and by

the Born approximation where the field in the random medium is replaced by the unperturbed field. Then, following Peake's (Reference 8) definition, the bistatic scattering coefficients are derived from the scattered fields. The cross-polarized scattering coefficients in the backscattering direction also vanish since the Born approximation is a single-scattering approximation which is only valid when the albedo is small.

Parashar et al. (Reference 9) considered the electromagnetic wave scattering from a slab of inhomogeneous medium with a slightly rough boundary surface. There has been much work on the electromagnetic wave scattering from a homogeneous medium with a rough surface but there is no previous work which accounts for both the volume scattering and the rough surface scattering characteristics of a medium. In the Parashar model the inhomogeneity in the medium is assumed to vary continuously in the vertical direction and has a small random variation in the horizontal direction. The scattering medium is assumed to consist of two layers where one region has increasing permittivity and the other region has decreasing permittivity in the vertical direction. Maxwell's equations are solved using the perturbation method together with Fourier transform technique. The resulting differential equations are solved by using WKB and variation of parameter methods. Field amplitudes in each medium are determined by taking boundary conditions into account and the expression for the first-order backscattering cross sections are obtained. Again the cross-polarized backscattering cross sections are zero.

Tsang and Kong (Reference 10) developed the radiative transfer theory to calculate the bistatic scattering coefficients and the backscattering cross-sections from a half-space random medium with lateral and vertical fluctuations. The radiative transfer equations without the usual emission terms are written down for the intensities in the random medium. The incident beam is taken into account by

choosing appropriate boundary conditions. Once the radiative transfer equations with the appropriate boundary conditions are solved for the intensities in the random medium, the intensities scattering into the non-random medium can be easily obtained. They solved the radiative transfer equations by an iterative process to the second order in the albedo. To the first order in the albedo, which is the same as taking the Born approximation in the wave approach, cross-polarized scattering coefficients are shown to vanish in the backscattering direction. However, in the second order they obtained cross-polarized scattering coefficients in the backscattering direction to exhibit depolarization effects of backscattered power.

(2) Discrete Scatterer Model:

Leader (Reference 11) studied the electromagnetic wave scattering from Rayleigh scatterers embedded in a dielectric slab. First the matrix doubling method developed by Twomey et al. (Reference 12) is extended to permit calculations of the polarization components of light intensities scattered in the plane of incidence from a mono-dispersive medium of Rayleigh scatterers. The technique developed by Twomey et al. provides a method for determining the scattering properties of the sum of two layers in terms of their respective properties. With this method the scattering properties of a thick scattering layer can be calculated from the knowledge of scattering properties of very thin layers whose scattering properties are approximated by the single scattering phase functions. The scattering matrix thus obtained is modified to account for dielectric discontinuities of the surfaces of a slab medium in which the scattering centers are embedded. Then the scattering cross-sections are obtained for scattered angles in the plane of incidence.

B. Passive

(1) Random Medium Model:

Gurvich et al. (Reference 13) first derived the expression for the emissivity of a half-space random medium with a laminar structure in the single scattering approximation. The emissivity is obtained by reciprocity after solving for the power coefficient of reflection from the surface and the power coefficient of scattering into the upper hemisphere. The single scattering approximation and the laminar structure of the medium are used to calculate the power coefficient of scattering.

Applying a radiative transfer approach, Tsang and Kong (Reference 14) solved the problem of microwave thermal emission from a half-space random medium with a laminar structure and nonuniform temperature distribution in the vertical direction. Because of the laminar structure of the problem considered, horizontally and vertically polarized intensities are uncoupled and the radiative transfer equations reduce from the usual integro-differential equation to a first order differential equation for each polarization. The radiative transfer equation is then solved for the intensities in the random medium, subject to the boundary conditions. After the upward intensity in the random medium is obtained, it is easily related to the brightness temperature in the upper medium. For constant absorption and scattering coefficients, the brightness temperature is determined by a simple closed-form formula. An iteration approach is also discussed for the general case when absorption and scattering coefficients are not constants.

The reflectivity of a wave at normal incidence upon a two-layer medium where top layer is a random medium with a laminar structure was derived by Tsang and Kong (Reference 6) by solving the MRT equations. This result can be applied to the passive remote sensin since by reciprocity emissivity is one minus reflectivity. They also derived the emissivity of a half-space random medium with

three-dimensional correlation functions by first calculating the bistatic scattering coefficients with the Born approximation and then obtaining emissivities following Peake's (Reference 7) definition.

Tsang and Kong (Reference 15) calculated the brightness temperature resulting from microwave thermal emission from half-space random medium with a nonuniform temperature profile in the vertical direction and a three-dimensional correlation function. The scattering phase functions and the scattering coefficients are first derived then are used in the radiative transfer equations. The radiative transfer equations for the random medium with three-dimensional correlation functions are two coupled integral-differential equations for the horizontally and vertically polarized intensities. The radiative transfer equations and the appropriate boundary conditions are cast into the integral equation form. Then by assuming a small albedo, an iterative approach is used to solve for the zeroth and the first order upward propagating intensities. Then for the general case the integro-differential radiative transfer equations are solved by a numerical approach. Following Chandrasekhar (Reference 167), the radiative transfer equations are cast into quadrature form by using the even-order Legendre polynomials. The radiative transfer equations are turned into a system of ordinary differential equations with constant coefficients. This is then solved by obtaining eigenvalues and eigenvectors and matching the boundary conditions.

Tsang (Reference 16) studied the thermal microwave emission from a scattering layer overlying a homogeneous half-space with a radiative transfer approach. The scattering layer has a nonuniform temperature profile and is characterized by three-dimensional correlation functions. The radiative transfer equations are cast into a system of first order differential equations using the Gaussian quadrature method. These equations are solved by both the classical

AD-A116 448   MASSACHUSETTS INST OF TECH CAMBRIDGE RESEARCH LAB OF--ETC F/G 17/9
PREDICTION OF BACKSCATTER AND EMISSIVITY OF SNOW AT MILLIMETER --ETC(U)
JAN 80   J A KONG, R T SHIN   F08635-78-C-0115

UNCLASSIFIED   AFATL-TR-80-33   NL

2 of 3
AD A
116448

method of calculating eigenvalues and eigenvectors, and the method of invariant imbedding.

Tsang and Kong (Reference 17) used a radiative transfer approach to study the thermal microwave emission from a inhomogeneous slab random medium bounded by different dielectrics on both sides. The random medium can have nonuniform absorption, scattering and temperature profiles and can be characterized by one-dimensional correlation functions or by three-dimensional correlation functions. With the method of invariant imbedding the boundary value problem of the radiative transfer equations is converted to a initial value problem starting at zero slab thickness. For the case of three-dimensional correlation functions, the Gaussian quadrature method is used to cast the radiative transfer equations into a system of first-order differential equations before they are solved by the method of invariant imbedding. The invariant imbedding equations so obtained are in the form of first-order ordinary equations and these equations can be solved by standard methods of initial value problems to get numerical results.

Fisher (Reference 18) also studied the thermal microwave emission from a inhomogeneous slab random medium with a radiative transfer approach. The scattering medium is characterized by three dimensional correlation functions, as well as nonrandom variations in permittivity, temperature and loss. The radiative transfer equations are solved by the Gaussian quadrature method and the invariant imbedding methods.

(2) Discrete Scatterer Model:

England (Reference 19) first studied the thermal microwave emission from a uniform half-space containing isotropic scatterers and possessing a nonuniform temperature profile with a radiative transfer approach. Isotropic scatterers are assumed to redistribute incident radiations in all directions evenly. Also assuming

that there is no exchange of energy between polarizations, resulting radiative transfer equations are cast into a system of ordinary first-order differential equations by the Gaussian quadrature method. These equations are solved by calculating the eigenvalues and eigenvectors, and by matching the boundary conditions. He then treated the case of scattering layer over a homogeneous half-space where scattering medium is characterized by a uniform layer containing Rayleigh scatterers (Reference 20). Then the resulting radiative transfer equations for the intensities in the scattering layer are solved numerically in the same way.

Chang et al. (Reference 21) studied the thermal microwave emission from a scattering layer on top of a homogeneous half-space. The scattering layer has the same background medium as the upper half-space and contains randomly spaced scattering spheres. The Mie theory is then used to calculate the extinction and scattering cross-sections of individual spheres. These quantities with the Mie-scattering phase functions are used in the radiative transfer equations. Then the radiative transfer equations are solved numerically for the intensities normal to the surface by a variation of the Gauss-Seidel method.

Tsang and Kong (Reference 22) also developed the theory of thermal microwave emission from a half-space homogeneous medium containing spherical scatterers with a radiative transfer approach using Mie-scattering phase functions. The radiative transfer equations are first solved by an iterative approach and a closed form solution is obtained. Then for the general case the Gaussian quadrature method is used to convert the radiative transfer equations into a system of ordinary first-order differential equations. The brightness temperature is solved for by calculating eigenvalues and eigenvectors and then matching the boundary conditions. Also, in addition to the monodisperse case involving only single size scatterers, they extended their result to the case involving a distribution of different size particles.

Tsang (Reference 16) also treated the more general case of thermal microwave emission from a homogeneous slab containing spherical scatterers overlying a different homogeneous half-space. The radiative transfer equations are cast into a system of ordinary first order differential equations and solved by both the classical method of calculating eigenvalues and eigenvectors and the method of invariant imbedding.

SECTION II
EXPERIMENTS

A. Active Remote Sensing

Sackinger and Byrd (References 23,24) studied the details of the electromagnetic wave backscattering at 35 GHz from snow-covered land, fresh ice and sea ice. Backscattering measurements were made as a function of angle of incidence for several different snow conditions. Both horizontal and vertical polarizations have been used, and using separate transmitting and receiving antennas, they made the backscattering measurements for horizontal, vertical, and cross-polarization cases.

Hoekstra and Spanogle (Reference 25) made measurements of the backscatterer from snow and ice surfaces for the design of a terrain avoidance system. The following two types of measurements were made on the snow surfaces:

(1) The terrain clutter from undisturbed snow surfaces was measured at frequencies of 10, 35 and 95 GHz, at grazing angles of 1 to 0.3 degrees. At 10 GHz the measurements were made for linear, circular and cross polarizations; at 35 GHz, for linear and cross polarizations; and at 95 GHz, for linear polarization.

(2) The terrain clutter from periodically spaced trenches in the snow surface was measured at 10 GHz and 35 GHz, at grazing angles of 1.0, 0.65 and 0.38 degrees, for linear polarization.

Currie et al. (Reference 26) made a series of radar measurements on the backscattering properties of smooth snow at 35 GHz

and 95 GHz. The bulk of the measurements were made at grazing angles between 8 and 15 degrees. The backscattering cross-sections were studied at 35 GHz and 95 GHz as functions of polarization, frequency, depression angle and time. The snowpack ground-truth data were collected in the conjunction with the radar measurements.

Ulaby et al. (Reference 27) investigated the angular, spectral, and polarization dependence of the backscattering coefficient on a select set of snow parameters-- depth, density, water equivalence, and temperature. The 1-8 GHz microwave active spectrometer (MAS) system was used to measure the backscattering response from ground covered with a relatively thin layer of snow. The scattering coefficients were measured for three linear polarization configurations (HH, VV, and HV) at angles of incident between nadir and 70 degrees. The ground data acquired in conjunction with the spectrometer measurements include soil moisture, soil temperatures at different locations and depths, air temperature, snow depth, snow density profile, and snow water equivalent profile.

B. Passive Remote Sensing

In a research conducted by the Geoscience Laboratory (References 28-30), Advanced Microwave Systems Division of Space-General Corporation, the microwave thermal emission characteristics of a number of natural surfaces including snow fields have been investigated. Both the laboratory measurements and the in-situ field measurements were made for various snow conditions at 13.5 GHz and 37 GHz as functions of angle as well as time.

Edgerton et al. (References 31, 32) also investigated the microwave thermal emission of snowpacks. Field measurements of brightness temperatures were conducted at wavelengths of 0.8, 2.2, 6 and 21 cm (37, 13.4, 4.99 and 1.42 GHz). The brightness

temperature is measured as a function of snow equivalence (water mass) for dry and wet snow on top of soil and for natural snow on top of aluminum plates.

During March of 1971, the NASA Convair 990 Airborne Observatory carrying microwave radiometers in the wavelength range of 0.8 to 21 cm was flown over dry snow fields with different substrata making brightness temperature measurements (Reference 33). At the same time the brightness temperature measurements were made on the plane, ground-truth measurements of each test site were also made.

Hofer and Schanda (Reference 34) started a long-term observational study of the microwave emission and scattering behavior of snow under quasi-controlled conditions, with five radiometers at frequencies of 4.9, 10.5, 21, 36, and 94 GHz. The brightness temperature measurements were made as a function of angle in the morning and afternoon measuring cycles. The brightness temperature measurements as a function of frequency at different angles are pointed out for morning and afternoon measuring cycles.

Another microwave remote sensing of snowpack experiment conducting in the Colorado Rocky Mountains is described by Shiue et al. (Reference 35). With four radiometers at frequencies of 5, 10.7, 18 and 37 GHz, the brightness temperature measurements were made as a function of angle by performing both the "swath" (or "elevation") scan and the "fixed spot" scan. Also the brightness temperature measurements were made as a function of snow depth for artificial snowpile and as a function of snow water equivalence for natural snowpacks. A portable single frequency at 35 GHz was used to measure brightness temperatures, as a function of angle with "fixed spot" scan, of two different sites where the main difference between two sites was the average grain size of snow.

SECTION III
RELATED INFORMATION

A. Remote Sensing of Snow, Ice, Vegetation, and Soil Moisture

In recent years the microwave remote sensing techniques have been applied to studies of the geophysical prospection of lake, sea ice, vegetation and soil moisture. The current results in these areas of investigation offer a tantalizing glimpse of what is expected in the next few years when such remote-sensing data become generally available. Since both active and passive remote sensing have their special advantages, active and passive sensing will be discussed separately. Nevertheless, the interpretation of surface characteristics from microwave sensor outputs alone is more effective when data is available from both active (radar) and passive (radiometer) sensors. This is because both outputs are determined by the complete scattering pattern of the medium; of which one aspect (backscattering) is estimated by radar and another (brightness temperature) is estimated by the radiometer (Reference 36).

(1) Active Microwave Remote Sensing

(a) Snow:

A high resolution monocycle v.h.f. radar was developed and tested over lake ice. These tests were conducted by the US Army Cold Regions Research and Engineering Laboratory using a boom as the antenna support in 1965, and using a moving helicopter as a support in 1966. Meyer (Reference 37) discussed the results of measurements of ice thickness and snow thickness by visual data reduction. They also discussed the application of these measurements to the determination of the dielectric constant. Waite and MacDonald (Reference 38) studied snowfield mapping with K-band radar. Analysis of K-band imagery from several snowfield areas

in the United States suggests that the distribution of perenial snc.. results in an anomalously high signal return. In contrast to normal snow survey methods, it appears feasible to map the extent of old snow areas irrespective of most weather conditions, and even when covered with new-fallen snow. Koehler and Kavadas (Reference 39) made a study to determine if conventional radar might provide useful measurements of snow depth. In the first part of the study, they examined the various system parameters of a radar in order to determine the maximum possible resolution in snow depth. It was concluded that one might expect to get depth resolution of the order of 3 cm without going beyond the present state of the art in radar technology. In the second part of the study, they dealt with properties of snow as a radar target. At radar frequencies, snow is a dielectric with a dissipative term which depends on, among other things, the temperature and the moisture content of the snow. It was found that the character of the echo also depends on the dielectric constant of the ground beneath the snow. Very few measurements of these properties have been made at microwave frequencies. They lead to the conclusion that the technique appears to be practical but that further study of the microwave properties of snow and the earth is necessary before any final conclusions can be formed.

Linlor (Reference 40) described the snowpack water content by remote sensing, based on plane-layered models consisting of air, snow, ice, water, and earth. The reflection coefficient was computed for a plane electromagnetic wave at normal incidence with frequencies between 10^6 and 10^{10} Hz. They also gave an example of the theoretical results, showing how the water content of the snow layer and thickness of the ice can be obtained from the shape of the curve of reflection coefficient versus frequency. The paper also briefly reviews other systems for electromagnetic remote sensing and discusses the electrical properties of snow. Possible

airborne applications of the proposed electromagnetic system are outlined. Vickers and Rose (Reference 41) describe in their paper a system which can be used to derive either the snow thickness, or the average snow density by measurement of the transit time of a one nanosecond radar pulse. Their data shows that the radar system can provide an accuracy of less than 10% in the measurement of the density of the snowpack.

Kunzi and Staelin (Reference 42) derived microwave signatures for snow covered land from data obtained by the microwave spectrometer NEMS on board the Nimbus-5 satellite. The emissivity at 31.4 GHz is lower by about 10% than that at 22.2 GHz, while the emissivities for uncovered land are $\simeq 0.95$ at both frequencies. Maps for snow cover over land are generated for the northern hemisphere and compared with data obtained by visible light imagery. Page and Ramseier (Reference 43) present in their paper an overview of the active microwave tools becoming available to the glaciologist with emphasis on recent radar developments as applied to floating ice. They give enough theory to allow the user to understand the techniques and they discuss the side-looking radar imagery using a number of examples resulting from the use of real and synthetic aperture, single and dual polarization. Recent studies of the microwave properties of ice and snow are also reviewed, and are shown to be leading to significant advances in high-resolution radar techniques for accurate sounding of these materials. Remote sensing of freshwater ice thickness is shown to be well established and operational, with similar techniques feasible in the near future for sea ice. It is pointed out that both imaging and probing radars applied to studies of sea ice and snow usually must be used in association with data from other sensors.

Meier (Reference 44) discusses in his paper the measurement of important snow properties using electromagnetic radiation. Ulaby (Reference 45) presents a perspective on the implementation of micro-

wave sensors in future airborne and spaceborne observations of hydrologic parameters. The rationale is based on a review of the status and future trends of active (radar) and passive (radiometer) microwave research as applied to the remote sensing of soil moisture content, snowpack water equivalent, freeze/thaw boundaries, lake ice thickness, surface water area, and the specification of watershed runoff coefficients. They also include analyses and observations based on data acquired from ground based, airborne and spaceborne platforms and an evaluation of advantages and limitations of microwave sensors.

(b) Ice:

Remote sensing of the Arctic ice is an important tool for the operation of shipping in ice covered waters. The most challenging problem in the investigation of sea ice is how to predict the ice thickness, and identify sea states and ice types by remote sensing techniques. In these papers (References 46-81), we can find the studies of high altitude, side looking radar images of sea ice, radio ice-sounding technique, ice type identification by radar, ice thickness and variability by a radar approach, etc. In the paper of N. W. Guinard (Reference 49), one learns about the Four-Frequency Radar System that has been used to measure the radar returns scattered from both sea and ice surfaces for the purpose of identifying sea state and ice types and to determine effective models of the scattering processes to aid in the design of optimum sensors. J. W. Rouse (Reference 50) mentions in his paper one of the most significant results of a radar experiment which was verfication of the ice type identification potential of a 2.25 cm-wavelength radar scatterometer. The results of the radar experiment are presented and the data is analyzed to determine the characteristics of radar backscatter from various Arctic ice types. A quantitative analysis of the data indicates that identifiable radar return "signatures" are obtained for each of several specific sea ice types.

The first successful radar echo sounding through glacier ice in Canada was carried out by the Dominion Observatory in 1965 on an outlet glacier of the Penny Ice Gap on Baffin Island (Reference 51). The radar soundings were generally in agreement, within the range of the reading accuracy of the oscilloscope (±15 m), with depths obtained seismically, gravimetrically, and by the electrical resistivity method. Radio echo sounding results are also discussed in References 71, 72, 78, 79.

K. J. Campbell and A. S. Orange (Reference 62) describe in their paper an impulse radar system that provides a continuous profile of sea and fresh water ice thickness. This was put into operational use in early 1973 and it can be considered as the electromagnetic equivalent of single-trace acoustic profiling systems used in marine subbottom profiling. For the radar system, an electromagnetic pulse is generated on the ice surface and the reflections from the surface and from the ice/water interface are displayed on a continuous strip-chart recorder. Travel times of the reflected pulses can be converted directly to ice thickness. It is likely that the system also can be applied to thickness measurement of glacial ice and to crevasse detection. Airborne profiling of ice thickness by a short pulse radar is also discussed by Vickers et al. (Reference 57).

The ability of radar to discriminate sea ice types and their thickness was studied by Parashar et al. (Reference 65). Radar backscatter measurements at 400 MHz (multi-polarization) and 13.3 GHz (vv polarization) obtained from NASA Earth Resources Aircraft Program Mission 126 were analyzed in detail. The scatterometer data were separated into seven categories of sea ice according to age and thickness as interpreted from stereo aerial photographs. The variations of radar backscatter cross-section (σ°) with sea ice thickness at various angles are presented at the two frequencies. An analytical theory of radar scatter from

sea ice was also developed in this paper. Sea ice was considered as an homogeneous medium in which the dielectric properties vary continuously in the vertical direction. In addition, a small random horizontal variation was considered. Polarized radar backscatter cross-section ($\sigma°$) was computed for six ice types at 400 MHz and 13.3 GHz by taking surface roughness into account. The results thus obtained are presented and are shown to be in general agreement with the experimental results.

Bryan and Larson (Reference 68) studied fresh-water lake ice using multiplexed imaging radar. Their analysis of ice in Whitefish Bay (Lake Superior) indicates that the combination of the ice/water interface and the ice/air interface is the major contributor to the radar backscatter as seen on the imagery. Although the ice thickness cannot be measured directly from the received signals, it is suspected that by combining the information pertaining to radar backscatter with data on the meteorological and sea-state history of the area, together with some basic ground truth data, better estimates of the ice thickness may be provided. In addition, certain ice features (e.g. ridges, ice-foot formation, areas of brash ice) may be identified with reasonable confidence. There is a continued need for additional ground work to verify the validity of imaging radars for these types of interpretations.

In the study of ice conditions and geological explorations, Side-Looking Airborne Radar (SLAR) has been used experimentally since the early 1960's. Its application and many results pertaining to ice are presented and discussed in References 46, 47, 53, 55, 56, 58, 59, 60, 64, 65, 66, 68, 69 and 74. The interpretation of ice features from the SLAR imagery was discussed, and the conclusion reached was that in spite of certain ambiguities the technique has great potential to improve with increasing resolution. Extent of coverage per distance flown and independence of light and cloud conditions make it unique among airborne sensors (Reference 74).

(c) Vegetation:

Vegetation analysis with radar imagery is discussed in References 82-96. Recent studies at Kansas University and by Raytheon Company have shown that vegetation analysis with radar imagery are possible within broad limits depending upon the geographic area being investigated. Imagery has been inspected for a wide range of climatic and topographic environments in the United States in all areas where the influence of vegetation upon radar returns was observable. There is sufficient information obtainable from this form of imagery to warrant its investigation both for use as a single sensor and for future use with other remote sensors (Reference 82). Radar imagery-- because it may be obtained through cloud cover, at night, and over large areas-- can provide valuable data for agricultural land-use mapping. Schwarz and Caspall (Reference 83) talk about the use of radar in the discrimination and identification of agricultural land use. Haralick, Caspall and Simonett (Reference 84) give a statistical study of radar imagery for crop discrimination. The influence of weather and season was also investigated by de Loor et al. (Reference 87). It was shown that if a single vegetation type is present, it behaves as a Rayleigh scatterer. The radar backscatter coefficient as a function of frequency and polarization proves to be the only usable classifier to classify vegetation with the aid of radar. Active microwave measurements of vegetation backscatter were conducted by Ulaby (Reference 91) to determine the utility of radar in mapping soil moisture through vegetation and in mapping crop types. Using a truck-mounted boom, spectral response data were obtained for four crop types (corn, milo, soybeams, and alfalfa) over the 4-8 GHz frequency band, at incidence angles of 0-70 degrees in 10 degree steps, and for all four linear polarization combinations. The results of Radar Response to Vegetation in the 8-18 GHz band were presented by Ulaby et al. (Reference 92), Bush and Ulaby (Reference 93), and Ulaby and Bush (Reference 94). Because the microwave dielectric

constant of dry vegetation matter is much smaller (by an order of magnitude or more) than the dielectric constant of water, and because a vegetation canopy is usually composed of more than 99% air by volume, it is proposed (Reference 95) that the canopy can be modeled as a water cloud whose droplets are held in place by the vegetative matter. Such a model was developed assuming that the canopy "cloud" contains identical water droplets randomly distributed within the canopy. By integrating the scattering and attenuation cross-section contributions of N droplets per unit volume over the signal path length through the canopy, an expression was derived for the backscattering coefficient as a function of three target parameters: volumetric moisture content of the soil, volumetric water content of the vegetation, and plant height. Regression analysis of the model predictions against scattering data acquired over a period of four months at several angles of incidence (0-70 degrees) and frequencies (8-18 GHz) for HH and VV polarizations yields correlation coefficients that range from 0.7 to 0.99 depending on frequency, polarization, and crop type.

(d) Soil Moisture:

The study of remote sensing of soil moisture is discussed in References 97-104. The effects of soil layering on the use of VHF radio waves for remote terrain analysis are discussed and illustrated by Nikodem (Reference 97). The radar response to soil moisture content was investigated using a truck-mounted 1-18 GHz Active Microwave Spectrometer (MAS) system (Reference 98). The sensitivity to soil moisture content and the accuracy with which it could be estimated were evaluated for both bare and vegetation-covered fields. The radar response to soil moisture was also experimentally determined (Reference 99) for each of three bare fields with considerably different surface roughness at eight frequencies

in the 2-8 GHz band for HH and VV polarizations. Analysis of the data indicates that the effect of roughness on the radar backscattering coefficient can be minimized by proper choice of the radar parameters. If, in addition, sensitivity to soil moisture content and system design constraints are considered, the following radar parameters are recommended for an operational soil moisture mapper: Radar Signal Frequency = 4 GHz. Angle of Incidence Range: 7 $\sim$ 15 degrees from nadir. Signal Polarization: HH or VV. The corresponding sensitivity is about 0.25 dB/0.01g/cm^3. Measurements of radar backscatter from bare soil at 4.7, 5.9, and 7.1 GHz for incident angles of 0-70 degrees have been analyzed to determine sensitivity to soil moisture (Reference 95). The effect of soil moisture on the radar backscattering coefficient was investigated by measuring the 4-8 GHz spectral response from two types of bare fields: slightly rough and very rough, in terms of the wavelength (Reference 102).

(2) Passive Microwave Remote Sensing

An experimental passive microwave radiometer measurement program is described in Reference 105. That program concerns itself primarily with the nature of the experiments, the equipment used, and of course the resulting data.

(a) Snow:

Meier (Reference 106) discussed the measurement of snow cover using passive microwave radiation. The snowline mapped from air photographs of Mount Rainer on 18 June 1968, is almost identical to the 270°K brightness temperature shown on a microwave image. Microwave brightness temperature of dry snow, wet snow, and snow-free terrain are unique. Thus the snow-covered area can be calculated from an average brightness temperature for an field of view. Kunzi et al. (Reference 107) studied the signatures of various earth

surfaces measured by the Nimbus-5 microwave spectrometer. The Nimbus-5 Meteorological Satellite is equipped with a 5-Channel microwave spectrometer. The two lowest channels (22.2 and 31.4 GHz) provide information on surface brightness temperature. Distinctive microwave signatures can be observed for snow, land ice, and sea ice in both polar regions. Moore and Hooper (Reference 108) used a very sensitive K_a-band microwave radiometer to map agricultural areas during winter, spring, and summer seasons, and at various altitudes. The microwave radiometer utilized in this program employs a parametric amplifier to achieve its ultra-high sensitivity. The mapping function is accomplished by rotating parabolic antennas which scan the beam in the cross-track direction. The forward motion of the aircraft provides the other dimension. The area mapped is a strip which as a width four times the altitude of the aircraft. The system is capable of rapid installation and removal. In this paper they gave the maps obtained at 300, 750, 1500 and 3000 meters during each season. Ground-truth data includes aerial photographs taken either simultaneously with the radiometric maps or a short time after the flight tests, or 2 to 8 years before the flight tests. Agricultural information, contour maps and observer comments have also been obtained. Mooney et al. (Reference 109) summarize in their paper the main conclusions of a preliminary study carried out into the role and technological consequence of spaceborne passive microwave radiometry intended for Earth observation. The Earth's oceans, ice and snow cover and atmosphere are considered the prime areas of interest for the technique with preferred payloads being a mix of profiling and imaging devices.

Kunzi et al. (Reference 110) also discussed the snow and ice surfaces measured by the Nimbus 5 microwave spectrometer. The 22.2 GHz and 31.4 GHz channels of the microwave spectrometer on board the Nimbus 5 earth observatory satellite provide information about the global distribution and character of various types

of snow and ice. Observations for the winter and summer of 1973 are presented for both polar regions. Well defined spectral signatures are found for snow, sea ice, and land ice in Greenland and Antarctica. A simple model with subsurface temperature gradients in a lossy homogeneous dielectric does not account for the observations; internal scattering effects appear to play a dominant role.

Zwally (Reference 111) formulates in his paper the radiative transfer theory to permit a meaningful definition of emissivity for bulk emitting media such as snow. The emissivity in the Rayleigh-Jeans approximation is then the microwave brightness temperature T_B divided by an effective physical temperature $\langle T \rangle$. The $\langle T \rangle$ is an average of the physical temperature, $T(z)$, weighted by a radiative transfer function $f(z)$. Similarly, $T_B = \int_0^\infty f(z)\, e(z)\, T(z)\, dz$, where $e(z)$ is the local emittance. It is shown that a mean emissivity which is equal to the mean annual T_B divided by the mean annual surface temperature T_m, is a useful quantity for comparing theory and observations. Snow-crystal size measurements, $r(z)$, at seven locations in Greenland and Antarctica are used to determine the Mie Rayleigh scattering coefficient $V_s(z)$ and to calculate the mean emissivities. In that paper, Zwally (Reference 111) defines the above effective physical temperature, then uses it to define the general bulk emissivity. He also uses an approximate radiative transfer function, which is valid if the volume scattering is small relative to the absorption, to calculate the brightness temperature, the effective physical temperature, and the emissivity in order to illustrate the effects of various absorption and scattering coefficients and temperature variations. It is also used to calculate emissivities based on snow crystal size measurements for comparison with observed emissivities and to estimate the sensitivity of the emissivity to changes in the snow characteristics.

(b) Ice:

Passive remote sensing in the microwave spectral region has proved to be a useful tool for determination of oceanographic phenomena such as sea state, pollution, and sea ice characteristics. Difference in radiometric brightness temperature of the sea surface of the order of 15°K have been readily detected during airborne measurements of the Salton Sea, California and the North Atlantic using scanning phased array radiometers (Reference 113).

The problem of remotely determining the thickness of sea ice over large areas is a difficult one and the attempts have not yet proven successful (Reference 114). The techniques most widely used involve observing the surface structure and surface pattern (visually or by a radar), and attempting to infer the thickness of the ice from such information. Adey et al. (Reference 114) have developed a technique using a UHF radiometer and have recently carried out the first field trials of the technique and of the instrumentation.

Rabinovich et al. (Reference 116) studied the determination of the Meteorological characteristics of the atmosphere and the earth's surface from airborne measurements of passive microwave radiation. Radiometric investigations of the earth were started in the USSR in 1968 by launching the satellite "Cosmos 243" equipped with microwave and infrared radiometers. Basharinov et al. (Reference 117) gave the data obtained from an experiment that was conducted over the Southern hemisphere during the spring season of 1970. The data allowed them to estimate the ocean-surface temperature, the boundary of floating ice around the Antarctic continent, the temperature and the state of continental ice covers, atmospheric water vapor content, the liquid water content of clouds, characteristics of rain and some other geophysical data. A combination of remote sensing from an aircraft and simultaneous surface measurements have

confirmed the feasibility of identifying old and new sea ice according to its emission of thermal radiation at wavelengths between 0.3 and 3 cm (Reference 118). Results derived from a comparative study of surface-based 13.4 GHz passive microwave measurements with detailed surface-truth measurements concerning the physical, chemical and structural properties of Arctic sea ice illustrate distinct decreasing microwave emissions for first-year, transitional and multi-year sea ice types (Reference 120). During the spring of 1975 an extensive experiment to determine the characteristics of sea ice in the Baltic Sea by passive and active remote sensing methods was performed. Tiuri et al. (Reference 121) give a report in which the preliminary results of UHF and microwave radiometer measurements are described. The results indicate that 600 MHz and 5 GHz radiometers can be used to determine the ice thickness in the case of low salinity ice. Tooma et al. (Reference 122) gave a comparison of sea-ice type identification between airborne dual-frequency passive microwave radiometry and standard laser/infrared techniques.

(c) Soil Moisture:

Several papers (References 123-135) discuss microwave remote sensing of soil moisture. Microwave radiometric temperature measurements using both vertical and horizontal polarization were taken with fixed-view angle traverse across three sites at two locations (Reference 124). The observational wavelengths were 21 cm, 2.2 cm, and 0.8 cm. Ground truth measurements included soil moisture, soil bearing strength, electrical resistivity, and thermal temperature. Jean et al. (Reference 125) compared a theoretical expression for the total apparent temperature of a smooth surface to *in situ* measurements, taken from a natural terrain. Although a good correlation was observed for certain incident angles, it was impossible to separate the effects of the various environmental parameters. In order to study the effects of these various surface parameters, they

constructed a controlled test site where radiometer measurements at 31.4 GHz were made. Then they compared the data obtained to a model of the apparent temperature of a smooth surface. Blinn et al. (Reference 127) discussed the results of microwave radiometric field observations conducted at wavelengths of 21, 2.8 and 9.95 cm to determine the microwave penetration depth of a number of sands and gravels as a function of particle size and moisture content. Observations of a reflecting plate covered with varying thicknesses of test material exhibit a pronounced oscillatory behavior that is consistent with established electromagnetic theory for plane-parallel layered media. Utilization of this interference effect is proposed as a microwave radiometric technique for determining the bulk electric properties of geologic materials readily adapted to layering experiments. They proposed that the extension of the technique could lead to a method for remotely determining layer thickness in certain naturally layered systems such as sea ice. Passive microwave observations of moist soil were performed at wavelengths of 0.8 and 3.4 cm from an aircraft. The data obtained is compared with the results of direct measurements of soil moisture content (Reference 128). The dependence of brightness temperature on the value of moisture content is observed as well as the influence of vegetation cover. Newton et al. (Reference 130) discussed the feasibility of remote monitoring of soil moisture with microwave sensors. They found that the airborne measurements of radiometric temperature at monitored sites located near Chickasha, Oklahoma, and Weslaco, Texas show that vegetation cover has the effect of masking the soil moisture dependence of the microwave data. Since Peake's (Reference 8) model is inappropriate for describing emission in the presence of a vegetative cover, therefore, a new model was developed which yields emissivity directly from the material properties of the subsurface medium and from the transmission coefficient of the surface. This work was

used to develop a model for the apparent microwave temperature and radar backscatter coefficient of vegetated terrain to illustrate the effects of vegetation on the sensitivity of these parameters to variations of soil moisture. A ground measurement program was established in order to obtain data to compare the predictions of the models. Microwave radiometry has also been used for remote sensing of soil moisture in a series of aircraft flights over an agricultural test area in the vicinity of Phoenix, Arizona (Reference 131). Ground truth in the form of gravimetric measurements of the soil moisture in the top 15 cm were obtained for 200 fields. The results indicate that it is possible to monitor soil moisture variations with airborne radiometers.

Peck et al. (Reference 133) presented a comparison of concurrent measurements of estimates of soil moisture from ground sampling and from measurements of passive microwave and passive gamma radiation made by aircraft. Although the good results obtained were based on ideal conditions (minimum change in vegetative cover, excellent ground fix for aerial surveys, extensive ground truth, etc.) they do point to the possible use of microwave techniques for aireal measurement of soil moisture under selective conditions for hydrologic purposes. Kondratyev et al. (Reference 134) summarize the work accomplished in the Voyeykov Main Geophysical Observatory on passive microwave remote sensing of soil moisture and discuss the theory and calculations of microwave emission from a medium with depth-dependent physical properties. They gave a technique for determining the amount of water in the 1 m layer which can be used by plants.

Njoku and Kong (Reference 135) developed the theory of microwave thermal emission from a nonscattering half-space medium for application to regions with nonuniform subsurface soil moisture and temperature variations. A coherent stratified model valid for nonuniform temperature profiles and rapidly varying moisture profiles

was presented. For naturally occurring profiles the stratified model gives more accurate results than the other approaches at frequencies below about 4 GHz. Experimental results from ground-based radiometric observations of a controlled target area agree with the brightness temperature predicted from the theoretical model to within 10°K. By using this model the thermal microwave emission spectrum is computed for a number of representative moisture and temperature profiles in the frequency range of 0.25 to 25 GHz. A regression technique is then used to show that multifrequency data can be used to obtain moisture and temperature gradients in the soil when an estimate of the surface temperature is available. Genda and Okayama (Reference 137) describe a simulation for remote sensing to confirm the properties and meaning of remote sensed information. The simulator, suitable for the measurement of soil moisture, consists of an optical source, a polarimeter, and a sample stage. SiC and MgO and beach sand were used to represent soil. They note that the degree of polarization increases with the moisture content and particle size of the sample.

Curtis (Reference 138) discusses requirements and presents prospects in the remote sensing of soil moisture. Moore et al. (Reference 139) studied the simultaneous active and passive microwave of the earth from the skylab radscat experiment. Campbell et al. (Reference 140) discussed mesoscale and macroscale studies of floating ice for three sensor categories: visual, passive microwave, and active microwave.

Sobti et al. (Reference 141) calculated the correlations between active and passive microwave responses received by the S-193 radiometer-scatterometer on Skylab. They found that over both land and sea the correlation between polarizations is high, but that the correlation between radiometer and scatterometer response at 30 degrees incidence is negligible. This suggests that multipolarization instruments with low resolution (greater than 10 km in all

cases) are redundant while a combination of radiometer and scatterometer is useful.

B. Electrical Properties of Snow, Ice and Soil

(1) Snow and Ice

Evans (Reference 142) gives a good review of dielectric properties of ice and snow. He considers the permittivity and loss tangent of naturally occurring ice and snow. In Appendix A, he gives a chornological annotated bibliography of published measurements. Readers interest in the measurements prior to 1965 should consult this paper. We shall review papers published after 1965. Gribbon (1967) (Reference 143) studied the dielectric relaxation of neve and glacial ice on two temperate glaciers in Greenland and France. Measurement of the audio-frequency capacitance and loss tangent of thin parallel wires placed on the surface of a glacier yield ε', the relative permittivity, and ε'', the loss factor of the neve. The relaxation time is expressed in terms of the frequency f_m at the maximum ε'' value of the Cole-Cole $\varepsilon'' - \varepsilon'$ diagrams obtained for different wire separations.

Philberth (Reference 144) suggests a simple device to measure the permittivity of deep ice layers under the normal temperature, pressure and grain structure. The electrical properties of and electrical relaxation in saline ice were discussed by Addison (references 146, 147). Webber et al. (Reference 148) studied the VLF ground-based measurements in Antarctica, and their relationship to stratifications in the subsurface terrain. Hoekstra et al. (Reference 149) discussed the dielectric properties of sea and sodium chloride ice at UHF and microwave frequencies. Peden et al. (Reference 150) described an experiment that had been designed to yield the dielectric and loss perperties of the ice cap near Byrd Station, Antarctica, in the VLF range, subsequent to the proper interpretation of the input admittance of an electrically short dipole probe.

Perry and Straiton (Reference 151) employed a quasioptical free-space technique to measure the complex dielectric constant of ice at 35.3 and 94.5 GHz. Bryan and Larson (Reference 152) discussed the application of dielectric constant measurements to radar imagery interpretation. They described several cases of radar-earth surface interaction and presented examples of radar imagery and some data on ice and snow. They concluded that the next logical step would be to quantify the radar ground truth in preparation for machine interpretation and automatic data processing of the radar imagery.

Shemelin (Reference 153) discusses the electrical and mechanical properties of ice which are of great importance in hydrology, glaciology, and meteorology. The appearance in the last 20 years of electron microscopy, neutron diffraction, and nuclear magnetic resonance has led to the broad development of physical ice and water studies. The most important results achieved in such studies in recent years are also discussed.

Campbell and Orange (Reference 154) observed sea ice electrical anisotropy in the horizontal plane with an impulse radar technique under development for profiling ice thickness. The radar technique used is the electromagnetic equivalent of the acoustic subbottom profiling method. The anisotropy is characterized by a marked change in amplitude of the vertically propagated signal reflected from the sea ice/water interface as the linearly polarized antenna was rotated in the horizontal plane on or above the ice surface. Vant et al. (Reference 155) studied the electrical properties of fresh and sea ice at 10 and 35 GHz. Addison (Reference 156) studied the electrical properties of saline ice for temperatures down to -150°C at 1 KHz. Bentley (Reference 157) provides a clear survey of advances in geophysical exploration of ice sheets and glaciers. Fitzgerald and Paren (Reference 158) studied the dielectric properties of Antarctic ice.

(2) Soil

Pearce et al. (Reference 163) developed the theory of a three component heterogeneous dielectric to provide a basis for an analytic description of the electromagnetic properties of soil systems. The theory is valid for frequencies where the electromagnetic wavelength is much greater than the soil particle size. Agreement between theory and experiments with coarse grained sand system at both audio and p-band radar frequencies is demonstrated in their paper. Leshchanskii et al. (Reference 164) used the short-circuit method based on measurement waveguides to measure the electrical parameters of sandy and loamy soils in the 0.8 to 2.26 cm range. They obtained the dependence of the permittivity and attenuation on the moisture content of the soil in the RF range. It is shown that in moist sandy soil the attenuation factor is determined by the absorption of radio waves by water molecules at all of the investigated wavelengths. In moist loamy soil the attenuation factor at centimeter wavelengths is primarily determined by the absorption of radio waves by the ions of the loamy soil. Hoekstra and Delaney (Reference 165) measured the complex dielectric constant of four types of soils, including a sand, a silt, and two clays, over the frequency range from 0.1 GHz to 26 GHz. Their results show that the relation between volumetric water content and the complex dielectric constant is realtively independent of soil types.

REFERENCES

1. A. Stogryn, "The brightness temperature of a vertically structured medium," Radio Science, 5, 1397-1406, Dec. 1970.

2. W. I. Linlor and G. R. Jiracek, "Electromagnetic reflection from multi-layered snow models," J. of Glaciology, 14, 501-515, 1975.

3. L. Tsang, E. Njoku, and J. A. Kong, "Microwave thermal emission from a stratified medium with nonuniform temperature distribution," J. Appl. Phys., 46, 5127-5133, Dec. 1975.

4. T. T. Wilheit, Jr., "Radiative transfer in a plane stratified dielectric," IEEE Trans. on Geoscience Electron., GE-16, 138-143, April 1978.

5. A. Stogryn, "Electromagnetic scattering by random dielectric constant fluctuations in a bounded medium," Radio Science, 9, 509-518, May 1974.

6. L. Tsang, "Microwave remote sensing of a two-layer random medium," IEEE Trans. on Antennas and Prop., AP-24, 283-288, May 1976.

7. L. Tsang and J. A. Kong, "Emissivity of half-space random media," Radio Science, 11, 593-598, July 1976.

8. W..H. Peake, "Interaction of electromagnetic waves with some natural surfaces," IRE Trans. on Ant. and Prop., S324-S328, Dec. 1959.

9. S. K. Parashar, A. K. Fung, and R. K. Moore, "A theory of wave scatter from an inhomogeneous medium with a slightly rough boundary and its application to sea ice," Remote Sensing of Environ., 7, 37-50, 1978.

10. L. Tsang and J. A. Kong, "Radiative transfer theory for active remote sensing of half space random media," Radio Science, to be published Sept. 1978.

11. J. C. Leader, "Polarization dependence in EM scattering from Rayleigh scatterers embedded in a dielectric slab. I. Theory," J. Appl. Phys., 46, 4371-4385, Oct. 1975.

12. S. Twomey, H. Jacobowitz, and H. B. Howell, "Matrix methods for multiple-scattering problems," J. Atmospheric Sci., 23, 289-296, May 1966.

13. A. S. Gurvich, V. I. Kalinin, and D. T. Matveyev, "Influence of the internal structure of glaciers on their thermal radio emission," Atm. and Oceanic Phys., 6, 1247-1256, 1973.

14. L. Tsang and J. A. Kong, "The brightness temperature of a half-space random medium with nonuniform temperature profile," Radio Science, 10, 1025-1033, Dec. 1975.

15. L. Tsang and J. A. Kong, "Thermal microwave emission from half-space random media," Radio Science, 11, 599-609, July 1976.

16. L. Tsang, "Theory of Thermal microwave emission from a two-layer medium," Pageoph, 114, Birkhauser Verlag, Basel, 1976.

17. L. Tsang and J. A. Kong, "Thermal microwave emission from a random inhomogeneous layer over a homogeneous medium using the method of invariant imbedding," Radio Science, 12, 185-194, Mar. 1977.

18. A. D. Fisher, "A model for microwave intensity propagation in an inhomogeneous medium," IEEE Trans. on Ant. and Prop., AP-25, 876-882, Nov. 1977.

19. A. W. England, "Thermal microwave emission from a half-space containing scatterers," Radio Science, 9, 447-454, April 1974.

20. A. W. England, "Thermal microwave emission from a scattering layer," J. Geophysical Res., 80, 4484-4496, Nov. 1975.

21. T. C. Chang, P. Gloersen, T. Schmugge, T. T. Wilheit, and H. J. Zwally, "Microwave emission from snow and glacier ice," J. of Glaciology, 16, 23-39, 1976.

22. L. Tsang and J. A. Kong, "Theory for thermal microwave emission from a bounded medium containing spherical scatterers," J. Appl. Phys., 48, 3593-3599, Aug. 1977.

23. W. M. Sackinger and R. C. Byrd, "Backscatter of millimeter waves from snow," IAEE Report 7207, Institute of Arctic Environmental Engineering, University of Alaska, June 1971.

24. R. C. Byrd, M. C. Yerkes, W. M. Sackinger, and T. E. Osterkamp, "Snow measurement using millimetre wavelengths," Proc. of the Bonff Sym., 1, 734-738, Sept. 1972.

25. P. Hoekstra and D. Spanogle, "Radar cross-section measurements of snow and ice," Cold Regions Research and Engineering Lab., Hanover, NH, Nov. 1972.

26. N. C. Currie and G. W. Ewell, "Radar millimeter backscatter measurements from snow," Final Report AFATL-TR-77-4, Engineering Experiment Station, Georgia Institute of Technology, Jan. 1977.

27. F. T. Ulaby, W. H. Stiles, L. F. Dellwig, and B. C. Hanson, "Experiments on the radar backscatter of snow," IEEE Trans. on Geoscience Electron., GE-15, 185-189.

28. J. M. Kennedy and R. T. Sakamoto, "Passive microw-ae determinations of snow wetness factors," Proc. of the-Fourth Sym. on Rem. Sen. of Environment, 12-14 April, 1966, University of Michigan, Ann Arbor, MI.

29. J. M. Kennedy, A. T. Edgerton, R. T. Sakamoto, and R. M. Mandl, "Passive microwave measurements of snow and soil," Tech. Report 2, SGC 829R-4, Aerojet-General Corp., El Monte, CA, Dec. 1965.

30. A. T. Edgerton et al., "Passive microwave measurements of snow, soils, and snow-ice water systems," Tech Report 4, SGD 829-6, Aerojet-General Corp., El Monte, CA, Feb. 1968.

31. A. T. Edgerton, A. Stogryn, and G. Poe, "Microwave radiometric investigations of snowpacks," Final Report 1285R-4, Aerojet-General Corp., El Monte, CA, July 1971.

32. M. F. Meier and A. T. Edgerton, "Microwave emission from snow-- A progress report," Proc. of the 7th International Sym. on Rem. Sen. of Environment, 2, University of Michigan, Ann Arbor, MI, 1977.

33. T. Schmugge, T. T. Wilheit, P. Gloersen, M. F. Meier, D. Frank, and I. Dirmhirn, "Microwave signatures of snow and fresh water ice," Presented at the Interdisciplinary Sym. on Adv. Concepts and Tech. in the Study of Snow and Ice Resources, Goddard Space Flight Center, Nov. 1973.

34. R. Hofer and E. Schanda, "Signatures of snow in the 5 to 94 GHz range," Radio Science, 13, 365-369, March 1978.

35. J. C. Shiue, A. T. C. Chang, H. Boyne, and D. Ellerbruch, "Remote sensing of snowpack with microwave radiometers for hydrologic applications," Proc. of the 12th International Sym. on Rem. Sen. of Environment, University of Michigan, Ann Arbor, MI, 1978.

36. W. H. Peake, R. L. Riegler, and C. H. Schultz, "The mutual interpretation of active and passive microwave sensor outputs," Proc. of the 4th Sym. on Rem. Sen. of Environment, University of Michigan, Ann Arbor, MI, April 1966.

37. M. A. Meyer, "Remote sensing of ice and snow thickness," Proc. of the 4th Sym. on Rem. Sen. of Environment, University of Michigan, Ann Arbor, MI, April 1966.

38. W. P. Waite and H. C. MacDonald, "Snowfield mapping with K-band radar," Rem. Sen. of Environment, 1, 143-150, 1970.

39. J. Koehler and A. Kavadas, "Radar as a possible instrument for snow depth measurements," Canadian Aeronautics and Space Journal, 17, 432, Dec. 1971.

40. W. I. Linlor, "Snowpack water content by remote sensing," Proc. of the Banff Sym., 1, 713-726, Sept. 1972.

41. R. S. Vickers and G. C. Rose, "High resolution measurements of snowpack stratigraphy using a short pulse radar," Proc. of the 8th International Sym. on Rem. Sen. of Environment, 1, University of Michigan, Ann Arbor, MI, Oct. 1972.

42. K. F. Kunzi and D. H. Staelin, "Measurements of snow cover over land with the Nimbus-5 microwave spectrometer," Proc. of the 10th International Sym. on Rem. Sen. of Environment, 2, University of Michigan, Ann Arbor, MI, Oct. 1975.

43. D. F. Page and R. O. Ramseier, "Application of radar techniques to ice and snow studies," Journal of Glaciology, 15, 171-191, 1975.

44. M. F. Meier, "Application of remote-sensing techniques to the study of seasonal snow cover," Journal of Glaciology, 15, 251-265, 1975.

45. F. T. Ulaby, "Microwave remote sensing of hydrologic parameters," Proc. of the 11th International Sym. on Rem. Sen. of Environment, 1, Ann Arbor, MI, April 1977.

46. V. H. Anderson, "High altitude, side-looking radar images of sea ice in the Arctic," Proc. of the 4th Sym. on Rem. Sen. of Environment, University of Michigan, Ann Arbor, MI, April 1966.

47. R. D. Leighty, "Terrain information from high altitude side-looking radar imagery of an arctic area," Proc. of the 4th Sym. on Rem. Sen. of Environment, University of Michigan, Ann Arbor, MI, April 1966.

48. J. N. Rinker, S. Evans, and G. Q. Robin, "Radio ice-sounding techniques," Proc. of the 4th Sym. on Rem. Sen. of Environment, University of Michigan, Ann Arbor, MI, April 1966.

49. N. W. Guinard, "The remote sensing of the sea and sea ice," Proc. of the 6th International Sym. on Rem. Sen. of Environ., 2, University of Michigan, Ann Arbor, MI, Oct. 1969.

50. J. W. Rouse, Jr., "Arctic ice type identification by radar," Proc. of the IEEE, 57, 605-611, April 1969.

51. J. R. Weber and P. Andrieux, "Radar soundings on the penny ice cap, Baffin Island," J. of Glaciology, 9, 49-54, 1970.

52. A. Biache, Jr., C. A. Bay, and R. Bradie, "Remote sensing of the Artic ice environment," Proc. of the 7th International Sym. on Rem. Sen. of Environment, 1, University of Michigan, Ann Arbor, MI, May 1971.

53. V. M. Glushkov and V. B. Komarov, "Side-looking imaging radar system Toros and its application to the study of ice conditions and geological explorations," Proc. of the 7th International Sym. on Rem. Sen. of Environment, 1, University of Michigan, Ann Arbor, MI, May 1971.

54. K. Iizuka, V. K. Nguyen, and H. Ogura, "Review of the electrical properties of ice and hiss down-looking radar for measuring ice thickness," Condensation, 17, 429-430, Dec. 1971.

55. J. D. Johnson and L. D. Farmer, "Determination of sea ice drift using side-looking airborne radar," Proc. of the 7th International Sym. on Rem. Sen. of Environment, 3, University of Michigan, Ann Arbor, MI, May 1971.

56. J. D. Johnson and L. D. Farmer, "Use of side-looking airborne radar for sea ice identification," J. of Geophysical Research., 76, 2138-2155, March 1971.

57. B. T. Larrowe, R. B. Innes, R. A. Rendelman, and L. J. Porcello, "Lake ice surveillance via airborne radar: some experimental results," Proc. of the 7th International Sym. on Rem. Sen. of Environment, 1, University of Michigan, Ann Arbor, MI, May 1971.

58. M. L. Bryan, "Utility of imaging radar for the study of lake ice," Proc. of the Banff Sym., 2, 1339-1349, Sept. 1972.

59. A. A. Zegarodnikov, V. S. Loshchilov, and K. B. Chelyshev, "Two-dimensional statistic analysis of radar imagery of sea ice," Proc. of the 8th International Sym. on Rem. Sen. of Environment, 1, University of Michigan, Ann Arbor, MI, Oct. 1972.

60. R. D. Ketchum, Jr., and S. A. Tooma, Jr., "Analysis and interpretation of air-borne multifrequency side-looking radar sea ice imagery," J. of Geophysical Res., 78, 520-538, Jan. 1973.

61. M. L. Bryan, "Ice thickness and variability on Silver Lake, Genesee County, Michigan: A radar approach," Presented at the Interdisciplinary Sym. on 'Advanced concepts and techniques in the study of snow and ice resources', National Academy of Sciences, Washington, DC, 1974.

62. K. J. Campbell and A. S. Orange, "Continuous sea and fresh water ice thickness profiling using an impulse radar system," Presented at the Interdisciplinary Sym. on 'Advanced concepts and techniques in the study of snow and ice resources', National Academy of Sciences, Washington, DC, 1974.

63. H. G. Hengeveld, "Remote sensing applications in Canadian ice reconnaissance," Presented at the Interdisciplinary Sym. on 'Advanced concepts and techniques in the study of snow and ice resources', National Academy of Sciences, Washington, DC, 1974.

64. R. J. Jirberg, R. J. Schertler, R. T. Gedney, and H. Mark, "Application of Slar for monitoring Great Lakes total ice cover," Presented at the Interdisciplinary Sym. on 'Advanced concepts and techniques in the study of snow and ice resources', National Academy of Sciences, Washington, DC, 1974.

65. S. K. Parashar, A. W. Biggs, A. K. Fung, and R. K. Moore, "Investigation of radar discrimination of sea ice," Proc. of the 9th International Sym. on Rem. Sen. of Environment, 1, University of Michigan, Ann Arbor, MI, April 1974.

66. S. K. Parashar, R. K. Moore, and A. W. Biggs, "Use of radar techniques for sea ice mapping," Presented at the Interdisciplinary Sym. on 'Advanced concepts and techniques in the study of snow and ice resources', National Academy of Sciences , Washington, DC, 1974.

67. R. S. Vickers, J. E. Heighway, and R. T. Gedney, "Airborne profiling of ice thickness using a short pulse radar," Presented at the Interdisciplinary Sym. on 'Advanced concepts

and techniques in the study of snow and ice resources', National Academy of Science, Washington, DC, 1974.

68. M. L. Bryan and R. W. Larson, "The study of fresh-water lake ice using multiplexed imaging radar," Journal of Glaciology, 14, 445-457, 1975.

69. C. Elachi and W. E. Brown, Jr., "Imaging and sounding of ice fields with airborne coherent radars," J. of Geophysical Res., 80, 1113-1119, Mar. 1975.

70. P. Gudmandsen, "Layer echoes in polar ice sheets," Journal of Glaciology, 15, 95-101, 1975.

71. V. I. Morgan and W. F. Budd, "Radio-echo sounding of the Lambert Glacier basin," Journal of Glaciology, 15, 103-111, 1975.

72. G. de Q. Robin, "Radio-echo sounding: Glaciological interpretations and applications," Journal of Glaciology, 15, 49-64, 1975.

73. T. Tabata, "Sea-ice reconnaissance by radar," Journal of Glaciology, 15, 215-224, 1975.

74. M. Dunbar, "Interpretation of Slar imagery of sea ice in Nares Strait and the Arctic Ocean," Journal of Glaciology, 15, 193-213, 1975.

75. C. Elachi and M. L. Bryan, "Imaging radar observations of frozen Arctic Lakes," Remote Sensing of Environment, 5, 169-175, 1976.

76. W. L. Flock, "Monitoring open water and sea ice in the Bering Strait by radar," IEEE Trans. on Geoscience Electron., GE-15, 196-202, Oct. 1977.

77. L. Gray, J. Cihlar, and S. Parashar, "Scatterometer results from shorefast and floating sea ice," Proc. of the 11th International Sym. on Rem. Sen. of Environment, 1, Ann Arbor, MI, April 1977.

78. P. Gudmandsen, "Studies of ice by means of radio echo sounding," Remote Sensing of the Terrestrial Environment, Proc. of the 28th Sym. of the Colston Res. Society, University of Bristol, April 1976.

79. J. F. Nye, "Remote sensing in glaciology and the physics of echoes," Remote Sensing of the Terrestrial Environment, Proc. of the 28th Sym. of the Colston Res. Society, University of Bristol, April 1976.

80. S. K. Parashar, R. M. Haralick, R. K. Moore, and A. W. Biggs, "Radar scatterometer discrimination of sea-ice types," IEEE Trans. on Geoscience Electron., GE-15, 83-87, April 1977.

81. W. F. Weeks, P. Sellmann, and W. J. Campbell, "Interesting features of radar imagery of ice-covered north slope lakes," Journal of Glaciology, 18, 129-136, 1977.

82. S. A. Morain and D. S. Simonett, "Vegetation analysis with radar imagery," Proc. of the 4th Sym. on Rem. Sen. of Environment, University of Michigan, Ann Arbor, MI, 1966.

83. D. E. Schwarz and F. Caspall, "The use of radar in the discrimination and identification of agricultural land use," Proc. of the 5th Sym. on Rem. Sen. of Environment, University of Michigan, Ann Arbor, MI, April 1968.

84. R. M. Haralick, F. Caspall, and D. S. Simonett, "Using radar imagery for crop discrimination: A statistical and conditional probability study," Remote Sen. of Environment, 1, 131-142, 1970.

85. F. T. Ulaby, R. K. Moore, R. Moe, and J. Holtzman, "On microwave remote sensing of vegetation," Proc. of the 8th International Sym. on Rem. Sen. of Environment, 2 University of Michigan, Ann Arbor, MI, Oct. 1972.

86. E. P. W. Attema, L. G. den Hollander, T. A. de Boer, D. Uenk, W. J. Eradus, G. P. de Loor, H. van Kasteren, and J. van Kuilenburg, "Radar cross sections of vegetation canopies determined by monostatic and bistatic scattero-

99. F. T. Ulaby and P. P. Batlivala, "Optimum radar parameters for mapping soil moisture," IEEE Trans. on Geoscience Electron., GE-14, 81-93, April 1976.

100. F. T. Ulaby and P. P. Batlivala, "Diurnal variations of radar backscatter from a vegetation canopy," IEEE Trans. on Ant. and Prop., AP-24, 11-17, Jan. 1976.

101. F. T. Ulaby, J. Cihlar, and R. K. Moore, "Active Microwave measurement of soil water content," Remote Sen. of Environ., 3, 185-203, 1974.

102. F. T. Ulaby, "Radar measurement of soil moisture content," IEEE Trans. on Ant. and Prop., AP-22, 257-265, Mar. 1974.

103. F. M. Dickey, C. King, J. C. Holtzman, and R. K. Moore, "Moisture dependency of radar backscatter from irrigated and non-irrigated fields at 400 MHz and 13.3 GHz," IEEE Trans. on Geoscience Electron., GE-12, 19-22, Jan. 1974.

104. H. C. MacDonald and W. P. Waite, "Soil moisture detection with imaging radars," Water Resources Research, 7, 100-110, Feb. 1971.

105. W. H. Conway and R. T. Sakamoto, "Microwave radiometer measurements program," Proc. of the 3rd Sym. on Rem. Sen. of Environment, University of Michigan, Ann Arbor, MI, Oct. 1964.

106. M. F. Meier, "Measurement of snow cover using passive microwave radiation," Proc. of the Banff Sym., 1, Sept. 1972.

107. K. F. Kunzi, R. L. Pettyjohn, D. H. Staelin, and J. W. Waters, "Signatures of various earth surfaces measured by the Nimbus-5 microwave spectrometer," Proc. of the 9th International Sym. on Rem. Sen. of Environment, 1, University of Michigan, Ann Arbor, MI, April 1974.

108. R. P. Moore and J. O. Hooper, "Microwave radiometric characteristics of snow-covered terrain," Proc. of the 9th International Sym. on Rem. Sen. of Environment, 3, University of Michigan, Ann Arbor, MI, April 1974.

109. H. McD. Mooney, E. P. L. Windsor, E. Nilsson, and L. Thrane, "Passive microwave radiometry from a European spacecraft," Remote Sen. of the Terrestrial Environment, Proc. of the 28th Sym. of the Colston Res. Society, University of Bristol, April 1976.

110. K. F. Kunzi, A. D. Fisher, D. H. Staelin, and J. W. Waters, "Snow and ice surfaces measured by the Nimbus 5 microwave spectrometer," Journal of Geophysical Res., 81, 4965-4980, Sept. 1976.

111. H. J. Zwally, "Microwave emissivity and accumulation rate of polar firn," J. of Glaciology, 18, 195-215, 1977.

112. H. G. Pascalar and R. T. Sakamoto, "Microwave radiometric measurements of ice and water," Proc. of the 3rd Sym. on Rem. Sen. of Environment, University of Michigan, Ann Arbor, MI, Oct. 1964.

113. A. T. Edgerton and D. T. Trexler, "Oceanographic applications of remote sensing with passive microwave techniques," Proc. of the 6th International Sym. on Rem. Sen. of Environment, 2, University of Michigan, Ann Arbor, MI, Oct. 1969.

114. A. W. Adey, T. R. Hartz, R. E. Barrington, W. L. Rolfe, and W. E. Mather, "Theory and field tests of UHF radiometer for determining sea ice thickness," Can. Aeronautics and Space Journal, 17, 425-426, Dec. 1971.

115. A. E. Basharinov, A. S. Gurvitch, and S. T. Igorov, "Features of microwave passive remote sensing," Proc. of the 7th International Sym. on Rem. Sen. of Environment, 1, University of Michigan, Ann Arbor, MI, May 1971.

116. Y. T. Rabinovich, G. G. Shchukin, and V. V. Melentyev, "The determination of the meteorological characteristics of the atmosphere and the Earth's surface from airborne measurements of passive microwave radiation," Proc. of the 7th International Sym. on Rem. Sen. of Environment, 3, University of Michigan, Ann Arbor, MI, May 1971.

117. A. E. Basharinov, A. S. Gurvitch, A. E. Gorodezky, S. T. Hgorov, B. G. Kutuza, A. A. Kurskaya, D. T. Matveev, A. P. Orlov, and A. M. Shutko, "Satellite measurements of microwave and infrared radiobrightness temperature of the Earth's cover and clouds," Proc. of the 8th International Sym. on Rem. Sen. of Environment, 1, University of Michigan, Ann Arbor, MI, Oct. 1972.

118. P. Cloersen, W. Nordberg, T. J. Schmugge, T. T. Wilheit, and W. J. Campbell, "Microwave signatures of first-year and multiyear sea ice," Journal of Geophysical Res., 78, 3564-3572, June 1973.

119. P. Gloersen, T. C. Chang, T. T. Wilheit, and W. J. Campbell, "Polar sea ice observations by means of microwave radiometry," Presented at the Interdisciplinary Sym. on 'Advanced Concepts and Techniques in the Study of Snow and Ice Resources', National Academy of Sciences, Washington, DC, 1974.

120. D. C. Meeks, R. O. Ramseier, and W. J. Campbell, "A study of microwave emission properties of sea ice-- Aidjex 1972," Proc. of the 9th International Sym. on Rem. Sen. of Environment, 1, University of Michigan, Ann Arbor, MI, Apr. 1974.

121. M. Tiuri, A. Lääperi, and K. Jokela, "Passive radiowave

sensing of the thickness and other characteristics of sea ice," Proc. of the 10th International Sym. on Rem. Sen. of Environment, 1, University of Michigan, Ann Arbor, MI, Oct. 1975.

122. S. G. Tooma, R. A. Mennella, J. P. Hollinger, and R. D. Kethum, Jr., "Comparison of sea-ice type identification between airborne dual-frequency passive microwave radiometry and standard laser infrared techniques," Journal of Glaciology, 15, 225-239, 1975.

123. A. T. Edgerton, "Engineering applications of microwave radiometry," Proc. of the 5th Sym. on Rem. Sen. of Environment, University of Michigan, Ann Arbor, MI, April 1968.

124. R. J. Hruby and A. T. Edgerton, "Subsurface discontinuity detection by microwave radiometry," Proc. of the 7th International Sym. on Rem. Sen. of Environment, 1, University of Michigan, Ann Arbor, MI, May 1971.

125. B. R. Jean, J. A. Richerson, and J. W. Rouse, Jr., "Experimental microwave measurements of controlled surfaces," Proc. of the 7th International Sym. on Rem. Sen. of Environment, 3, University of Michigan, Ann Arbor, MI, May 1971.

126. K. Y. Kondratyev, Y. M. Timofeev, and Y. M. Shulgina, "On the feasibility of determining surface soil characteristics from remotely sensed microwave radiation," Proc. of the 7th International Sym. on Rem. Sen. of Environment, 3, University of Michigan, Ann Arbor, MI, May 1971.

127. J. C. Blinn, III, and J. E. Connel, "Microwave emission from geological materials: Observations of interference effects," Journal of Geophysical Res., 77, 4366-4378, Aug. 1972.

128. A. E. Basharinov, L. F. Borodin, and A. M. Shutko, "Passive microwave sensing of moist soils," Proc. of the 9th International Sym. on Rem. Sen. of Environment, 1, University of Michigan, Ann Arbor, MI, April 1974.

129. A. E. Basharinov, L. F. Borodin, and A. M. Shutko, "Passive microwave sensing of moist soils," Proc. of URSI Specialist Meeting on Microwave Scat. and Emis. from the Earth, Nov. 1974.

130. R. W. Newton, S. L. Lee, J. W. Rouse, Jr., and J. F. Paris, "On the feasibility of remote monitoring of soil moisture with microwave sensors," Proc. of the 9th International Sym. on Rem. Sen. of Environment, 1, University of Michigan,

Ann Arbor, MI, April 1974.

131. T. Schmugge, P. Gloersen, T. Wilheit, and F. Geiger, "Remote sensing of soil moisture with microwave radiometers," Journal of Geophysical Res., 79, 317-323, Jan. 1974.

132. A. E. Basharinov, L. F. Borodin, and A. M. Shutko, "Hydrological applications of microwave radiometry data," Proc. of the 10th International Symposium on Rem. Sen. of Environment, 2, University of Michigan, Ann Arbor, MI, Oct. 1975.

133. E. L. Peck, L. W. Larson, R. K. Farnsworth, and T. L. Dietrich, "Comparison of aerial passive gamma and passive microwave techniques for measurement of soil moisture," Proc. of the 10th International Sym. on Rem. Sen. of Environment, 2, University of Michigan, Ann Arbor, MI, Oct. 1975.

134. K. Y. Kondratyev, V. V. Melentyev, Y. I. Rabinovich, and E. M. Shulgina, "Passive microwave remote sensing of soil moisture," Proc. of 11th International Sym. on Rem. Sen. of Environment, 2, University of Michigan, Ann Arbor, MI, April 1977.

135. E. G. Njoku and J. A. Kong, "Theory for passive microwave remote sensing of near-surface soil moisture," Journal of Geophysical Res., 82, 3108-3118, July 1977.

136. R. K. Moore, F. T. Ulaby, and A. Sobti, "The influence of soil moisture on the microwave response from terrain as seen from orbit," Proc. of the 10th International Sym. on Rem. Sen. of Environment, 2, University of Michigan, Ann Arbor, MI, Oct. 1975.

137. H. Genda and H. Okayama, "Simulator for remote sensing and its application to soil moisture measurements," Appl. Optics, 17, 807-813, March 1978.

138. L. F. Curtis, "Remote sensing of soil moisture: User requirements and present prospects," Remote Sensing of the Terrestrial Environment, Proc. of the 28th Sym. of the Colston Res. Society, Bristol, April 1976.

139. R. K. Moore, J. P. Claassen, A. C. Cook, D. L. Fayman, W. J. Pierson, V. J. Cardone, J. Hayes, W. Spring, R. J. Kern, and N. M. Hatcher, "Simultaneous active and passive microwave response of the Earth-- The Skylab radscat experiment," Proc. of the 9th International Sym. on Rem. Sen. of Environment, 1, University of Michigan, Ann Arbor, MI, April 1974.

140. W. J. Campbell, W. F. Weeks, R. O. Ramseier, and P. Gloersen, "Geophysical studies of floating ice by remote sensing," Journal of Glaciology, 15, 305-328, 1975.

141. A. Sobti and R. K. Moore, "Correlation between microwave scattering and emission from land and sea at 13.9 GHz," IEEE Trans. on Geoscience Electron., GE-14, 93-96, April 1976.

142. S. Evans, "Dielectric properties of ice and snow-- A review," Journal of Glaciology, 5, 773-792, Oct. 1965.

143. P. W. F. Bribbon, "Dielectric relaxation in temperate Glaciers," Journal of Glaciology, 6, 897-909, 1967.

144. B. Philberth, "Measurement of the permittivity of ice," Journal of Glaciology, 765-766, 1967.

145. T. Yoshino, "The reflection properties of radio waves on the ice cap," IEEE Trans. on Ant. and Prop., AP-15, 542-551, July 1967.

146. J. R. Addison, "Electrical properties of saline ice," Journal of Appl. Phys., 40, 3105-3114, July 1969.

147. J. R. Addison, "Electrical relaxation in saline ice," Journal of Appl. Phys., 41, 54-63, Jan. 1970.

148. G. E. Webber and I. C. Peden, "VLF ground-based measurements in Antarctica: Their relationship to stratifications in the subsurface terrain," Radio Science, 5, 655-662, Apr. 1970.

149. P. Hoekstra and P. Cappillino, "Dielectric properties of sea and sodium Chloride ice at UHF and microwave frequencies," Journal of Geophysical Res., 76, 4922-4931, July 1971.

150. I. C. Peden and J. C. Rogers, "An experiment for determining the VLF permittivity of deep Antarctic ice," IEEE Trans. on Geoscience Electron., GE-9, 224-233, Oct. 1971.

151. J. W. Perry and A. W. Straiton, "Dielectric constant of ice at 35.3 and 94.5 GHz," J. Appl. Phys., 43, 731-733, Feb. 1972.

152. M. L. Bryan and R. W. Larson, "Application of dielectric constant measurements to radar imagery interpretation," Remote Sensing of Earth Resources, 2, Conf. on Earth Resources Observation and Information Analysis System, Tullahoma, TN, March 1973.

153. A. K. Shemelin, "Electrical and mechanical properties of ice," Sov. Hydrology: Selected Papers, Issue No. 1, 1973.

154. K. J. Campbell and A. S. Orange, "The electrical anisotropy of sea ice in the horizontal plane," Journal of Geophysical Res., 79, 5059-5063, Nov. 1974.

155. M. R. Vant, R. B. Gray, R. O. Ramseier, and V. Makios, "Dielectric properties of fresh and sea ice at 10 and 35 GHz," Journal of Appl. Phys., 45, 4712-4717, Nov. 1974.

156. J. R. Addison, "Electrical properties of saline ice at 1 kHz down to -150°C," Journal of Appl. Phys., 46, 513-522, Feb. 1975.

157. C. R. Bentley, "Advances in geophysical exploration of ice sheets and glaciers," Journal of Glaciology, 15, 113-135, 1975.

158. W. J. Fitzgerald and J. G. Paren, "The dielectric properties of Antarctic ice," Journal of Glaciology, 15, 39-48, 1975.

159. J. W. Glen and J. G. Paren, "The electrical properties of snow and ice," Journal of Glaciology, 15, 15-38, 1975.

160. M. Mellor, "Engineering properties of snow," Journal of Glaciology, 19, 15-66, 1977.

161. J. Schwarz and W. F. Weeks, "Engineering properties of sea ice," Journal of Glaciology, 19, 499-531, 1977.

162. G. C. Thomann, "Experimental results of the remote sensing of sea-surface salinity at 21-cm wavelength," IEEE Trans. on Geoscience Electron., GE-14, 198-214, July 1976.

163. D. C. Pearce, W. H. Hulse, Jr., and J. W. Walker, "The application of the theory of heterogeneous dielectrics to low surface area soil systems," IEEE Trans. on Geoscience Electron., GE-11, 167-170, Oct. 1973.

164. Y. I. Leshchanskii, G. N. Lebedeva, and V. D. Shumilin, "The electrical parameters of sandy and loamy soils in the range of centimeter, decimeter, and meter wavelengths," Moscow Physicotechnical Institute, trans. from Izvestiya Vysshikh Uchebnykh Zavedenii, Radiofizika, 14, 562-569, April 1972.

165. P. Hoekstra and A. Delany, "Dielectric properties of soils at UHF and microwave frequencies," Journal of Geophysical Res., 79, 1699-1708, April 1974.

166. F. C. Karal, Jr., and J. B. Keller, "Elastic, electromagnetic, and other waves in a random medium," Journal of Mathematical Physics, 5, 537-547, April 1964.

167. S. Chandrasekhar, Radiative Transfer, Dover Publications, New York, 1960.

APPENDIX B

GROUND-TRUTH OF SNOW FIELDS IN THE ROME, NEW YORK AREA DURING JANUARY, 1979*

by

ROBERT T. SHIN+

and

MICHAEL A. ZUNIGA+

---

* This work was supported by NASA Contract NAS5-24139 and the AIR FORCE/EGLIN Contract F08635-78-C-0115.

+ Department of Electrical Engineering and Computer Science and Research Laboratory of Electronics, Massachusetts Institute of Technology, Cambridge, Massachusetts 02139

TABLE OF CONTENTS

LIST OF FIGURES

LIST OF TABLES

LIST OF TABLES (CONCLUDED)

SECTION I
INTRODUCTION

This report contains ground-truth measurements of snow fields performed during January 1979 at four sites in the Rome, New York area. The general locations of the sites are shown in Figure B-1 and they are referred to as Rome A, Rome E, Ava B and Ava C. The measurements were taken in connection with planned AIR FORCE SAR IMAGING flights. Two flights were made and these occurred on January 16 and January 29, 1979. The ground-truth acquired on these two days is supplemented by measurements made on six other days. This data was taken by Robert Shin and Michael Zuniga with Shun-Lien Chuang (MIT) assisting.

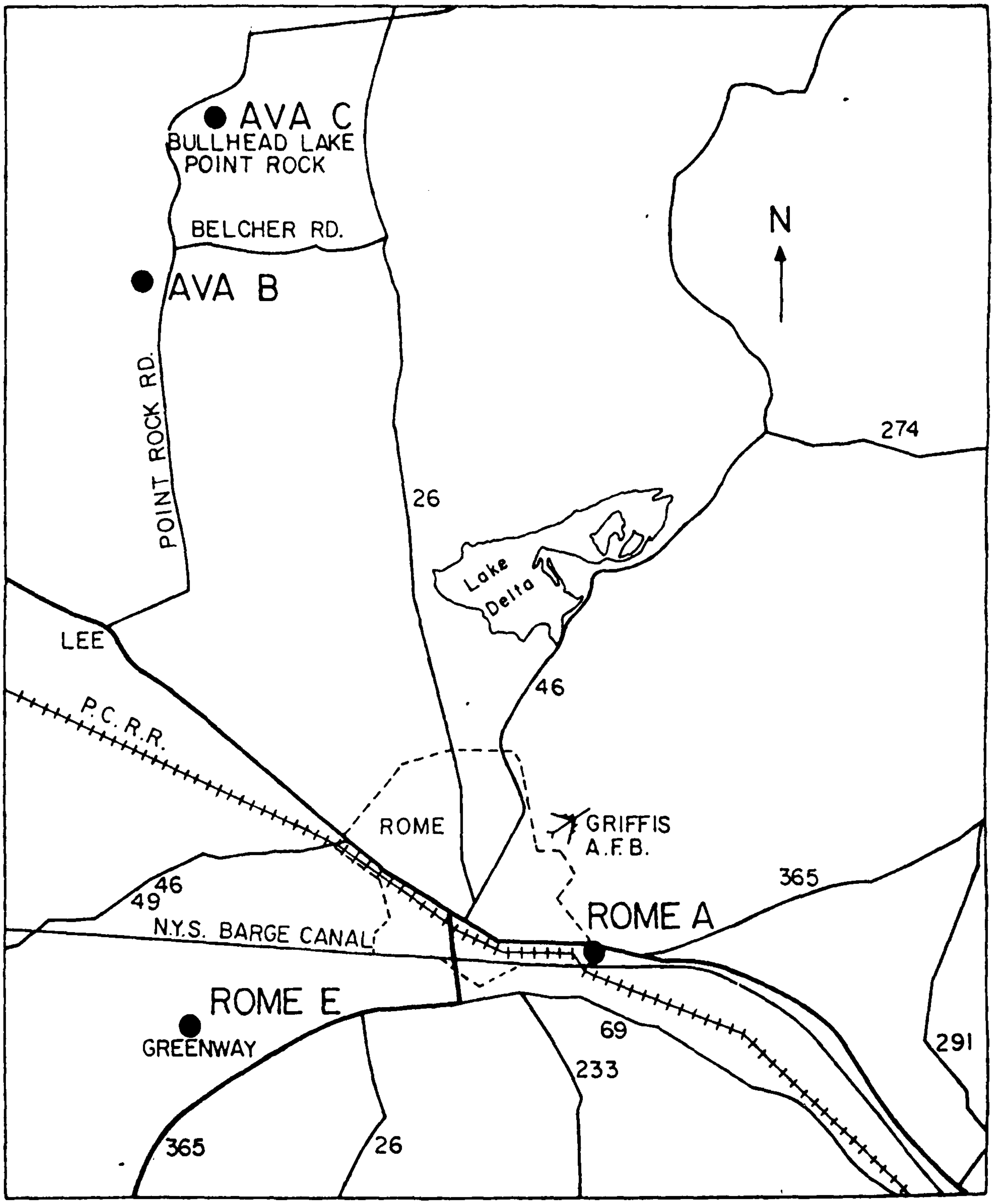

Figure B-1. General Area Map

SECTION II

SITES IN ROME AREA

A. Rome A Site

Two photographs of the site are presented in Figure B-2. The site is a fuel storage area located next to Route 49 near the Rome business district. In Figure B-3 we have a map of the site with the location indicated where snow profile and associated ground-truth measurements were made.

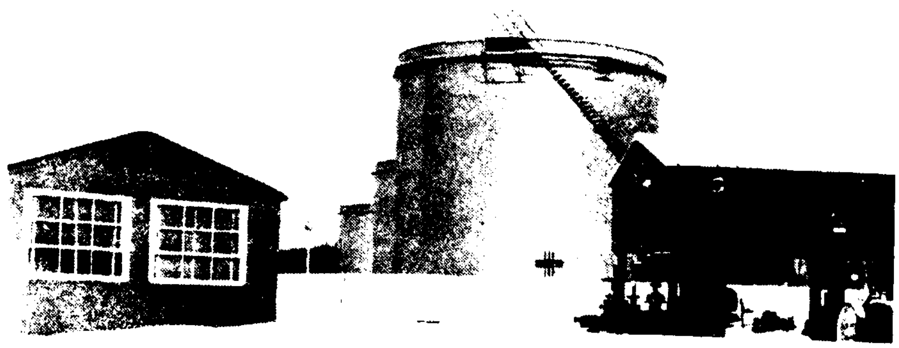

Figure B-2a. Photograph of Rome A Site.

Figure B-2b. Photograph of Rome A Site (Concluded).

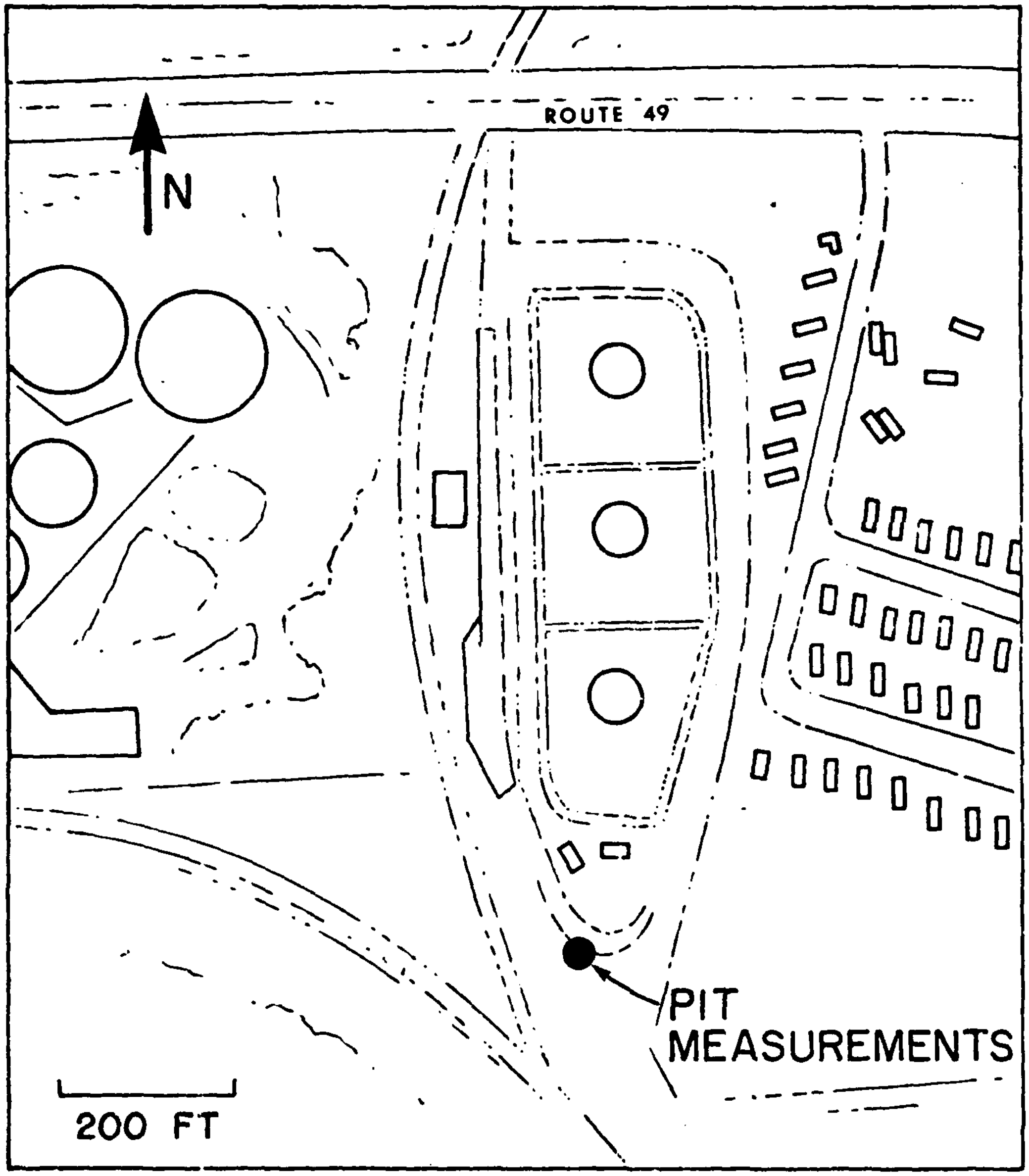

Figure B-3. Map of Rome A Site.

B. Rome E Site

This site is a flat open field located on Greenway Road next to the Greenway Cemetery in Rome. The northwest edge of the site is bounded by deciduous trees. The western and southern edges are bounded by an open field. Photographs and a map of this site are shown in Figure B-4 and Figure B-5, respectively.

Figure B-4a. Photograph of Rome E Site.

Figure B-4b. Photograph of Rome E Site (Concluded).

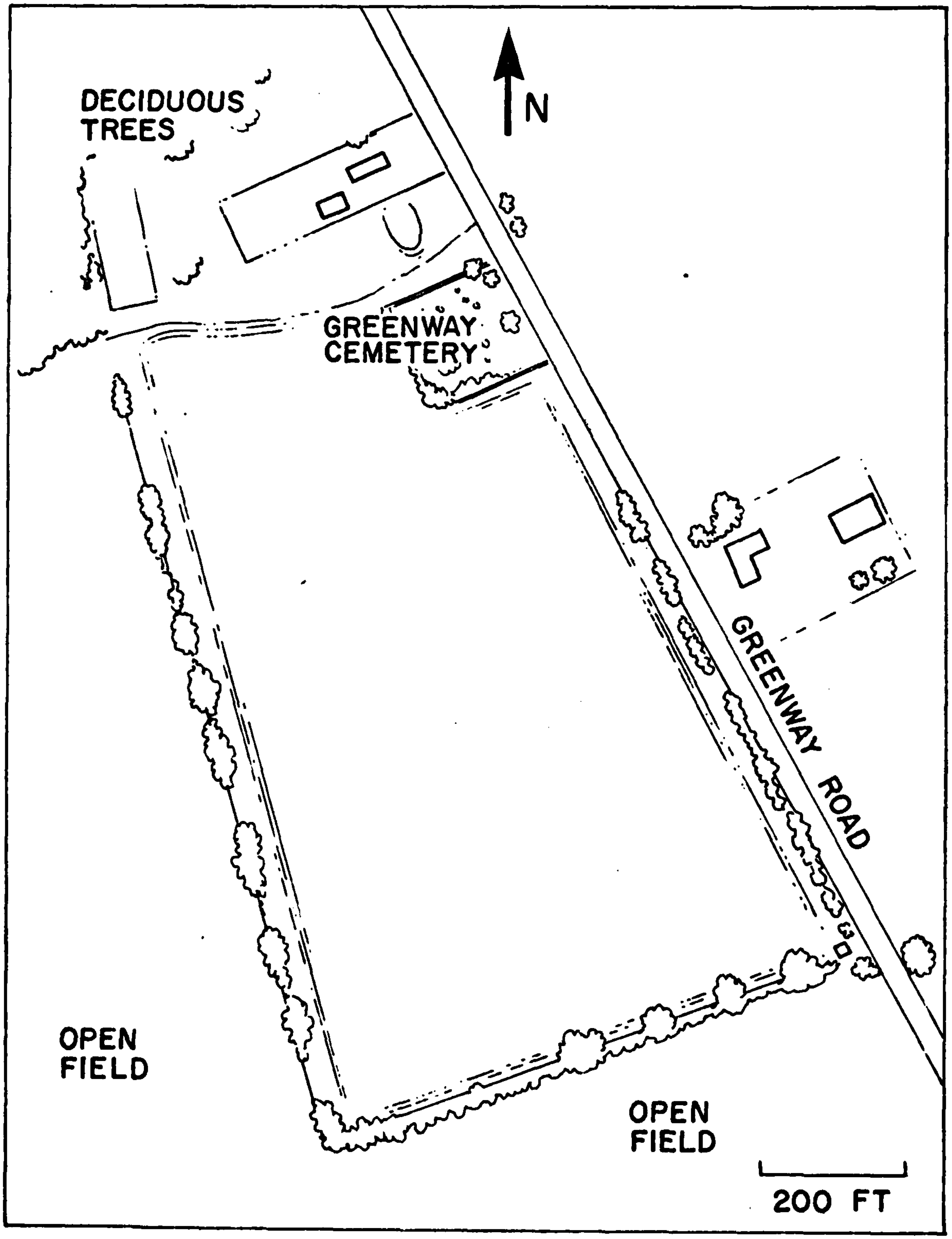

Figure B-5. Map of Rome E Site.

C. Ava B Site

This is a large open field located near the intersection of Belcher Road and Point Rock Road in the town of Lee, north of Rome. The region near the center of the site consisted of hilly terrain. The areas adjacent to Point Rock Road and to the trees in the north-west corner were flat. In Figure B-6 we have a photograph of the site and in Figure B-7 a map of the site with the features of the terrain noted.

Figure B-6a. Photograph of Ava B Site.

Figure B-6b. Photograph of Ava B Site (Continued).

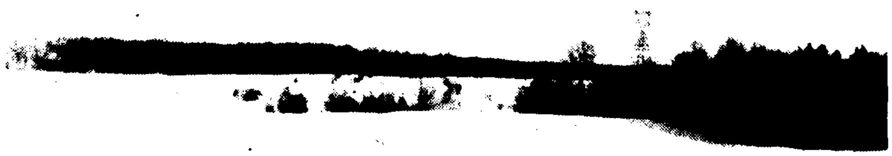

Figure B-6c. Photograph of Ava B Site (Concluded).

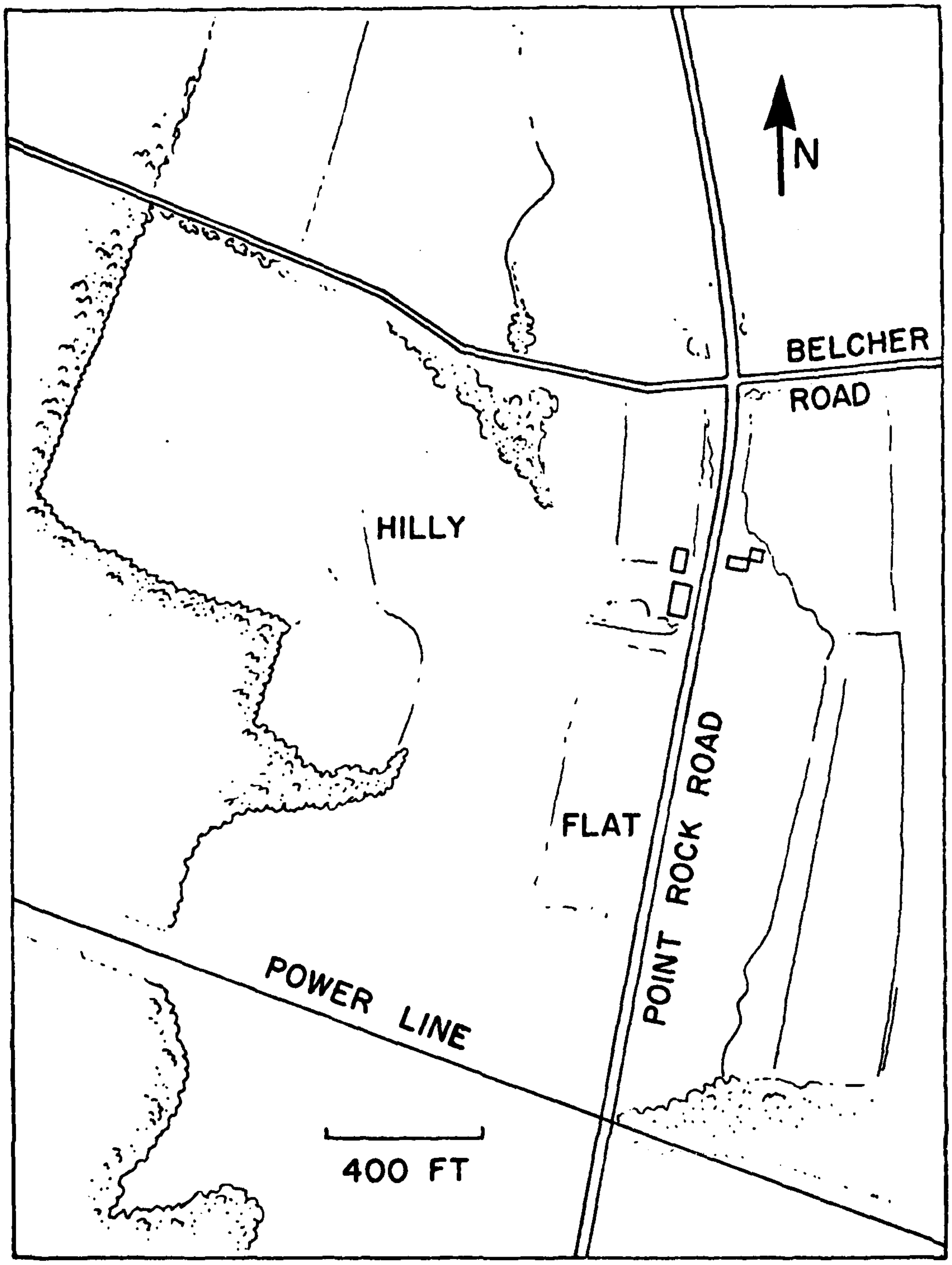

Figure B-7. Map of Ava B Site.

D. Ava C Site

This site is a lake (Bullhead Lake), situated at Kingsley Boyscout Camp in the two of Ava, north of Rome. In Figure B-8 and Figure B-9 we have photographs and a map of the site. The location where the snow profile and associated ground truth measurements were made is noted on the map.

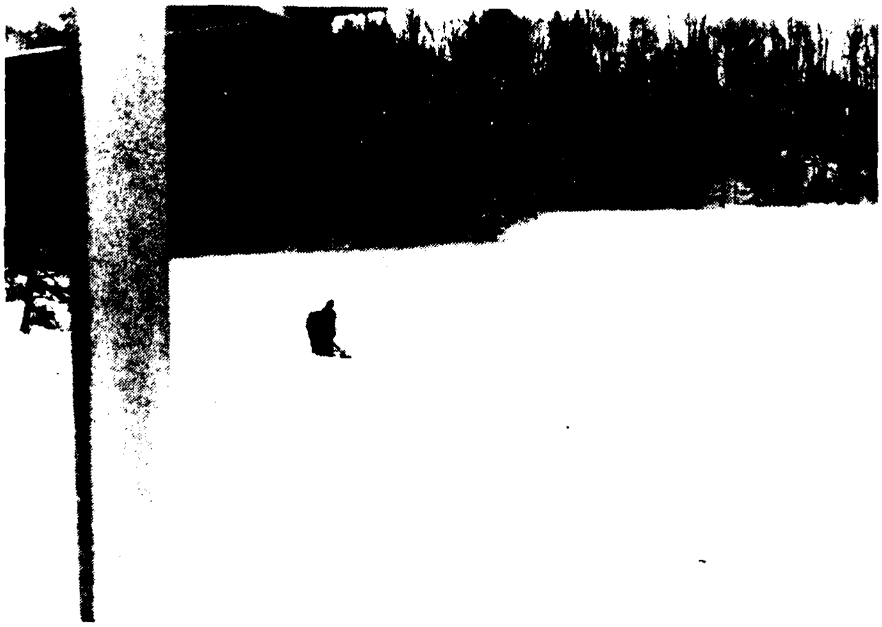

Figure B-8a. Photograph of Ava C Site.

Figure B-8b. Photograph of Ava C Site (Concluded).

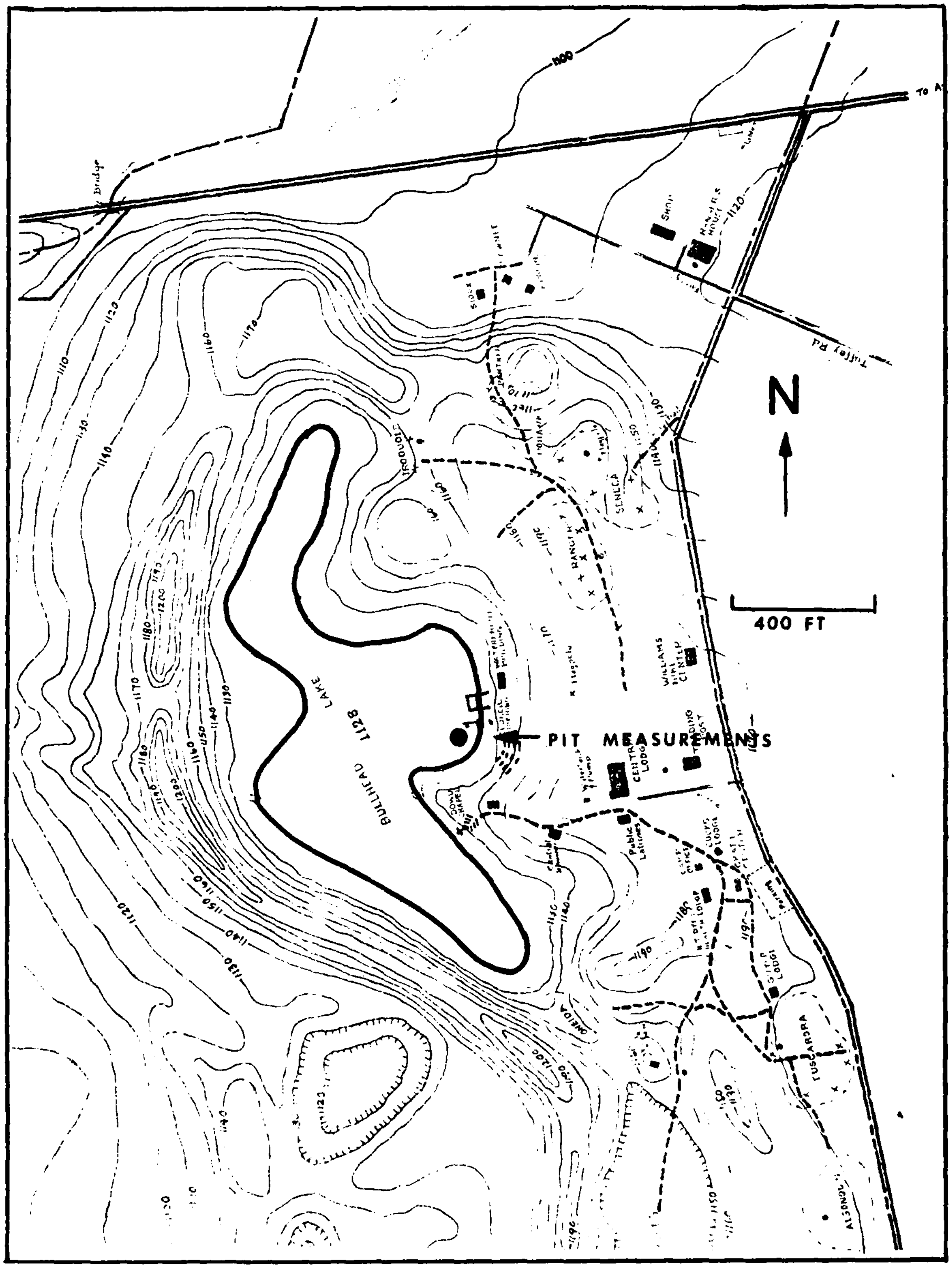

Figure B-9. Map of Ava C Site

SECTION III
GROUND-TRUTH MEASUREMENTS

The ground-truth data gathered at the four sites were acquired using the following procedure:

1. Snow Profile Characterization

Snow profiles were characterized by digging a pit in the snowpack and examining a selected cross sectional area of the snow layer. The various layers in the snowpack were identified and the temperature, average grain size, thickness, and density of each layer were recorded. In some cases, layer was too thin for a density measurement to be made.

2. Free Water Measurement

A freezing calorimetric technique was used to find the percentage by weight of the free water content in the snow.

3. Depth Measurement

Two snow depth measurements were made every 20 meters around the field in order to check for variability.

In Table B-1 we summarized the measurements made at the four sites.

TABLE B-1. SUMMARY OF MEASUREMENTS PERFORMED

Date	Time	Sites and Measurements Made	
January 9	1130 ∿ 1430	Ava B:	Snow Profile and Depth Measurements
January 10	0900 ∿ 1230	Rome E:	Snow Profile, Free Water, and Depth Measurements
	1500 ∿ 1600	Ava C:	Snow Profile and Depth Measurements
January 12	0700 ∿ 0900	Rome A:	Snow Profile and Free Water Measurements
January 16	1200 ∿ 1430	Rome A:	Snow Profile and Free Water Measurements
	1515 ∿ 1730	Ava B:	Snow Profile, Free Water, and Depth Measurements
	1800 ∿ 1830	Ava C:	Snow Profile
January 17	0930 ∿ 1030	Rome E:	Snow Profile and Depth Measurements
January 23	1115 ∿ 1400	Ava B:	Snow Profile and Free Water Measurements
January 29	0900 ∿ 1115	Rome A:	Snow Profile and Free Water Measurements
	1200 ∿ 1400	Ava B:	Snow Profile, Free Water and Depth Measurements
	1515 ∿ 1745	Rome E:	Snow Profile, Free Water and Depth Measurements
January 30	1030 ∿ 1130	Ava C:	Snow Profile

A. January 9, 1979

Ava B Site (1130 ∿ 1430)

TABLE B-2. SNOW PROFILE CHARACTERISTICS OF AVA B SITE

Layer No.	Thickness (cm)	Density (g/100 cc)	Average Grain Size (mm)	Temperature (°C)	Remarks
1	1	4.5	0.2	-6.0	wind blown, light snow
2	19	13	0.3 ∿ 0.4	-3.0	
3	1		0.5 ∿ 1.0		crusty top layer (grains frozen together)
4	6	13	0.7	-3.0	slightly frozen together, packed tightly
5	1		0.5		like third layer
6	4.5	29	0.5	-2.0	
7	3		1.0		like third layer
8	1				ice layer
9	9	32	0.7	0	tightly packed
10	7.5		0.7 ∿ 0.9		like third layer
	ground			0	not frozen

Total Depth: 53 cm

Air Temperature: -10°C

Weather: Sunny

See Figure B-10 for the location of the pit

TABLE B-3. DEPTH MEASUREMENTS OF AVA B SITE

Location No.	Depth Measurements (cm)	Location No.	Depth Measurements (cm)
1	53; 54	18	61; 63
2	55; 55	19	65; 63
3	54; 53	20	65; 65
4	54; 55	21	64; 74
5	55; 54	22	67; 68
6	47; 46	23	75; 73
7	53; 49	24	61; 64
8	57; 57	25	61; 61
9	46; 46	26	60; 60
10	45; 45	27	56; 54
11	55; 53	28	58; 61
12	56; 57	29	45; 46
13	61; 63	30	51; 52
14	61; 63	31	58; 62
15	62; 63	32	53; 54
16	69; 69	33	58; 63
17	62; 64	34	51; 50

Average Depth: 57.9 cm

See Figure B-10 for location of the measurements.

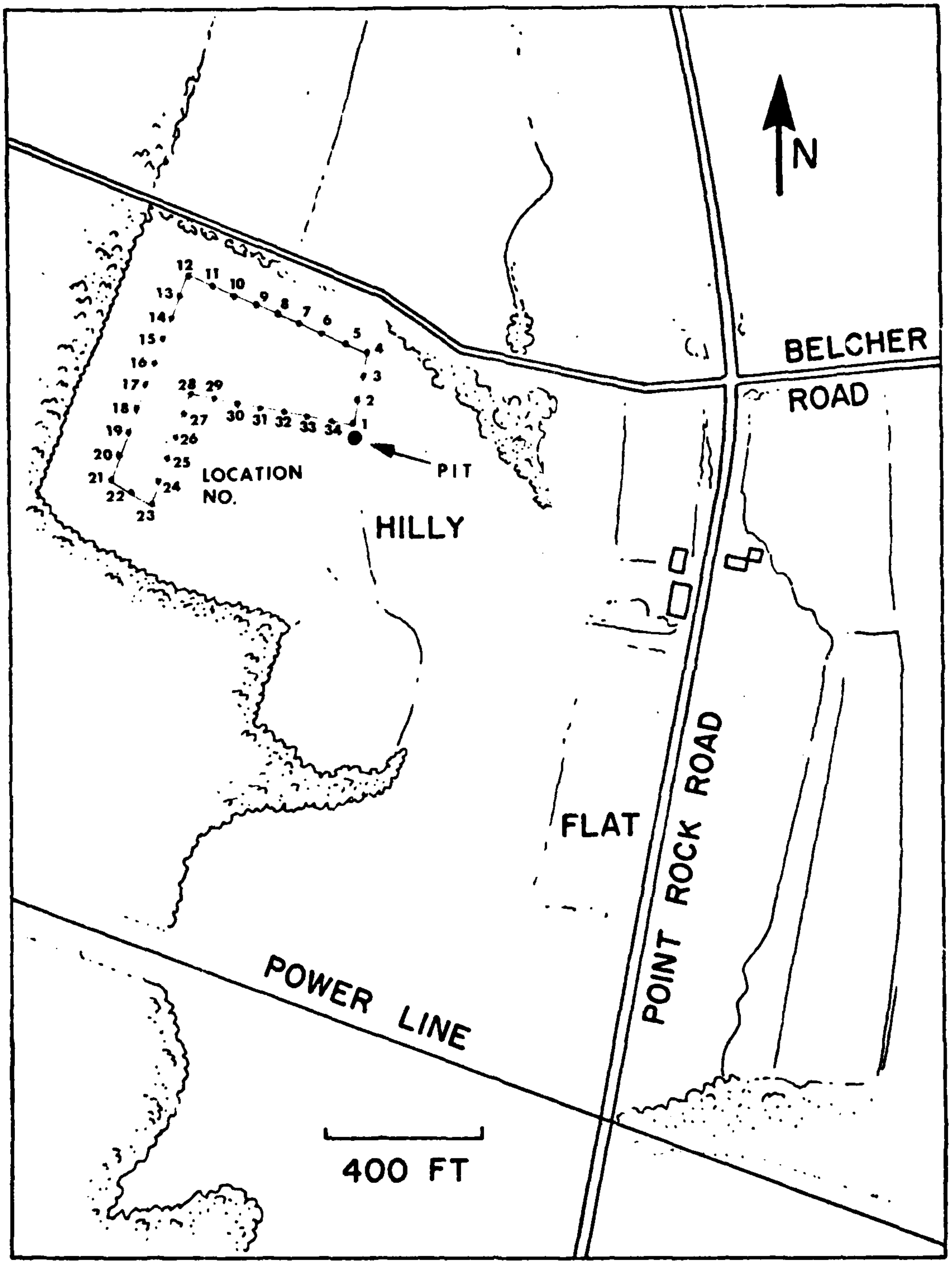

Figure B-10. Map of Ava B Site

B. January 10, 1979

Rome E Site (0900 ∿ 1230)

TABLE B-4. SNOW PROFILE CHARACTERISTICS OF ROME E SITE

Layer No.	Thickness (cm)	Density (g/100 cc)	Average Grain Size (mm)	Temperature (°C)	Remarks
1	2	7.0	0.5	-20	wind blown, light snow
2	17	18.0	0.5 ∿ 0.7	-11	layer appears to be more tightly packed with depth
3	3	43.0	0.8	-4	hard, crusty, tightly packed (grains frozen together)
4	1				ice layer
5	9	32.0	1.0 ∿ 1.5	-1	similar to layer three (not as tightly packed or frozen together)
	ground				

Total Depth: 32 cm

Air Temperature: -20°C

Weather: Sunny, not windy

See Figure B-11 for the location of the pit.

TABLE B-5. FREE WATER CONTENT MEASUREMENTS AT ROME E SITE

Time	Free Water Content (% by weight)	Snow Temp. (°C)	Air Temp. (°C)	Remarks
1000 ∿ 1020	2.7	-13	-13	sunny, not windy
1100 ∿ 1125	2.8	-9	-9	sunny, not windy

Average Free Water Content: 2.8% by weight

The samples were taken from the top 5 cm next to the pit.

TABLE B-6. DEPTH MEASUREMENTS OF ROME E SITE

Location No.	Depth Measurement (cm)	Location No.	Depth Measurement (cm)	Location No.	Depth Measurement (cm)
1	35; 36	16	58; 59	31	36; 36
2	28; 23	17	38; 40	32	44; 48
3	52; 45	18	58; 63	33	38; 44
4	31; 29	19	41; 50	34	41; 52
5	36; 42	20	32; 43	35	45; 51
6	32; 40	21	40; 52	36	40; 42
7	37; 38	22	41; 38	37	53; 55
8	36; 34	23	62; 59	38	47; 49
9	36; 36	24	36; 40	39	48; 48
10	32; 32	25	34; 45	40	56; 58
11	71; 73	26	39; 40	41	56; 56
12	27; 27	27	37; 43	42	48; 44
13	70; 43	28	37; 40	43	40; 37
14	37; 67	29	36; 36		
15	63; 69	30	30; 46		

Average Depth: 43.7 cm

See Figure B-11 for the location of the measurements.

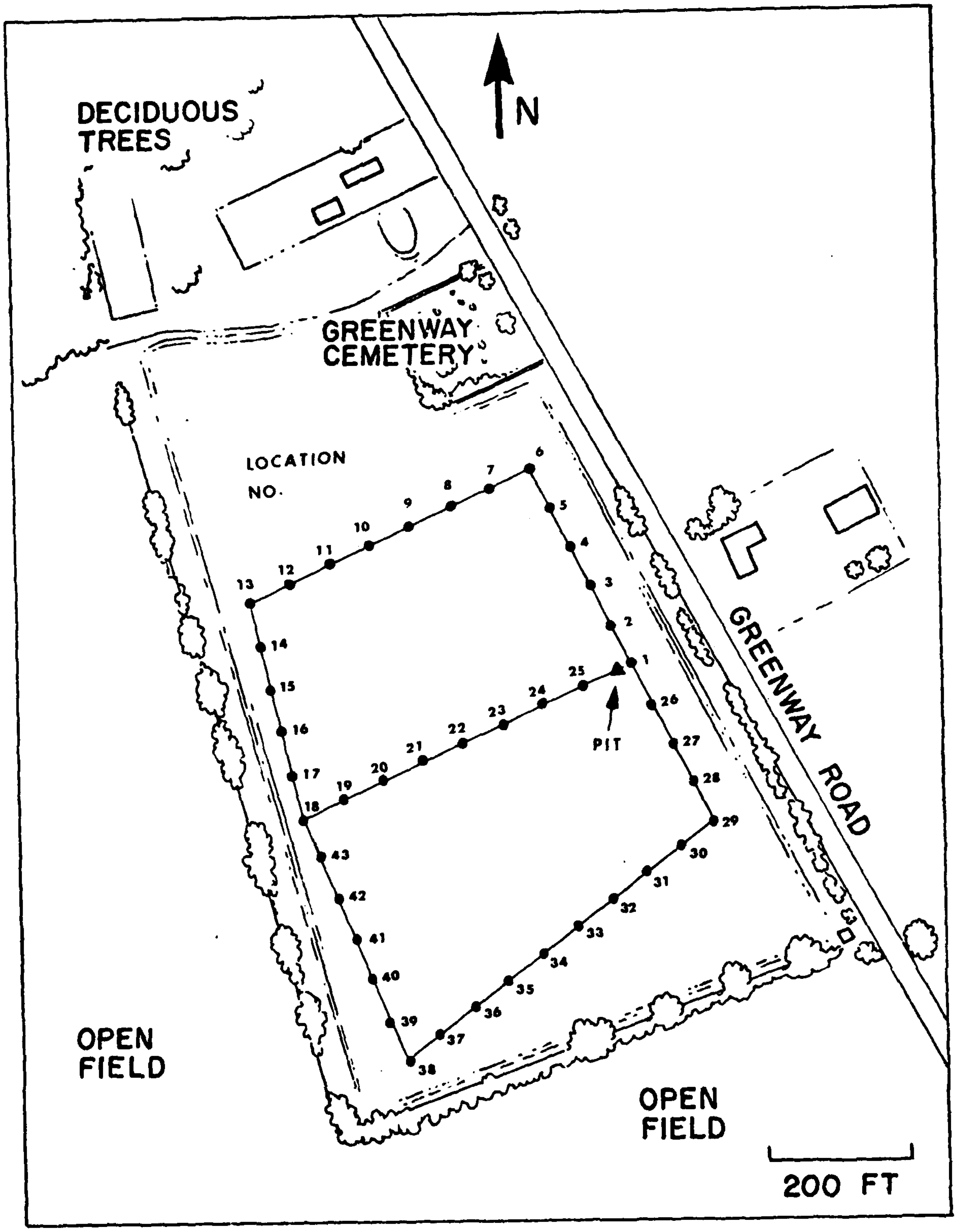

Figure B-11. Map of Rome E Site

Ava C Site (1500 ∿ 1600)

TABLE B-7. SNOW PROFILE CHARACTERISTICS OF AVA C SITE

Layer No.	Thickness (cm)	Density (g/100 cc)	Average Grain Size (mm)	Temperature (°C)	Remarks
1	2	5	0.4	-9	wind blown, loosely packed
2	18.6	13.5	0.5	-7	
3	2		1.0	-1	loosely packed ice grains, not hard
4	5				ice layer
	water				

Total Depth: 22.6 cm (snow depth)

Air Temperature: -9°C

Weather: snowing lightly

See Figure B-12 for the location of the pit.

TABLE B-8. DEPTH MEASUREMENTS OF AVA C SITE

Location No.	Depth Measurements (cm)	Location No.	Depth Measurements (cm)
1	23; 23	5	24; 24
2	22; 22	6	23; 23
3	25; 25	7	23; 23
4	22; 23		

Average Depth: 23.2 cm

See Figure B-12 for the location of the measurements.

Unlike other sites the distance between the measurements is not 20 m.

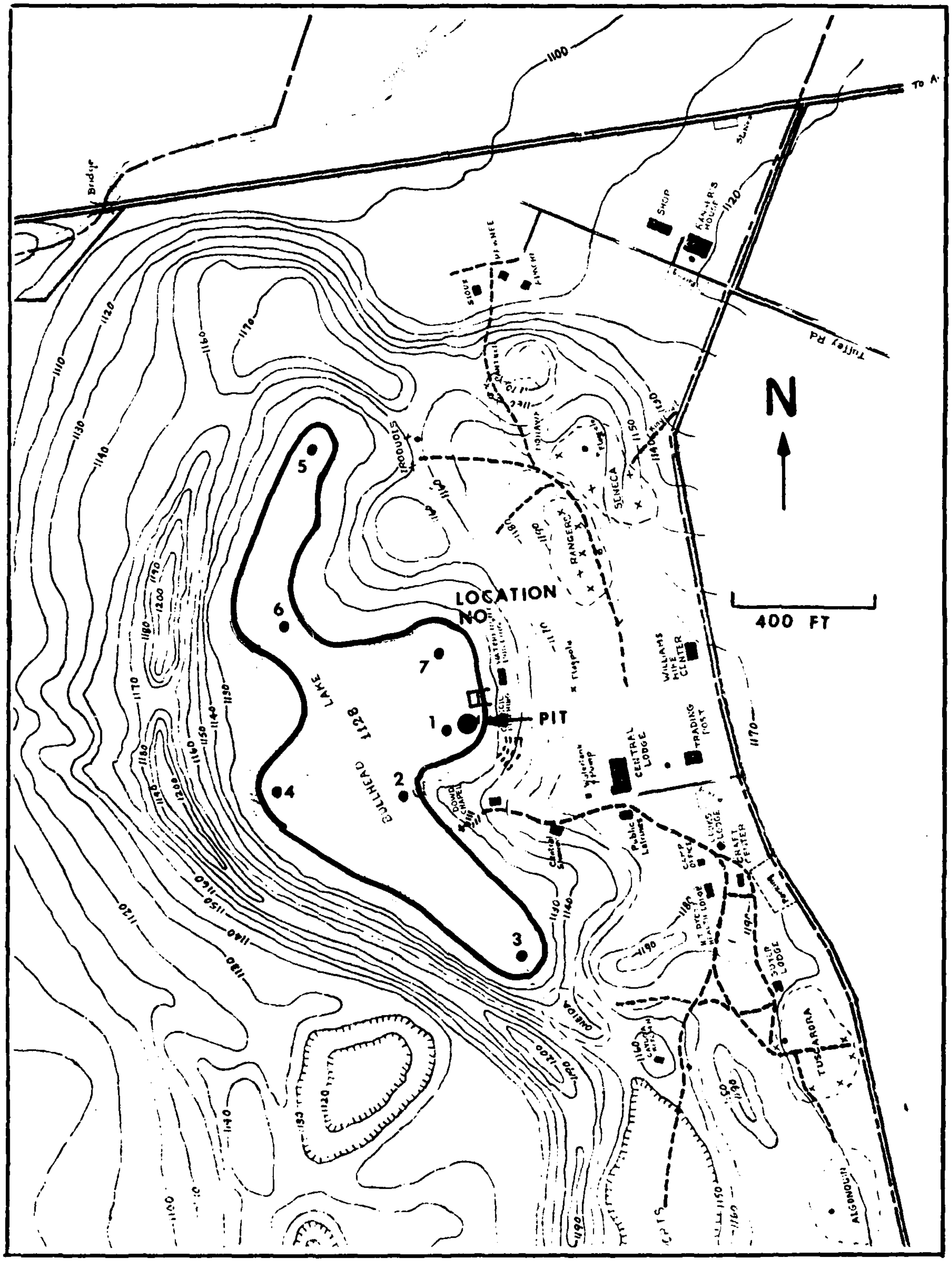

Figure B-12. Map of Ava C Site

C. January 12, 1979

Rome A Site (0700 ∿ 0900)

TABLE B-9. SNOW PROFILE CHARACTERISTICS OF ROME A SITE

Layer No.	Thickness (cm)	Density (g/100 cc)	Average Grain Size (mm)	Temperature (°C)	Remarks
1	2	7	0.2 ∿ 0.4		wind blown, lightly packed
2	15	17	0.8		
3	2	20	1.0		
4	5	28	1.0 ∿ 1.5		crusty, tightly packed (grains frozen together)
5	1				ice layer
6	1				hard, crusty, tightly packed (grains frozen together)
7	1				ice layer
8	2				same as layer 6
	Ground				

Total Depth: 29cm

Air Temperature: -24°C

Weather: Clear, sunny

See Figure B-3 for the location of the pit.

TABLE B-10. FREE WATER CONTENT MEASUREMENTS AT ROME A SITE

Time	Free Water Content (% by weight)	Snow Temp. (°C)	Air Temp. (°C)	Remarks
0715 ∿ 0735	3.0	-16	-24	sunny, not windy
0750 ∿ 0810	1.3	-17	-21	sunny, not windy
0820 ∿ 0840	1.9	-15	-21	sunny, not windy

<u>Average Free Water Content</u>: 2.1% by weight

The samples were taken from the top 5 cm next to the pit.

D. January 16, 1979

Rome A Site (1200 ∿ 1430)

TABLE B-11. SNOW PROFILE CHARACTERISTICS OF ROME A SITE

Layer No.	Thickness (cm)	Density (g/100 cc)	Average Grain Size (mm)	Temperature (°C)	Remarks
1	6	10	1.0 ∿ 1.5	-3	loosely packed (grains are flat in shape)
2	1				ice layer
3	3	32	0.5 ∿ 1.0	-3	hard, crusty, tightly packed
4	11	22	0.5 ∿ 1.0	-2	loosely packed
5	7	35	1.0 ∿ 2.0		hard, crusty, tightly packed (like layer 3)
6	3				ice layer
	ground				

Total Depth: 31 cm

Air Temperature: -5°C

Weather: overcast, snowing lightly

See Figure B-3 for the location of the pit.

TABLE B-12. FREE WATER CONTENT MEASUREMENTS AT ROME A SITE

Time	Free Water Content (% by weight)	Snow Temp. (°C)	Air Temp. (°C)	Remarks
1230 ∿ 1245	6.1	-3	-5	partially sunny
1310 ∿ 1330	6.0	-2	-5	snowing lightly
1340 ∿ 1400	3.6	-3	-4	snowing lightly
1405 ∿ 1430	4.9	-3.5	-5	snowing lightly

<ins>Average Free Water Content</ins>: 5.2% by weight

The samples were taken from the top 5 cm next to the pit.

Ava B Site (1515 ∿ 1730)

TABLE B-13. SNOW PROFILE CHARACTERISTICS OF AVA B SITE

Layer No.	Thickness (cm)	Density (g/100 cc)	Average Grain Size (mm)	Temperature (°C)	Remarks
1	2	5	1.5 ∿ 2.0 (flake size)	-8	very lightly packed (windblown flakes, flat with rib-like structure)
2	7	13	0.2 ∿ 0.5	-6	lightly packed
3	7	45	0.5 ∿ 1.0	-5	hard, crusty layer (spherical like grains frozen together)
4	7	21	0.5 ∿ 1.0	-4	lightly packed
5	6	46	1.0	-3	similar to layer 3
6	12	25	1.0	-1	loosely packed crusty layer
7	18	unable to penetrate	1.0 ∿ 2.0	0	very hard crusty layer (like ice layer) spherical grains frozen solidly together
	ground				

Total Depth: 59 cm

Air Temperature: -8°C

Weather: Partially sunny to snowing moderately

See Figure B-13 for the location of the pit.

TABLE B-14. FREE WATER CONTENT MEASUREMENTS AT AVA B SITE

Time	Free Water Content (% by weight)	Snow Temp. (°C)	Air Temp. (°C)	Remarks
1525∿1545	5.0	-4	-8	partially sunny
1555∿1618	6.2	-6	-8	cloudy
1622∿1640	3.5	-7	-9	snowing lightly
1645∿1705	3.4	-7	-9	snowing moderately

Average Free Water Content: 4.5% by weight

The samples were taken from the top 5 cm next to the pit.

TABLE B-15. DEPTH MEASUREMENTS OF AVA B SITE

Location No.	Depth Measurements (cm)	Location No.	Depth Measurements (cm)
1 (pit)	59	7	41; 45
2	60; 59	8	63; 64
3	51; 52	9	56; 60
4	59; 58	10	53; 56
5	50; 51	11	66; 68
6	50; 54	12	63; 68

Average Depth: 56.8 cm

See Figure B-13 for the location of the measurements.

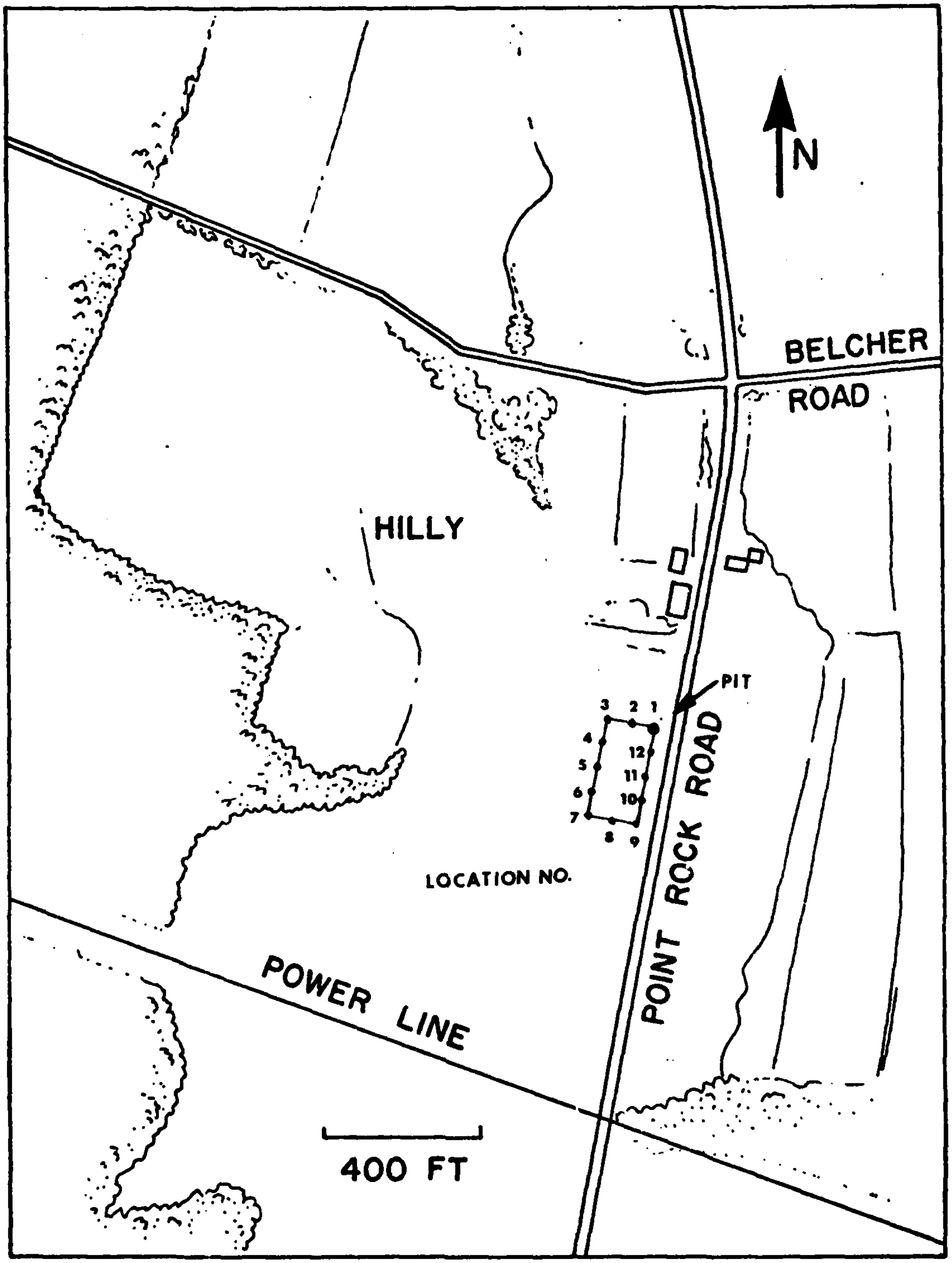

Figure B-13. Map of Ava B Site

Ava C Site (1800 ∿ 1830)

TABLE B-16. SNOW PROFILE CHARACTERISTICS OF AVA C SITE

Layer No.	Thickness (cm)	Density (g/100 cc)	Average Grain Size (mm)	Remarks
1	9 ∿ 10	5.5	3.0[a]	freshly fallen snow, lightly packed, rough surface[b]
2	6.5	14	0.2 ∿ 0.3	
3	1.5		1.0	snow grains frozen together (hard, almost like ice)
4	4	32	0.5 ∿ 0.7	crusty snow
5	1			wet slush
	ice layer			

Total Depth: 22 ∿ 23 cm

Weather: moderately snowing

a 3 mm is a size of snow flakes

b rough surface-- about 1 cm fluctuations in the vertical direction and about 2 cm fluctuations in the horizontal direction.

See Figure B-9 for the location of the pit.

E. January 17, 1979

Rome E (0930 ∿ 1030)

TABLE B-17. SNOW PROFILE CHARACTERISTICS OF ROME E SITE

Layer No.	Thickness (cm)	Density (g/100 cc)	Average Grain Size (mm)	Temperature (°C)	Remarks
1	4	11	0.5	-9	light, wind blown loosely packed
2	7	17.5	0.5	-8	
3	2				ice layer
4	13	21	0.5 ∿ 1.0	-5	granular, slightly frozen together
5	0.5				ice layer
6	6.5	32	1.0 ∿ 1.5	0	very hard crusty snow (grains frozen together)
	ground				

Total Depth: 33 cm

Air Temperature: -10°C

Weather: cloudy

See Figure B-14 for the location of the pit.

TABLE B-18. DEPTH MEASUREMENTS OF ROME E SITE

Location No.	Depth Measurements (cm)	Location No.	Depth Measurements (cm)
1 (pit)	33	7	55; 57
2	23; 26	8	56; 58
3	33; 40	9	48; 50
4	34; 38	10	51; 50
5	46; 50	11	45; 46
6	48; 53	12	46; 43

Average Depth: 44.7 cm

See Figure B-14 for the location of the measurements.

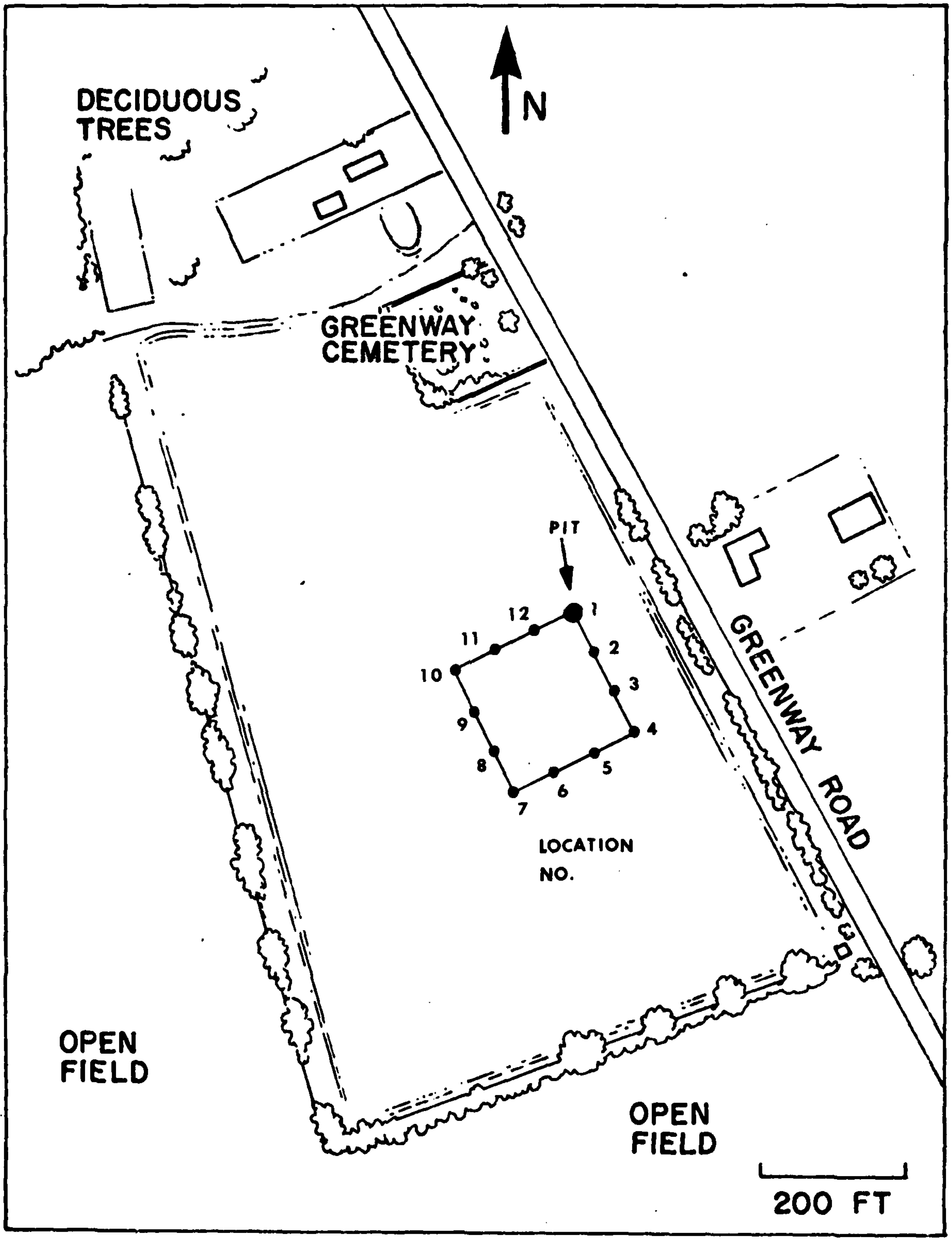

Figure B-14. Map of Rome E Site

F. January 23, 1979

Ava B Site (1115 ∿ 1400)

TABLE B-19. SNOW PROFILE CHARACTERISTICS OF AVA B SITE

Layer No.	Thickness (cm)	Density (g/100 cc)	Average Grain Size (mm)	Temperature (°C)	Remarks
1	1.5	8	0.2 ∿ 0.5	0	freshly fallen snow
2	7	12.5	0.2 ∿ 0.5	0	
3	2.4		0.5 ∿ 1.0		snow grains frozen together
4	10	18	0.5	-1.5	tightly packed snow
5	4		0.5 ∿ 1.0		snow grains frozen together solidly
6	10	21.5	0.5 ∿ 0.8	0	
7	1				ice layer
8	14	27.5	0.5 ∿ 1.0	0	crusty, snow grains not frozen together
9	4		0.5 ∿ 1.0		snow grains frozen together solidly
10	8	30.5	1.0	0	crusty snow layer
11	4				ice layer
	ground				

Total Depth: 65 cm Weather: cloudy Air Temperature: -1°C

See Figure B-13 for the location of the pit.

TABLE B-20. FREE WATER CONTENT MEASUREMENTS AT AVA B SITE

Time	Free Water Content (% by weight)	Snow Temp. (°C)	Air Temp. (°C)	Remarks
1135 ∿ 1155	4.6	-1	-1	cloudy
1220 ∿ 1240	1.9	0	0	cloudy
1255 ∿ 1320	4.8	-1	-1.5	cloudy
1330 ∿ 1350	5.7	0	0	cloudy

Average Free Water Content: 4.3% by weight

The samples were taken from the top 5 cm next to the pit.

AD-A116 448 MASSACHUSETTS INST OF TECH CAMBRIDGE RESEARCH LAB OF--ETC F/G 17/9
PREDICTION OF BACKSCATTER AND EMISSIVITY OF SNOW AT MILLIMETER --ETC(U)
JAN 80 J A KONG, R T SHIN F08635-78-C-0115
UNCLASSIFIED AFATL-TR-80-33 NL

3 of 3
AD A
116448

END
DATE
FILMED
7-82
DTIC

G. January 29, 1979

Rome A Site (0900 ∿ 1115)

TABLE B-21. SNOW PROFILE CHARACTERISTICS OF ROME A SITE

Layer No.	Thickness (cm)	Density (g/100 cc)	Average Grain Size (mm)	Temper-ature (°C)	Remarks
1	4	8	1.0 ∿ 2.0[a]	0	loosely packed snow layer
2	12	39	0.8 ∿ 1.0	0	crusty snow layer (grains frozen together) appears very wet
3	7	26	0.5	0	crusty snow layer, not frozen together
4	5	34	1.0	0	crusty snow (grains frozen together)
5	4				ice layer
	ground				

Total Depth: 32 cm

Air Temperature: -1°C

Weather: cloudy (snow flurries on and off)

a length measurement of needle-like ice crystals

See Figure B-3 for the location of the pit.

TABLE B-22. FREE WATER CONTENT MEASUREMENTS AT ROME A SITE

Time	Free Water Content (% by weight)	Snow Temp. (°C)	Air Temp. (°C)	Remarks
0925∿0948	5.1	0	-1	cloudy

The sample was taken from the top layer (4 cm) of snow next to the pit.

TABLE B-23. FREE WATER CONTENT MEASUREMENTS AT ROME A SITE

Time	Free Water Content (% by weight)	Snow Temp. (°C)	Air Temp. (°C)	Remarks
0955∿1015	8.9	0	-1	light snow flurries
1020∿1040	11.7	0	-1	snow flurries light snow
1045∿1105	10.5	0	-1	cloudy

Average Free Water Content: 10.4% by weight

The samples were taken from the top 10 cm (which included the wet second layer) next to the pit.

Ava B Site (1200 ∿ 1400)

TABLE B-24. SNOW PROFILE CHARACTERISTICS OF AVA B SITE

Layer No.	Thickness (cm)	Density (g/100 cc)	Average Grain Size (mm)	Temperature (°C)	Remarks
1	3	18	0.5 ∿ 1.0[a]	-3	loosely packed, wind blown
2	8	42.5	1.5 ∿ 2.0	0	grains frozen solidly together (almost like an ice layer)
3	5	44	0.5 ∿ 1.0	0	grains frozen together (not solidly)
4	6	39	1.5 ∿ 2.0	0	like layer 2
5	16	30.5	0.5 ∿ 1.0	0	like layer 3
6	2				ice layer
7	13	26	0.8 ∿ 1.0	0	like layer 3
8	13		2.0 ∿ 3.0		like layer 2
	ground				

Total Depth: 66 cm

Air Temperature: -4°C

Weather: snowing lightly to snowing moderately

a length measurement of needle-like crystals.

See Figure B-15 for the location of the pit.

TABLE B-25. FREE WATER CONTENT MEASUREMENTS AT AVA B SITE

Time	Free Water Content (% by weight)	Snow Temp. (°C)	Air Temp. (°C)	Remarks
1200 ∿ 1220	4.1	-1	-4	snowing lightly
1230 ∿ 1255	5.2	-2.5	-4	snowing lightly
1300 ∿ 1320	8.1	-3	-4	snowing lightly
1325 ∿ 1340	5.8	-3	-4	snowing moderately

Average Free Water Content: 5.8% by weight

The samples were taken from the top wind blown layer, next to the pit.

TABLE B-26. DEPTH MEASUREMENTS OF AVA B SITE

Location No.	Depth Measurements (cm)	Location No.	Depth Measurements (cm)
1 (pit)	66	6	60; 62
2	58; 54	7	55; 54
3	61; 62	8	55; 56
4	51; 52	9	63; 65
5	62; 57	10	62; 64

<u>Average Depth</u>: 58.9 cm

See Figure B-15 for the location of the measurements.

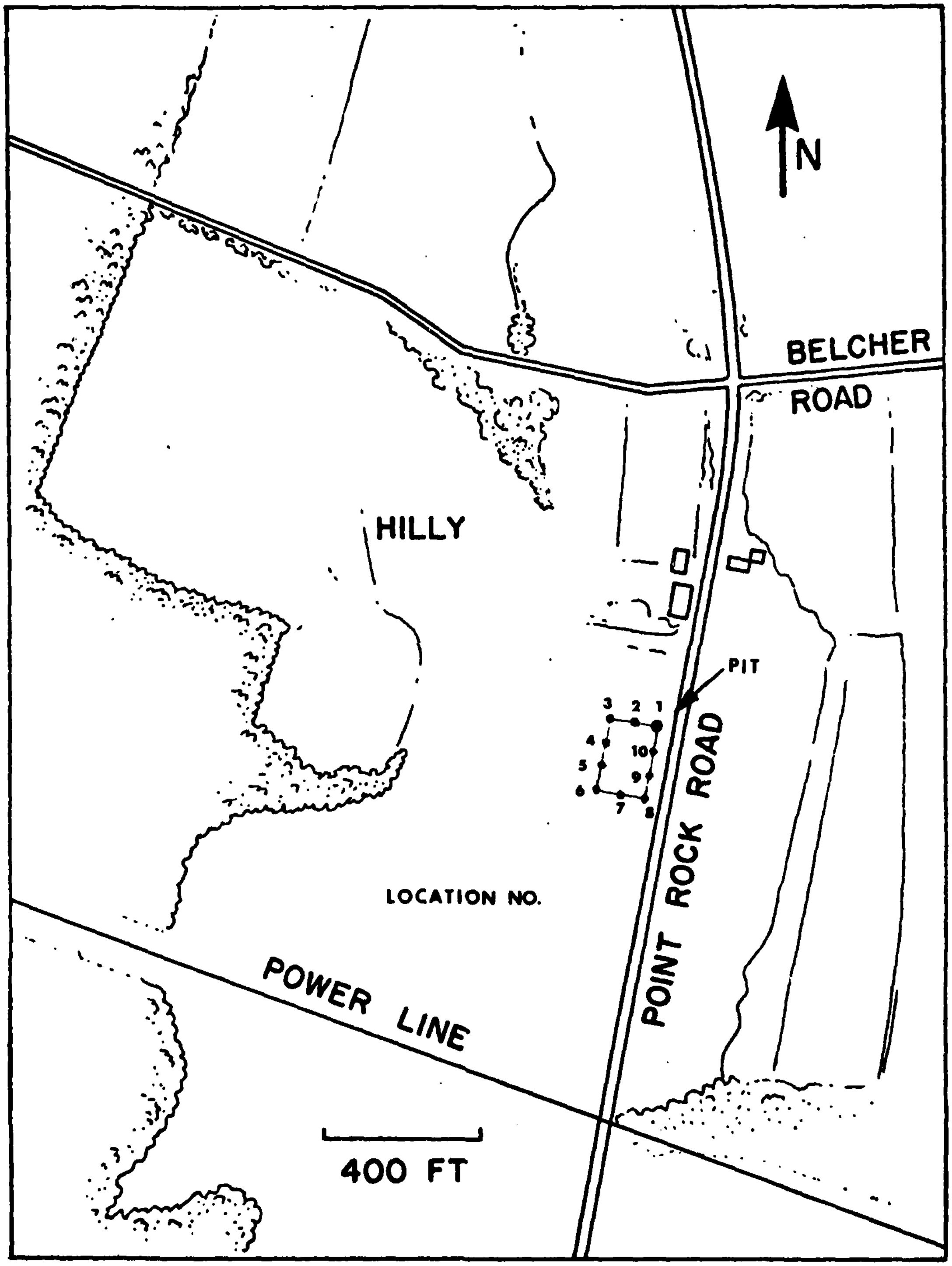

Figure B-15. Map of Ava B Site

Rome E Site (1515 ∿ 1745)

TABLE B-27. SNOW PROFILE CHARACTERISTICS OF ROME E SITE

Layer No.	Thickness (cm)	Density (g/100 cc)	Average Grain Size (mm)	Temperature (°C)	Remarks
1	4	18	0.5[a]	-2	wind blown layer
2	4	43	1.0 ∿ 2.0	0	grains frozen solidly together (almost like an ice layer)
3	16	47	1.0 ∿ 1.5	0	grains frozen together (not solidly), appears to be wet
4	2				ice layer
5	5	32	1.5 ∿ 2.0	0	grains not frozen together (very loosely packed)
	ground				

Total Depth: 31 cm

Air Temperature: -2°C

Weather: cloudy

a length measurement of needle-like ice crystals

See Figure B-14 for the location of the pit.

TABLE B-28. FREE WATER CONTENT MEASUREMENTS AT ROME E SITE

Time	Free Water Content (% by weight)	Snow Temp. (°C)	Air Temp. (°C)	Remarks
1525 ∿ 1545	3.8	0	-2	cloudy
1610 ∿ 1625	4.8	-3	-3	cloudy

Average Free Water Content: 4.3% by weight

The samples were taken from the top wind blown layer, next to the pit.

TABLE B-29. FREE WATER CONTENT MEASUREMENTS AT ROME E SITE

Time	Free Water Content (% by weight)	Snow Temp. (°C)	Air Temp. (°C)	Remarks
1548 ∿ 1610	16.3	0	-3	cloudy
1630 ∿ 1650	15.0	0	-3	cloudy
1655 ∿ 1710	4.6	0	-3	cloudy
1715 ∿ 1735	10.8	0	-3	cloudy

Average Free Water Content: 12.9% by weight

The samples were taken from the wet third layer, next to the pit.

TABLE B-30. DEPTH MEASUREMENTS OF ROME E SITE

Location No.	Depth Measurements (cm)	Location No.	Depth Measurements (cm)
1 (pit)	31	7	47; 49
2	48; 48	8	45; 60
3	46; 47	9	58; 58
4	49; 50	10	57; 54
5	47; 49	11	52; 50
6	38; 40	12	50; 47

<u>Average Depth</u>: 48.7 cm

See Figure B-15 for the location of the measurements.

H. January 30, 1979

Ava C Site (1030 ∿ 1130)

TABLE B-31. SNOW PROFILE CHARACTERISTICS OF AVA C SITE

Layer No.	Thickness (cm)	Density (g/100 cc)	Average Grain Size (mm)	Temperature (°C)	Remarks
1	1		0.5 ∿ 1.0[a]	-2	wind blown, dry
2	3	15	0.5 ∿ 1.0	-1	
3	3.5	37	1.0 ∿ 2.0	0	crusty, grains frozen together (not solidly)
4	0.5				ice layer
5	4		1.0 ∿ 2.0	0	like layer 3
6	2			0	ice-slush mixture
	water				

Total Depth: 14 cm

Air Temperature: -6°C

Weather: cloudy

a length measurements of needle-like ice crystals

See Figure B-9 for the location of the pit.

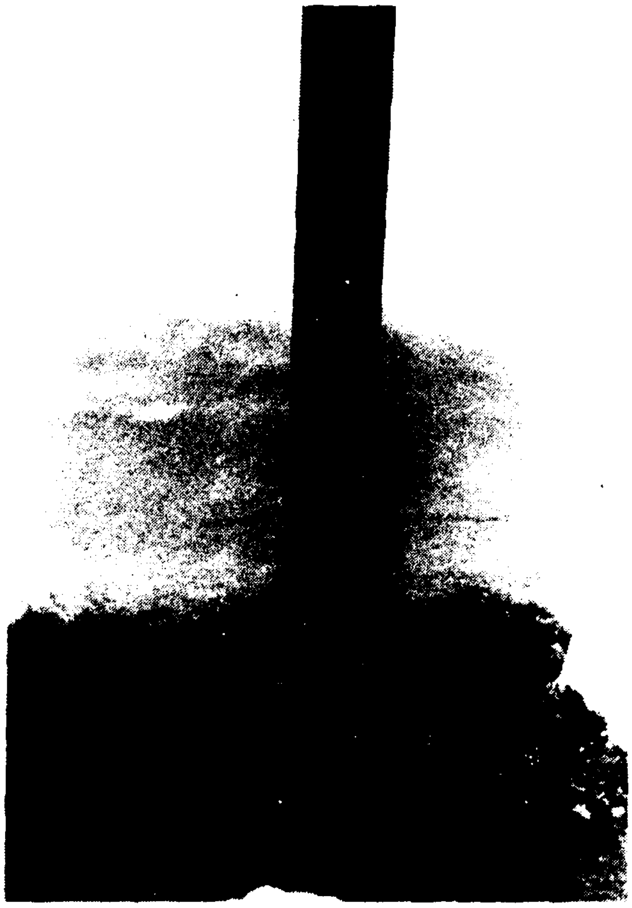

Figure B-16. Photograph of Snowpack Cross-Section at Ava C Site.

APPENDIX C

GROUND-TRUTH OF SNOW FIELDS IN THE ROGERS CITY, MICHIGAN AREA DURING FEBRUARY, 1979*

by

ROBERT T. SHIN+

and

MICHAEL A. ZUNIGA+

---

* This work was supported by NASA Contract NAS5-24139 and the AIR FORCE/EGLIN Contract F08635-78-C-0115.

+ Department of Electrical Engineering and Computer Science and Research Laboratory of Electronics, Massachusetts Institute of Technology, Cambridge, Massachusetts 01293

TABLE OF CONTENTS

LIST OF FIGURES

LIST OF TABLES

SECTION I
INTRODUCTION

This report contains ground-truth measurements performed during February 7 and 8, 1979 of snow fields at two sites in the Rogers City, Michigan area. The general locations of the sites are shown in Figure C-1 and they are referred to as Site E and Site F. The measurements were taken in region to an AIR FORCE SAR IMAGING flight of February 5, 1979. Also, the snowfall and air temperature measurements on February 5, 6, 7, 1979 were obtained from National Weather Service, Alpena Station and included in Tables C-9 through C-12. Figure C-2 shows the relative position of the sites and the Alpena National Weather Service Station.

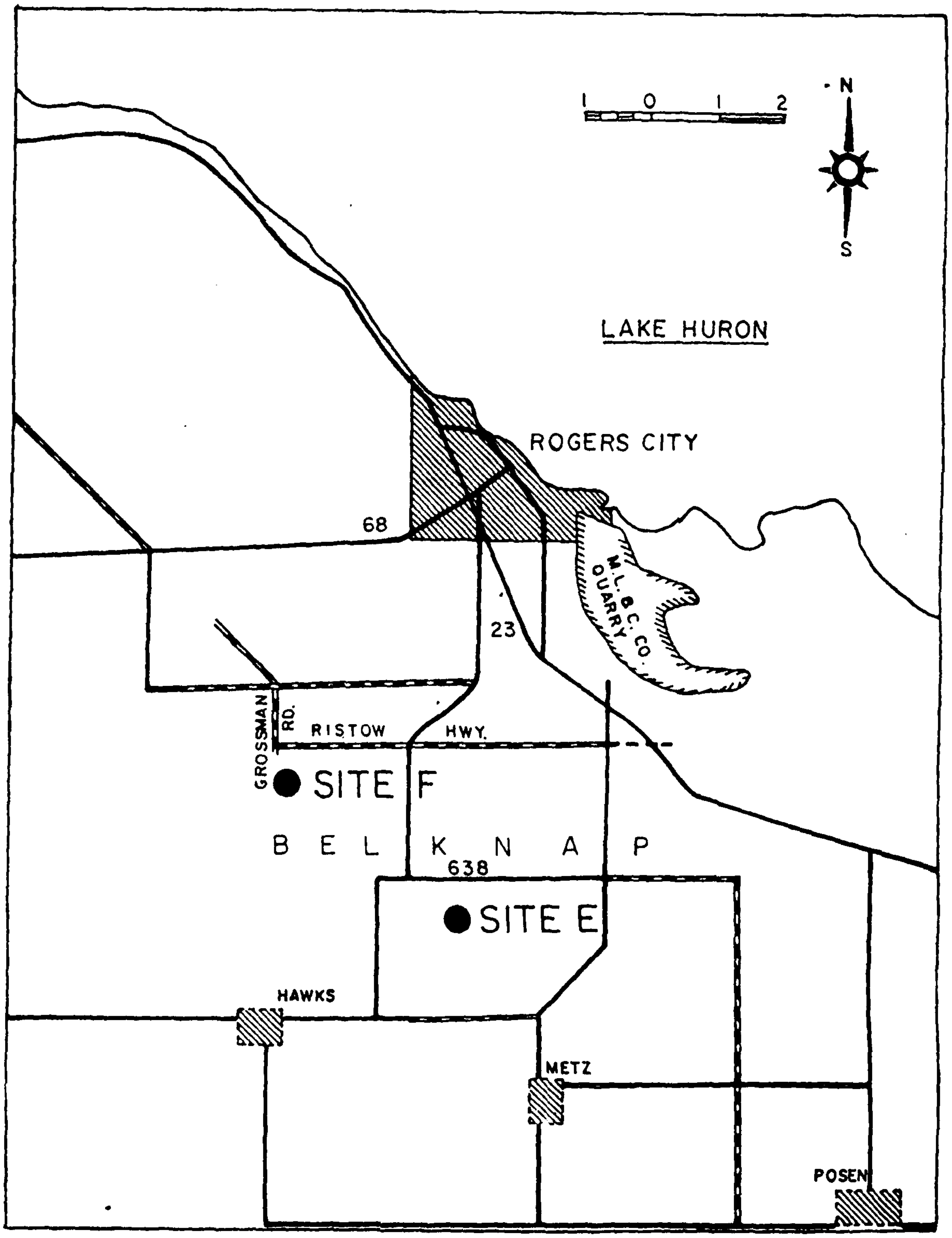

Figure C-1. General Area Map

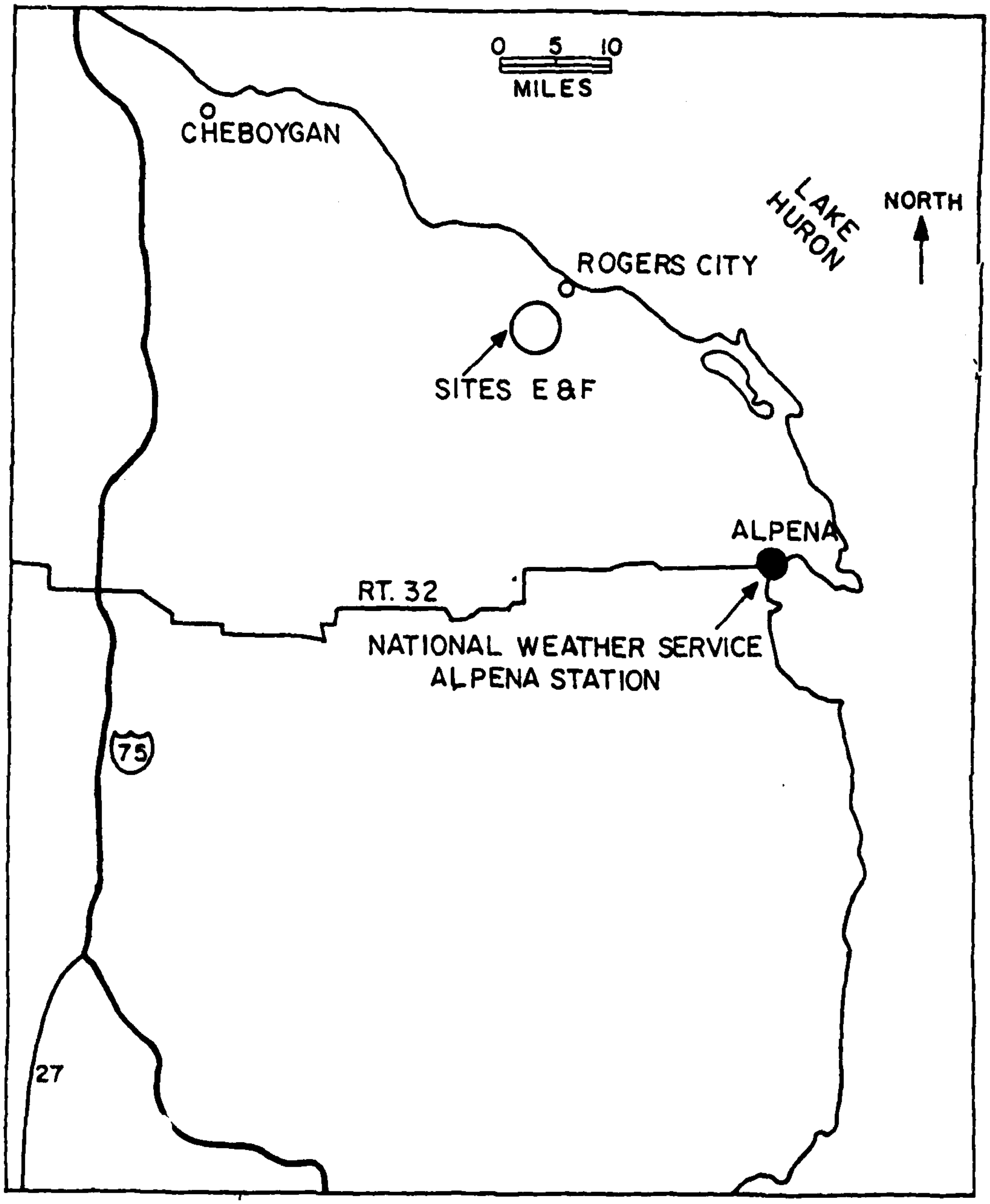

Figure C-2. Location of Alpena National Weather Service Station

SECTION II

SITES IN ROGERS CITY AREA

A. Site E

This site is a flat open field location next to the intersection of 451 Road and 638 Highway in the town of Belknap, south of Rogers City. The western edge of the site is bounded by a mixture of deciduous and pine trees. Photographs and a map of this site are shown in Figures 3 and 4, respectively.

Figure C-3a. Photograph of Site E

Figure C-3b. Photograph of Site E (Concluded)

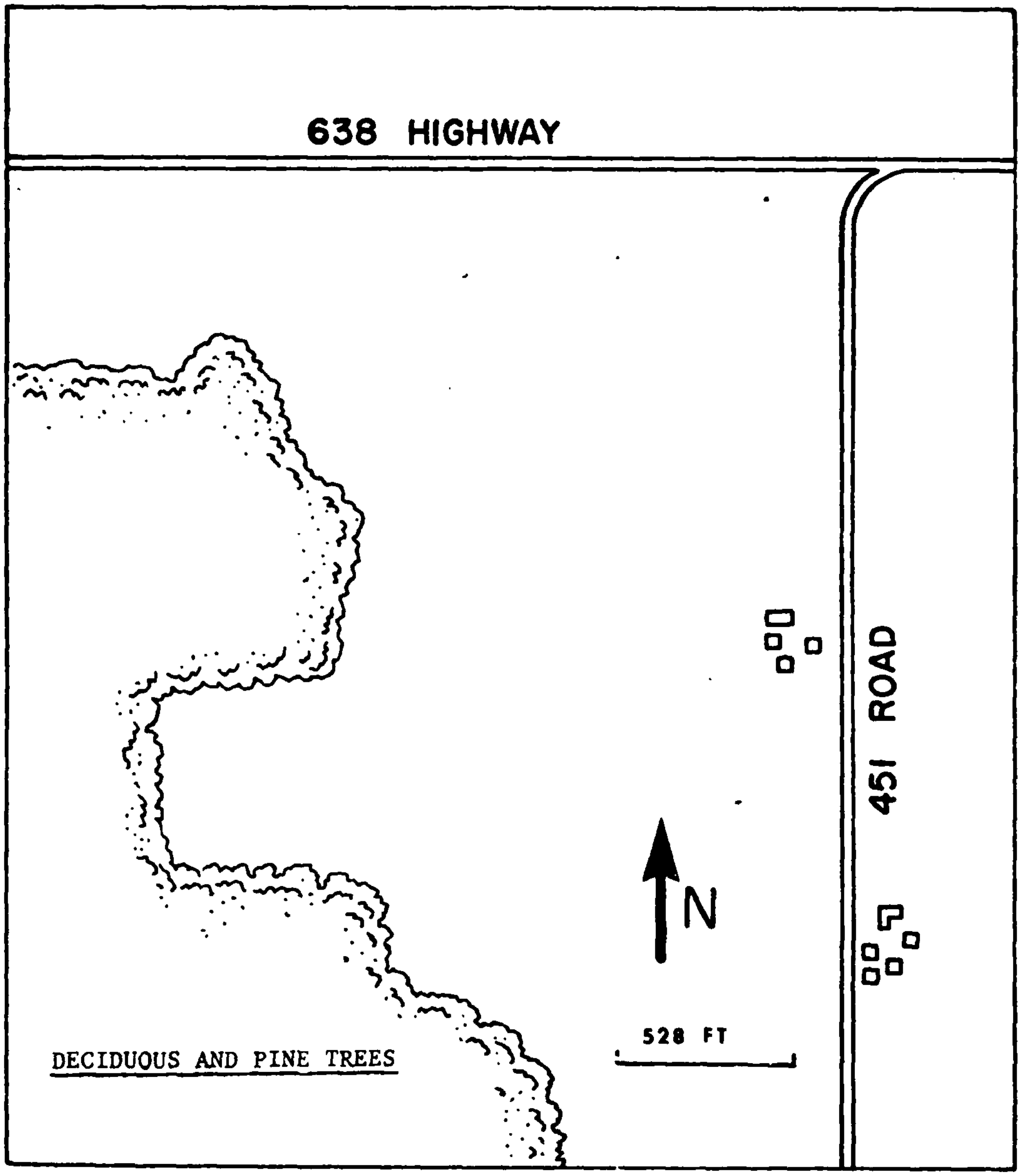

Figure C-4. Map of Site E

B. Site F

This site is a pond (Klees Pond), situated near the intersection of Grossman Road and West Ristow Highway in the town of Belknap, south of Rogers City. In Figures 5 and 6 we have photographs and a map of the site.

Figure C-5a. Photograph of Site F

Figure C-5b. Photograph of Site F (Concluded)

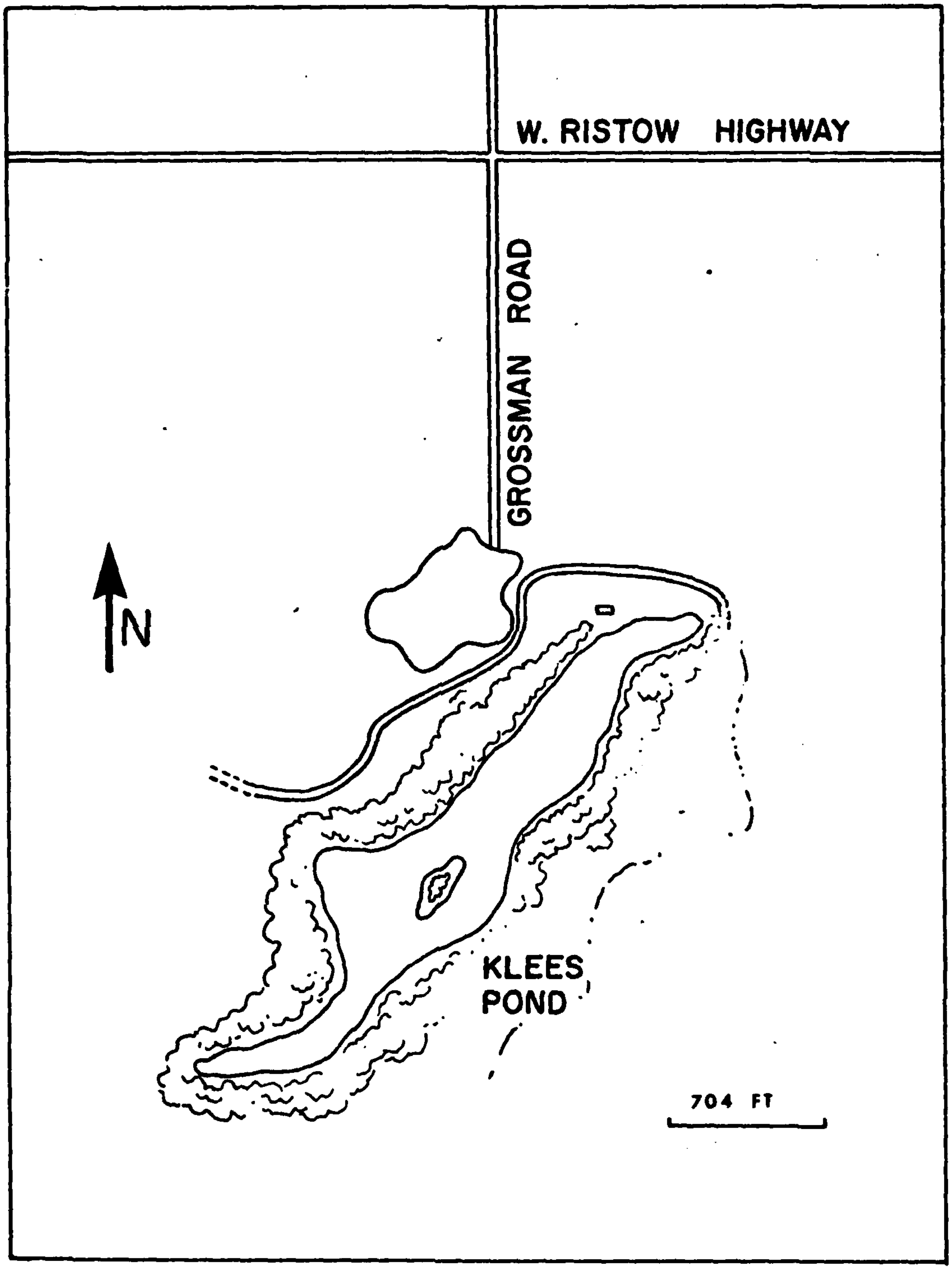

Figure C-6. Map of Site F

SECTION III
GROUND-TRUTH MEASUREMENTS

The ground truth data gathered at the two sites were acquired using the following procedures:

1. Snow Profile Characterization

Snow profiles were characterized by digging a pit in the snowpack and examining a selected cross sectional area of the snow layer. The various layers in the snowpack were identified and the temperature, average grain size, thickness, and density of each layer were recorded. In some cases, layer was too thin for a density measurement to be made.

2. Depth Measurement

Two snow depth measurements were made every 20 meters either around or across the field in order to check for variability.

Measurements on two sites, Site E and Site F, were made on both February 7 and 8, 1979.

A. February 7, 1979

Site E (1125 1400)

TABLE C-1. SNOW PROFILE CHARACTERISTICS OF SITE F

Layer No.	Thickness (cm)	Density (g/100 cc)	Average Grain Size (mm)	Temperature (°C)	Remarks
1	5	4	$2 \sim 4^a$	-3.0	freshly fallen snow rough surface, very loosely packed
2	9	21	$0.5 \sim 1.0$	-4.6	slightly crusty, granular
3	14	26	$0.5 \sim 1.0$	-5.6	same as layer 2, except this layer is more tightly packed
4	5	30	1.0	-5.0	same as layer 3
5	12	27.5	1.0	-3.7	same as layer 3
6	6	27.5	$1.0 \sim 1.5$	-2.0	same as layer 3
7	10	24.5	$1.5 \sim 2.0$	+0.4	granular, loosely packed (grains are not held together)
	ground				

Total Depth: 61 cm

Air Temperature: -5.4°C

Weather: snowing lightly

a Size of snow flakes

See Figure C-7 for the location of the pit.

TABLE C-2. DEPTH MEASUREMENTS OF SITE E

Location No.	Depth Measurements (cm)	Location No.	Depth Measurements (cm)
1 (pit)	61	23	56; 57
2	68; 64	24	59; 60
3	57; 59	25	62; 63
4	59; 57	26	63; 66
5	56; 56	27	64; 66
6	61; 61	28	54; 55
7	58; 60	29	66; 70
8	55; 55	30	63; 64
9	54; 56	31	62; 63
10	63; 64	32	62; 66
11	63; 60	33	59; 56
12	58; 60	34	64; 67
13	56; 57	35	64; 59
14	60; 64	36	61; 62
15	61; 63	37	65; 67
16	52; 53	38	63; 64
17	65; 63	39	72; 74
18	49; 48	40	65; 66
19	50; 50	41	56; 60
20	59; 59	42	54; 53
21	50; 54	43	57; 57
22	51; 52	44	61; 62

Average Depth: 59.9 cm

See Figure C-7 for the location of the measurements.

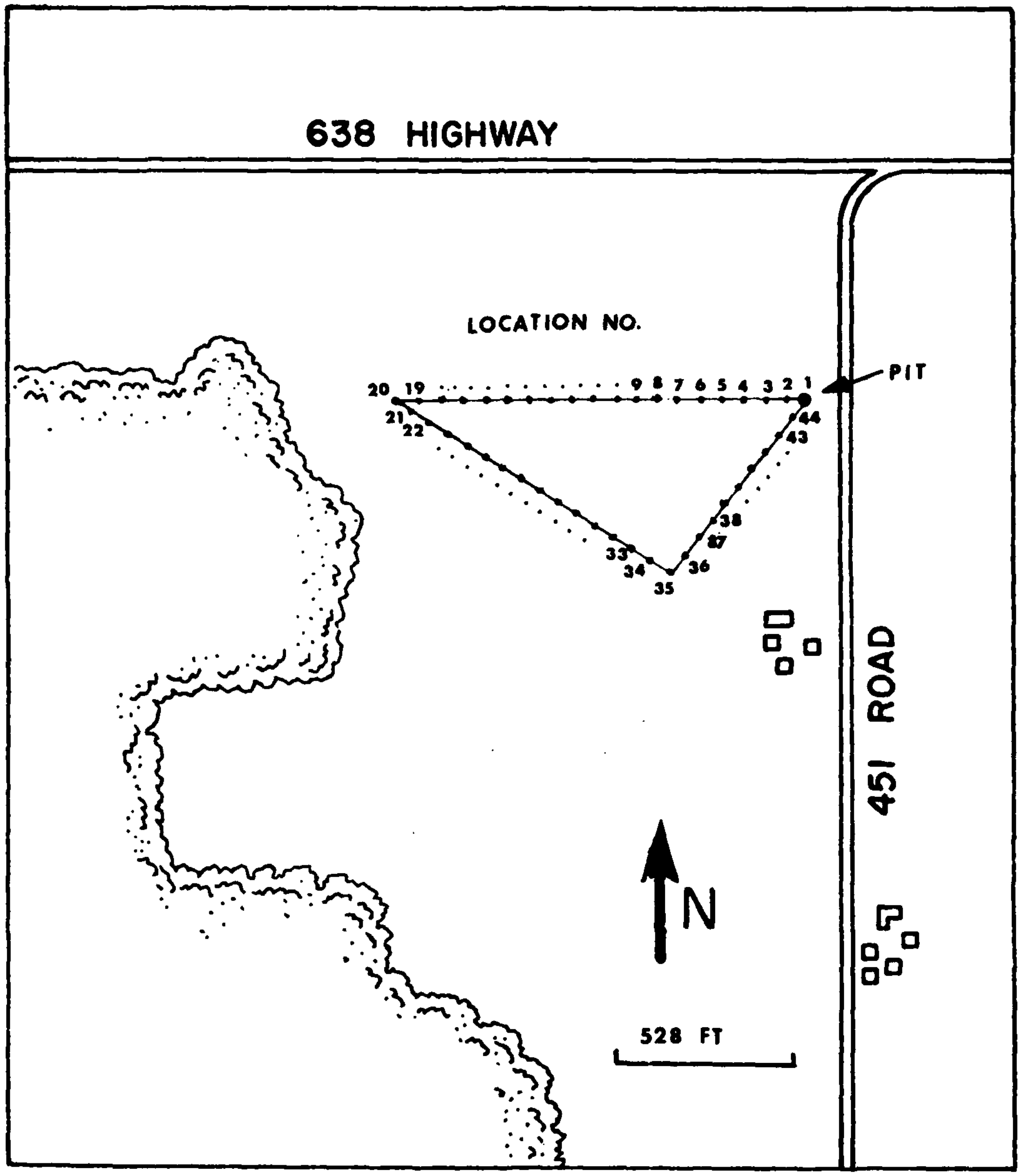

Figure C-7. Map of Site E

Site F (1630 ∿ 1715)

TABLE C-3. SNOW PROFILE CHARACTERISTICS OF SITE F

Layer No.	Thickness (cm)	Density (g/100 cc)	Average Grain Size (mm)	Temperature (°C)	Remarks
1	3.5	3	2.0 ∿ 4.0[a]	-4.0	freshly fallen snow flakes
2	5.5	10	1.0[b]	-2.0	broken flakes
3	0.5		1.0 ∿ 1.5		grains frozen together
4	14.5	22.5	1.0 ∿ 1.5	+1.0	granular, loosely packed
	ice				

Total Depth: 24 cm

Air Temperature: -8.0°C

Weather: cloudy

a size of snow flakes

b length measurement of needle-like broken flakes

See Figure C-8 for the location of the pit.

TABLE C-4. DEPTH MEASUREMENTS OF SITE F

Location No.	Depth Measurements (cm)	Location No.	Depth Measurements (cm)
1	19; 21	4	19; 20
2	21; 20	5	19.5; 19.5
3	20; 20		

Average Depth: 19.9 cm

See Figure C-8 for the location of measurements.

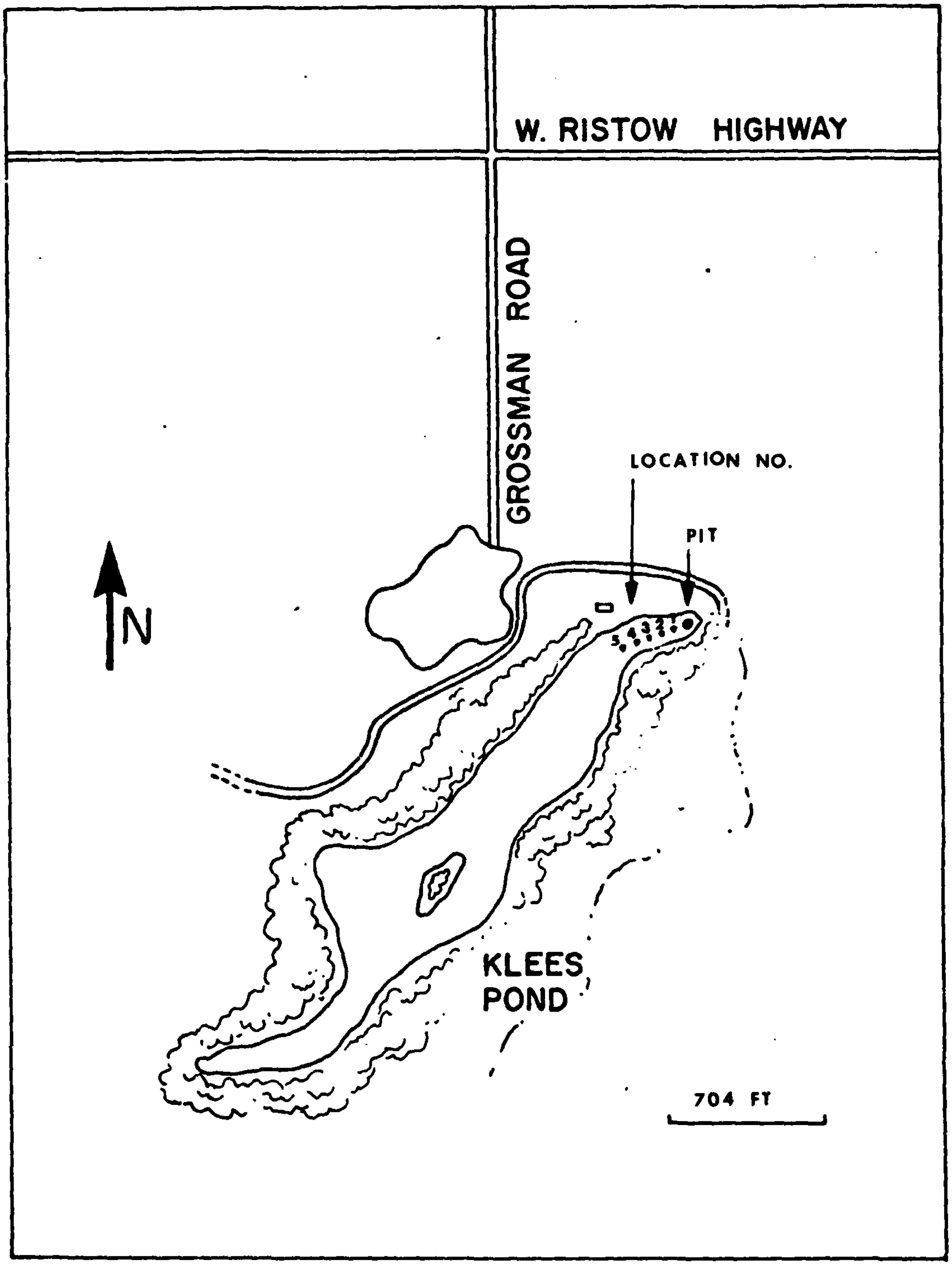

Figure C-8. Map of Site F

B. February 8, 1979

Site E (1250 ∿ 1430)

TABLE C-5. SNOW PROFILE CHARACTERISTICS OF SITE E

Layer No.	Thickness (cm)	Density (g/100 cc)	Average Grain Size (mm)	Temperature (°C)	Remarks
1	1		0.3	-11.7	tightly wind packed
2	10.5	6	1.0 ∿ 1.5[a]	-9.4	broken flakes
3	0.5		0.5 ∿ 1.0		crusty, grains frozen together, fractures easily
4	8.5	28.5	0.7	-6.5	granular, tightly packed (not frozen together)
5	4.5	31	0.5	-4.9	granular, packed together
6	37				granular, packed together
		27	0.7	-3.9	at 34 cm from the bottom
		28	0.7 ∿ 1.0	-2.9	at 29 cm from the ground
		28	1.0	-1.8	at 23 cm from the ground
		28	1.0	-1.4	at 18 cm from the ground
		28	1.0	+0.6	at 12 cm from the ground
	ground				

Total Depth: 61 cm   Air Temperature: -15°C   Weather: clear sunny

a Size of snow flakes. See Figure C-9 for the location of the pit.

TABLE C-6. DEPTH MEASUREMENTS OF SITE E

Location No.	Depth Measurements (cm)	Location No.	Depth Measurements (cm)
1 (pit)	61	11	61; 63
2	50; 54	12	58; 59
3	60; 61	13	64; 65
4	61; 64	14	60; 65
5	65; 65	15	64; 70
6	68; 60	16	57; 55
7	65; 67	17	63; 67
8	59; 60	18	61; 63
9	62; 63	19	61; 59
10	60; 62		

Average Depth: 61.7 cm

See Figure C-9 for the location of measurements.

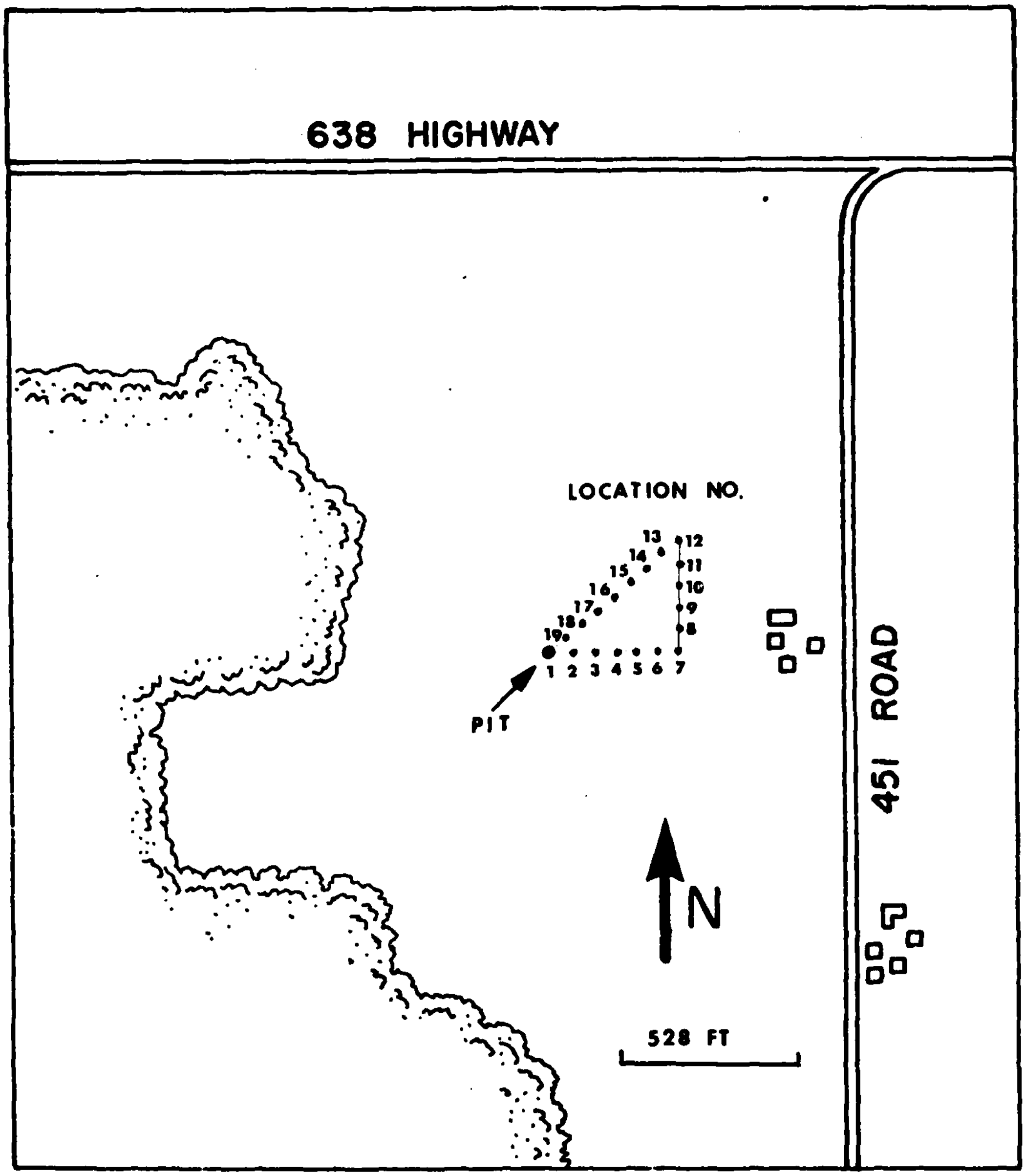

Figure C-9. Map of Site E

Site F (1617 ∿ 1715)

TABLE C-7. SNOW PROFILE CHARACTERISTICS OF SITE F

Layer No.	Thickness (cm)	Density (g/100 cc)	Average Grain Size (mm)	Temperature (°C)	Remarks
1	0.5		0.3		tightly wind packed layer
2	6.5	6.5	2.0 ∿ 4.0[a]	-4.0	very light, like fresh fallen snow consists of broken snow flakes
3	0.5		0.5		crusty, granular (grains frozen together)
4	9.5	21	1.0	-1.9	granular, packed together
5	20		2.0	+0.8	granular, loosely packed together
	ice				

Total Depth: 19 cm

Air Temperature: -14.5°C

Weather: clear, sunny

a Size of broken snow flakes

See Figure C-10 for the location of the pit.

TABLE C-8. DEPTH MEASUREMENTS OF SITE F

Location No.	Depth Measurements (cm)	Location No.	Depth Measurements (cm)
1	18; 19	5	19.5; 19.5
2	19; 19.5	6	21; 21.5
3	21; 21.5	7	18.5; 18.5
4	20; 21	8	18; 18.5

Average Depth: 19.6 cm

See Figure C-10 for the location of measurements.

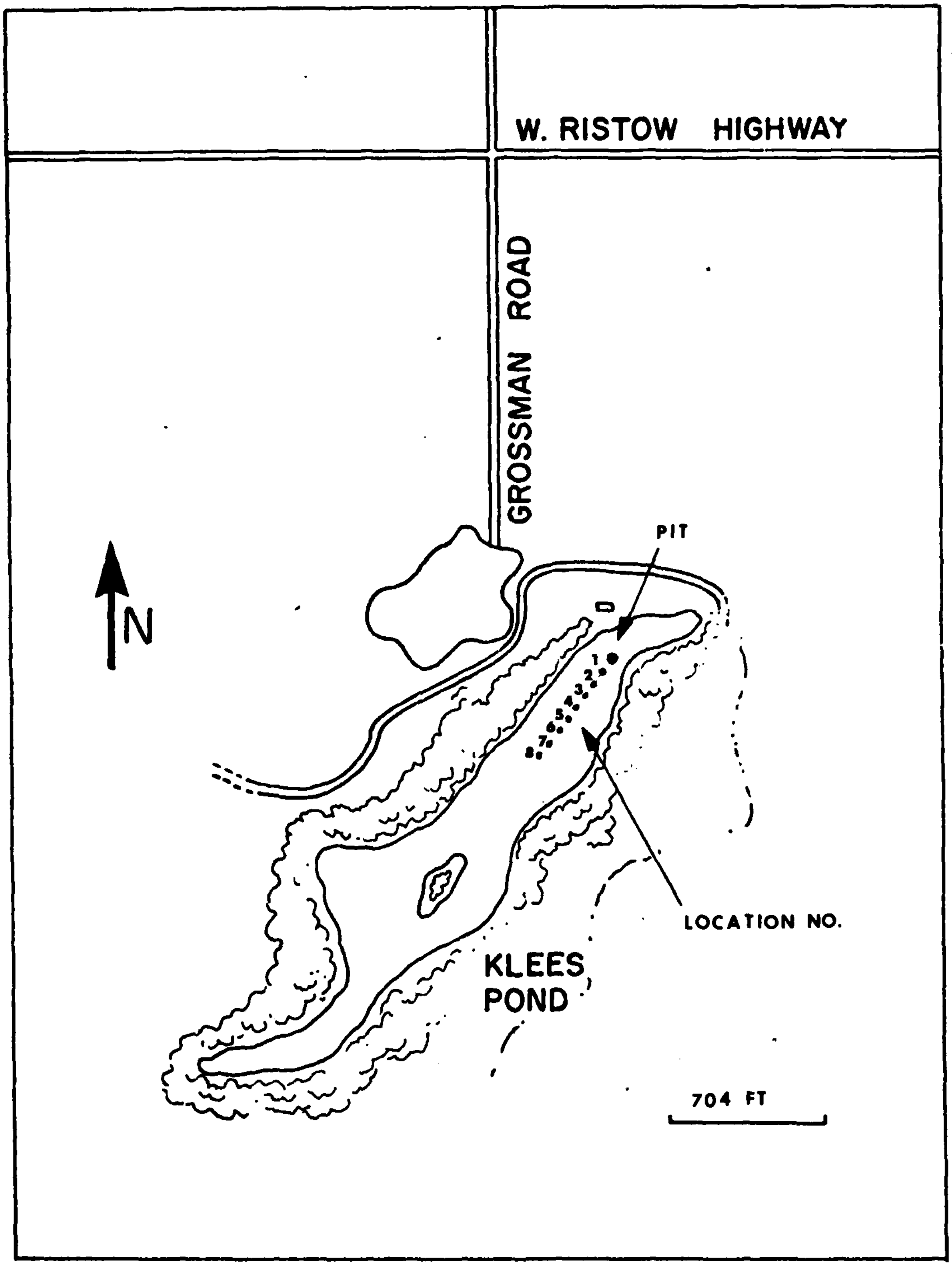

Figure C-10. Map of Site F

TABLE C-9. AIR TEMPERATURE MEASUREMENTS ON FEBRUARY 5, 1979

Time	Temperature (°F)	Time	Temperature (°F)	Time	Temperature (°F)
0057	4	0856	1	1658	9
0158	4	0955	3	1756	8
0255	4	1055	5	1857	6
0357	3	1154	6	1955	5
0458	2	1256	8	2058	2
0558	2	1354	9	2155	-1
0654	1	1455	9	2256	-1
0755	0	1555	10	2350	-1

TABLE C-10. AIR TEMPERATURE MEASUREMENTS ON FEBRUARY 6, 1979

Time	Temperature (°F)	Time	Temperature (°F)	Time	Temperature (°F)
0058	-3	0856	6	1655	14
0153	-7	0958	9	1755	14
0258	-5	1056	10	1857	14
0356	-4	1153	11	1955	15
0453	-1	1257	12	2055	16
0558	3	1353	14	2156	16
0655	5	1453	14	2255	17
0752	5	1554	14	2355	17

TABLE C-11. AIR TEMPERATURE MEASUREMENTS ON FEBRUARY 7, 1979

Time	Temperature (°F)	Time	Temperature (°F)	Time	Temperature (°F)
0058	17	0858	18	1655	17
0157	18	0957	18	1755	17
0259	18	1058	20	1857	15
0357	19	1157	22	1955	15
0457	19	1258	22	2055	14
0557	18	1358	22	2156	12
0654	18	1457	21	2255	10
0752	18	1556	20	2355	8

TABLE C-12. SNOWFALL MEASUREMENTS ON FEBRUARY 5, 6, 7, 1979

February 5, 1979		February 6, 1979		February 7, 1979	
time interval	Snow Fall (cm)	time interval	Snow Fall (cm)	time interval	Snow Fall (cm)
0000 ∿ 0300	0	0000 ∿ 0300	0	0000 ∿ 0300	0.3
0300 ∿ 0600	0	0300 ∿ 0600	0.25	0300 ∿ 0600	0
0600 ∿ 0900	0	0600 ∿ 0900	0.5	0600 ∿ 0900	0
0900 ∿ 1200	0	0900 ∿ 1200	1.0	0900 ∿ 1200	1.4
1200 ∿ 1500	0	1200 ∿ 1500	0.25	1200 ∿ 1500	0.7
1500 ∿ 1800	0	1500 ∿ 1800	0.5	1500 ∿ 1800	0.5
1800 ∿ 2100	0	1800 ∿ 2100	0	1800 ∿ 2100	0
2100 ∿ 2400	0	2100 ∿ 2400	0.25	2100 ∿ 2400	0
Total	0	Total	2.8 cm	Total	2.9 cm

(The reverse of this page is blank)

DA

FILM

7 –